

https://dspace.org/

The purification of the polymer membrane fuel cell (PEMFC) reformate as by the methanation reaction with the use of platinum group metals (PGMs) on TiO2 support

Mgcima, Zolani

2012-07-03
http://hdl.handle.net/10539/11591

Downloaded from a DSpace repository. https://dspace.org/

The purification of the polymer membrane fuel cell (PEMFC) reformate as by the methanation reaction with the use of platinum group metals (PGMs) on TiO_2 support.

By

Zolani Mgcima

Submitted in the fulfillment of the requirements for the degree of Master of Science in the Faculty of Science

Supervisor: Professor M.S. Scurrell

Co-supervisor: Professor N.J. Coville

Declaration

I declare that this MSc dissertation is my own, unaided work under the supervision of Professor M.S. Scurrell. It is being submitted for the degree of Master of Science in the University of Witwatersrand, Johannesburg. It has not been submitted before for any degree or examination in any other University.

.....

(Signed) Zolani Mgcima

..... Day of 2012

Abstract

The catalytic performance of TiO_2 supported PGMs (Pd, Ru, Pt, Rh) was investigated for the CO , CO_2 and CO/CO_2 methanation reactions with respect to metal loading. The Pd/TiO_2 and Ru/TiO_2 catalysts were prepared by both the deposition-precipitation method and the wet-incipient method. In the latter case catalysts were either subjected to calcination or were left uncalcined. From TEM and TPR analysis it was noted that the uncalcined Pd/TiO_2 and Ru/TiO_2 catalysts demonstrated different characteristics such as having smaller particle sizes and the presence of a second reduction peak which was not present in the other differently prepared catalysts. This peak was assumed to be due to metal-support interactions. The Pd/TiO_2 catalysts did not display significant differences in activity. However the uncalcined Ru/TiO_2 catalysts displayed higher activities for the CO methanation reaction; hence the Pt/TiO_2 and Rh/TiO_2 catalysts were prepared with this method. The catalytic activity for the CO methanation reaction of the catalysts was observed to vary in the order of $Rh/TiO_2 > Ru/TiO_2 > Pd/TiO_2 > Pt/TiO_2$. A similar ranking of aluminia supported PGMs has been reported in several studies.[1,2] All of the investigated catalysts lead to the production of one hydrocarbon which was methane even at lower temperatures such as 240 ^{0}C. Higher hydrocarbons were not observed and the extent to which methane was produced increased with increasing temperature. For all of the investigated catalysts activity was observed to decrease with decreasing metal loading.

During the CO_2 methanation reaction compared to the Pd and Pt catalysts, the Rh and Ru catalysts displayed the highest relative activity for CO_2 methanation. Plots which compared CO methanation with CO_2 methanation showed that the Rh/TiO_2 and Ru/TiO_2 catalysts had the largest temperature window at which CO methanation was at a maximum while CO_2 methanation was at a minimum. The Pt/TiO_2 and Pd/TiO_2 catalysts had the smallest temperature window of operation. The Pt/TiO_2 catalysts appeared to have higher tendencies for CO_2 methanation and not CO methanation. For all catalysts investigated the methanation of CO_2 lead to the production of CO via the reverse water gas shift reaction (RWGS) at high temperatures. In order to determine the selectivity of the catalysts for the CO methanation reaction compared to

CO_2 methanation, R values were calculated and it was established that the Rh/TiO_2 and Ru/TiO_2 catalysts had the highest maximum R values and thus better selectivity towards CO methanation.

Compared to the CO and CO_2 methanation results, the CO/CO_2 methanation results were different as the catalysts would reach maximum CO conversion at a certain temperature and then decrease with further increase of temperature due to the RWGS reaction. However the Pd and Pt catalysts displayed similar results as in the CO_2 methanation reaction, because they demonstrated a higher affinity for the RWGS reaction during the CO/CO_2 methanation reaction. The Rh and Ru catalysts displayed the highest activity for the selective methanation of CO in the CO/CO_2 gas mixture. The formation of CH_4 was determined for the Rh/TiO_2 and Ru/TiO_2 catalysts since they displayed the best performance for the selective methanation of CO in the CO/CO_2 gas mixture. It was noted that the CH_4 present also results from the methanation of CO_2 and that a temperature range at which complete CO methanation and negligible CO_2 methanation occurs is not present.

References:

(1) Panagiotopoulou, P; Kondarides, D.I; Verykios, X.E. *Applied Catalysis A: General,* 2008, 344, 45-54.

(2) Vannice; M.A. Journal of Catalysis, 1975, 37,449-461.

Presentations

- Z. Mgcima and M.S. Scurrell, The purification of the polymer electrolyte membrane fuel cell (PEMFC) reformate gas by the selective methanation reaction with the use of noble metals on titania (TiO_2) support, CATSA conference, Worcester, (2009)

- Z. Mgcima and M.S. Scurrell, The purification of reformate gas by the selective methanation reaction using noble metals on titania support for use in a polymer electrolyte membrane fuel cell (PEMFC), CATSA conference, Bloemfontein, (2010)

Acknowledgements

I would like to thank my supervisor Prof Michael Scurrell for introducing me to the world of fuel cells. I really enjoyed working under your supervision and thank you for all the excellent ideas and advice you give me for my project. To my co-supervisor Prof Neil Coville, thank you for contribution to my research and all the solutions to some of the questions I encountered in my research. The year 2010 was a very tragic year for me and I would like to thank you for your support and patience, you guys will always be my role models both academically and personally.

Mr Basil Chassoulas, thank you for the technical support. I will always remember the late nights we spent fixing my catalytic test units and all the jokes you used to crack. You truly are a technical guru.

To Prof M.J. Witcomb and Prof Ziegler, thank you for teaching me how to use the Tecnai G^2 Spirit TEM. To Prof Ziegler thank you for going beyond the call of duty to ensure that I receive the appropriate images for my project. To Prof D. Billing thank you for teaching me and allowing me to use the D2.

To the CATOMAT group, thank you guys for all the assistance and being such a friendly group.

To the NRF and HYSA thank you for the financial support. I would have not been able to perform this research without your financial support.

To my family, Phindile, Monde, Velaphi and Nolubabalo I would not have done it without your support and encouragement. Lastly to the Lord Almighty, thank you for always being there for me, you truly are the Alpha and Omega.

Table of contents

Abstract		i
Presentations		iii
Acknowledgements		iv
Table of contents		v
List of Figures		x
List of Tables		xix
Nomenclature		xx

Chapter 1: Introduction

1.1.	Aim of this study	1
1.2.	Fuel cells	1
1.3.	History of fuel cell	4
1.4.	Polymer electrolyte membrane fuel cell	8
1.5.	The methanation reaction	13
1.6.	Justification	17
1.7.	References	18

Chapter 2: Literature review

2.1.	CO methanation studies with PGMs	20
2.2.	CO methanation studies with supported PGMs	21

2.3. Objectives of the project 27
2.4. References 28

Chapter 3: Experimental

3.1. Introduction 30

3.2. Catalyst preparation 30

3.2.1. Preparation of the uncalcined TiO_2 supported Ru, Rh, Pt and Pd catalysts by the wet-incipient method 30

3.2.2. Preparation of the Ru/TiO_2 and Pd/TiO_2 catalysts by the deposition precipitation method. 31

3.2.3. Preparation of the catalysts by the wet-incipient method followed by calcination. 32

3.2.4. Preparation of the 5wt% Ru/TiO_2 uncalcined catalyst with 1/2wt% of the Cl^- ion. 33

3.3. Catalyst characterization procedures 34

3.3.1. Brunauer-Emmett-Teller (BET) analysis 34

3.3.2. Temperature Programmed Reduction (TPR) analysis 36

3.3.3. Transmission Electron Microscopy (TEM) 37

3.3.4. Powder X-ray diffraction (PXRD) 38

3.4. Catalysts performance test 39

3.4.1. Set up for the catalyst performance test. 39

3.4.2. Catalyst performance test. 40

3.4.2.1. Blank runs 40

3.4.2.2. Actual catalytic runs 42

3.4.2.3. Calculations used to determine conversions and yields 42

3.5. References 44

Chapter 4: Results and discussion

4.1. Introduction 45

4.2. Catalyst characterization results 45

4.2.1. Powder X-ray diffraction (PXRD) analysis of the Ru/TiO_2 catalysts. 45

4.2.2. Brunauer-Emmett-Teller (BET) analysis of the Ru/TiO_2 catalysts 48

4.2.3. Transmission Electron Microscopy (TEM) analysis of the Ru/TiO_2 catalysts 50

4.2.3.1. TEM analysis of the calcined $5\%Ru/TiO_2$ catalyst 51

4.2.3.2. TEM analysis of the deposition-precipitation $5\%Ru/TiO_2$ catalyst. 52

4.2.3.3. TEM analysis of the uncalcined $5\%Ru/TiO_2$ catalyst. 53

4.2.4. Temperature Programmed Reduction (TPR) analysis of the Ru/TiO_2 catalysts 54

4.2.4.1. TPR of the calcined Ru/TiO_2 catalysts 54

4.2.4.2. TPR of the Ru/TiO_2 catalysts which were prepared by the deposition precipitation method. 55

4.2.4.3. TPR of the uncalcined Ru/TiO_2 catalysts 56

4.2.5. Powder X-ray diffraction (PXRD) analysis of the Pd/TiO_2 catalysts. 60

4.2.6. BET analysis of the Pd/TiO_2 catalysts 62

4.2.7. Transmission Electron Microscopy (TEM) analysis of the Pd/TiO_2 catalysts 63

4.2.7.1. TEM analysis of the calcined 5 wt% Pd/TiO_2 catalyst 64

4.2.7.2. TEM analysis of the deposition-precipitation $5\%Pd/TiO_2$ catalyst. 65

4.2.7.3. TEM analysis of the uncalcined Pd/TiO_2 catalysts 66

4.2.8. Temperature Programmed Reduction (TPR) analysis of the Pd/TiO_2 catalysts 67

4.2.8.1. TPR of the calcined 5 wt% Pd/TiO_2 catalyst and the TPR of the

Pd/TiO_2 catalyst which was prepared by the deposition-precipitation method. 67
4.2.8.2. TPR of the uncalcined 1 wt% and 5 wt% Pd/TiO_2 catalysts. 68
4.2.9. X-ray diffraction XRD analysis of the 1 wt%, 3 wt% and 5 wt% Rh/TiO_2 catalysts. 69
4.2.10. BET analysis of the 1 wt%, 3 wt% and 5 wt% Rh/TiO_2 catalysts. 71
4.2.11. TEM analysis of the 5 wt% Rh/TiO_2 catalysts. 71
4.2.12. TPR of the calcined 1 wt%, 3 wt% and 5 wt% Rh/TiO_2 catalysts. 73
4.2.13. X-ray diffraction XRD analysis of the 1 wt%, 3 wt% and 5 wt% Pt/TiO_2 catalysts. 74
4.2.14. BET analysis of the 1wt%, 3wt% and 5wt% Pt/TiO_2 catalysts. 76
4.2.15. TEM analysis of the 5 wt% Pt/TiO_2 catalysts. 76
4.2.16. TPR of the calcined 1wt%, 3wt% and 5wt% Pt/TiO_2 catalysts. 77

4.3. Catalytic performance tests 79
4.3.1. CO methanation results 79
4.3.1.1. CO methanation results of the 5 wt% Ru/TiO_2 catalysts 79
4.3.1.2. CO methanation results of the 1wt% and 3wt% Ru/TiO_2 catalysts 82
4.3.1.3. CO methanation over the 5wt% Pd/TiO_2 catalysts 84
4.3.1.4. CO methanation results of the 1wt% and 3wt% Pd/TiO_2 catalysts 85
4.3.1.5. CO methanation results of the 1wt%,3wt% and 5wt% Rh/TiO_2 catalysts 86
4.3.1.6. CO methanation results of the 1 wt%,3 wt% and 5 wt% Pt/TiO_2 catalysts 88
4.3.1.7. Summary of the CO methanation results of the 4 PGMs on TiO_2 support catalysts. 90
4.3.2. CO_2 methanation results 93
4.3.2.1. CO_2 methanation results of the Rh/TiO_2 catalyst. 93
4.3.2.2. CO_2 methanation results of the Ru/TiO_2 catalyst. 95
4.3.2.3. CO_2 methanation results of the Pd/TiO_2 catalyst. 96
4.3.2.4. CO_2 methanation results of the Pt/TiO_2 catalyst. 97
4.3.2.5. Summary of the CO_2 methanation results of the 4 PGMs on TiO_2 support catalysts. 98

4.3.3. CO/CO_2 methanation results. 102
4.3.3.1. CO/CO_2 methanation results for the 5wt% Rh/TiO_2 catalyst. 102
4.3.3.2. CO/CO_2 methanation results for the 5wt% Ru/TiO_2 catalyst. 103
4.3.3.3. CO/CO_2 methanation results for the 5wt% Pd/TiO_2 catalyst. 103
4.3.3.4. CO/CO_2 methanation results for the 5wt% Pt/TiO_2 catalyst. 104
4.3.3.5. Summary of the CO/CO_2 methanation results of the 4 PGMs on TiO_2 support catalysts. 106
4.4. References 110

Chapter 5: Conclusions and Recommendations

5.1. Conclusions 113

5.2. Recommendations for future work 115

Appendices

Appendix A 117

List of Figures

Chapter 1

Figure 1.1: Picture of William Grove the inventor of the first fuel cell and the set-up he used to come up with his invention (taken from Ref 4). 5

Figure 1.2: Picture of Thomas Grubb and Leonard Niedrach who were the inventors of the first PEM fuel cell (taken from Ref.4). 6

Figure 1.3: Illustration of how a typical PEMFC operates.Taken from: www.fctec.com/images/fctype.PEMFC.jpg 8

Figure 1.4: Flow diagram of the purification of the PEMFC fuel (modified from Ref. 3). 11

Figure 1.5: Mechanism of CO methanation to form methane and water. 14

Figure 1.6: Volcano curve which was obtained by Bligaard et al. where he measured CO methanation activities against the calculated dissociative CO adsorption energies.(taken from Ref.17) 16

Chapter 2

Figure 2.1: Selective methanation of CO in CO_2 and H_2 gas mixtures which was performed by Panagiotopoulou et al. (Taken from Ref. 14). 22

Figure 2.2: CO conversion results which were reported by Galletti et.al.(Taken from Ref.15). 23

Figure 2.3: Selective methanation of CO in CO_2 and H_2 gas mixture with the use of Ru on different supports performed by Panagiotopoulou et al. (Taken from Ref.1). 25

Chapter 3

Figure 3.1: Flow diagram illustrating how the uncalcined catalysts were prepared. 31

Figure 3.2: Set-up used for the preparation of the Ru/TiO_2 and Pd/TiO_2 catalysts by the deposition-precipitation method. 32

Figure 3.3: Schematic of the preparation of the calcined catalysts. 33

Figure 3.4: Picture of the Micromeritics Flow Prep 060 sample degas system. 34

Figure 3.5: Picture of the Micromeritics Tristar surface area and porosity analyzer. 35

Figure 3.6: Picture of the Micromeritics Autochem II chemisorptions analyzer system. 36

Figure 3.7: Picture of the Tecnai G^2 spirit TEM instrument. 37

Figure 3.8: Picture of the D2 Bruker Phaser Powder X-ray diffraction instrument. 38

Figure 3.9: Schematic representation of the set-up used for the catalytic performance tests. 40

Figure 3.10: Blank run for the CO methanation reaction. 41

Figure 3.11: Blank run for the CO_2 methanation reaction. 41

Figure 3.12: Blank run for the selective methanation of CO in a CO_2 and H_2 gas mixture. 42

Chapter 4

Figure 4.1: PXRD pattern of the three 5 wt% Ru/TiO_2 catalysts.(a)Prepared by wetness-incipient method, dried at 110 ^{0}C and calcined at 400 ^{0}C for 5 hours (**b)** Prepared by wetness-incipient method, dried at 110 ^{0}C and not calcined **(c)** prepared by deposition-precipitation method and calcined at 400 ^{0}C for 5 hours. 46

Figure 4.2: PXRD pattern of the reduced 5 wt% Ru/TiO_2 catalysts. **(a)**Prepared by wetness-incipient method, dried at 110 ^{0}C and calcined at 400 ^{0}C for 5 hours (**b)** Prepared by wetness-incipient method, dried at 110 ^{0}C and not calcined **(c)** prepared by deposition-precipitation method and calcined at 400 ^{0}C for 5 hours. 47

Figure 4.3: Example of how the pore volume increases. 49

Figure 4.4: TEM images of the 5wt% Ru/TiO_2 catalysts before they were reduced. **(a)** dried at 110^0C for 24 hours and calcined at 400 ^{0}C for 5 hours, **(b)** prepared by deposition-precipitation method, vacuum dried for 20 hours and calcined at 400 ^{0}C for 5 hours and **(c)** dried at 110 ^{0}C for 24 hours. 50

Figure 4.5: TEM image of the 5 wt% Ru/TiO_2 catalyst which was calcined at 400 ^{0}C for 5 hours. 51

Figure 4.6: TEM image of the 5 wt% Ru/TiO_2 catalyst which was prepared by the deposition-precipitation method and calcined at 400 ^{0}C for 5 hours. 52

Figure 4.7: TEM image of the 5wt% Ru/TiO_2 catalyst which was dried at 110 ^{0}C and not subjected to calcination. 53

Figure 4.8: TPR profile of the Ru/TiO_2 catalysts calcined at 400 ^{0}C for 5 hours. **(a)** 5 wt% Ru/TiO_2,**(b)** 3 wt% Ru/TiO_2 and **(c)** 1 wt% Ru/TiO_2. 54

Figure 4.9: TPR profile of the Ru/TiO_2 catalysts prepared by the deposition-precipitation method and calcined at 400 ^{0}C for 5 hours. **(a)** 5 wt% Ru/TiO_2, **(b)** 3 wt% Ru/TiO_2 and **(c)** 1 wt% Ru/TiO_2. 55

Figure 4.10: TPR profile of the Ru/TiO_2 catalysts prepared by the incipient wetness impregnation and not subjected to calcination.**(a)** 5 wt% Ru/TiO_2, **(b)** 3 wt% Ru/TiO_2 and **(c)** 1 wt% Ru/TiO_2. 57

Figure 4.11: TPR profiles of the **(a)** 5 wt% Ru/TiO_2 with 0.5 wt% Cl^- and the **(b)** 5 wt% Ru/TiO_2 uncalcined catalyst. 58

Figure 4.12: Proposed mechanism of how the 330 ^{0}C reduction peak might arise in the TPR profile of the uncalcined catalysts. 59

Figure 4.13: PXRD pattern of the three 5 wt% Pd/TiO_2 catalysts. **(a)** Prepared by deposition-precipitation method and calcined at 400 ^{0}C for 5 hours,**(b)** dried at 110 ^{0}C and not calcined and **(c)** calcined at 400 ^{0}C for 5 hours. 60

Figure 4.14: PXRD patterns of the reduced Pd/TiO_2 catalysts, **(a)** Prepared by deposition-precipitation method and calcined at 400 ^{0}C for 5 hours,**(b)** dried at 110 ^{0}C and not calcined and **(c)** calcined at 400 ^{0}C for 5 hours. 61

Figure 4.15: TEM images of the 5 wt% Pd/TiO_2 catalysts before they were reduced.**(a)** dried at 110 ^{0}C for 24 hours and calcined at 400 ^{0}C for 5 hours, **(b)** prepared by deposition-precipitation method, vacuum dried for 20 hours and calcined at 400 ^{0}C for 5 hours and **(c)** dried at 110 ^{0}C for 24 hours. 63

Figure 4.16: TEM image of the 5wt% Pd/TiO_2 catalyst which was calcined at 400 ^{0}C for 5 hours. 64

Figure 4.17: TEM image of the 5 wt% Pd/TiO_2 catalyst which was prepared by the deposition-precipitation method and calcined at 400 ^{0}C for 5 hours. 65

Figure 4.18: TEM image of the 5 wt% Pd/TiO_2 catalyst which was dried at 110 ^{0}C and uncalcined. 66

Figure 4.19: TPR profiles of the **(a)** 5wt% Pd/TiO_2 catalyst which was calcined and the **(b)** 5wt% Pd/TiO_2 catalyst prepared by the deposition-precipitation method. 67

Figure 4.20: The TPR profile of the **(a)** 1 wt% and **(b)** 5 wt% Pd/TiO_2 catalysts which were prepared by the wet-incipient method and left uncalcined. 68

Figure 4.21: PXRD pattern of the Rh/TiO_2 catalysts with different metal loadings (**a)** 5 wt% (**b)** 3 wt% and **(c)** 1 wt%. 69

Figure 4.22: PXRD pattern of the 5 wt% Rh/TiO_2 catalysts **(a)** 5 wt% Rh/TiO_2 not reduced and **(b)** 5 wt% Rh/TiO_2 reduced. 70

Figure 4.23: TEM image of the 5 wt% Rh/TiO_2 catalyst **(a)** TEM image and **(b)** Particle distribution,**(c)** EDX results. 72

Figure 4.24: TPR profile of the Rh/TiO_2 catalysts with different metal loadings **(a)** 1 wt% Rh/TiO_2, **(b)** 3 wt% Rh/TiO_2 and **(c)** 5 wt% Rh/TiO_2. 73

Figure 4.25: PXRD pattern of the Pt/TiO_2 catalysts with different metal loadings (**a)** 5 wt% Pt/TiO_2, **(b)** 3 wt% Pt/TiO_2 and **(c)** 1 wt% Pt/TiO_2. 74

Figure 4.26: PXRD pattern of the 5 wt% Pt/TiO_2 catalysts **(a)** 5 wt% Pt/TiO_2 not reduced and **(b)** 5 wt% Pt/TiO_2 reduced. 75

Figure 4.27: TEM image of the 5 wt% Pt/TiO_2 catalyst **(a)** TEM image and **(b)** Particle size distribution 77

Figure 4.28: TPR profiles of the Pt/TiO_2 catalysts **(a)** 5 wt %, **(b)** 3 wt% and **(c)** 1 wt%. 78

Figure 4.29: Conversions of CO as function of temperature obtained over 5 wt% Ru/TiO_2 catalysts prepared by different methods. **(a)** Dried at 110 ^{0}C for 24 hours and calcined at 400 ^{0}C for 5 hours, **(b)** dried at 110 ^{0}C for 24 hours and **(c)** prepared by deposition-precipitation method, vacuum dried for 20 hours and calcined at 400 ^{0}C for 5 hours. 79

Figure 4.30: Conversions of CO as function of temperature obtained from 1 wt%

and 3 wt% Ru/TiO_2 catalysts prepared by different methods. **(a)** Dried at 110 ^{0}C for 24 hours and calcined at 400 ^{0}C for 5 hours, **(b)** dried at 110 ^{0}C for 24 hours and **(c)** prepared by deposition-precipitation method, vacuum dried for 20 hours and calcined at 400 ^{0}C for 5 hours. 82

Figure 4.31: Conversions of CO as function of temperature obtained over 5 wt% Pd/TiO_2 catalysts prepared by different methods. **(a)** Dried at 110 ^{0}C for 24 hours and calcined at 400 ^{0}C for 5 hours, **(b)** dried at 110 ^{0}C for 24 hours and **(c)** prepared by deposition-precipitation method, vacuum dried for 20 hours and calcined at 400 ^{0}C for 5 hours. 84

Figure 4.32: Conversions of CO as function of temperature obtained over 1 wt% and 3 wt% Pd/TiO_2 catalysts prepared by different methods. **(a)** Dried at 110 ^{0}C for 24 hours and calcined at 400 ^{0}C for 5 hours, **(b)** dried at 110 ^{0}C for 24 hours and **(c)** prepared by deposition-precipitation method, vacuum dried for 20 hours and calcined at 400 ^{0}C for 5 hours. 86

Figure 4.33: Conversions of CO as function of temperature obtained over Rh/TiO_2 catalysts with different metal loadings. **(a)** 5 wt %,**(b)** 3 wt% and **(c)** 1 wt%. 87

Figure 4.34: Conversions of CO as a function of temperature obtained over Pt/TiO_2 catalysts with different metal loadings. **(a)** 5 wt%, (**b)** 3 wt% and **(c)** 1 wt%. 89

Figure 4.35: Conversions of CO as a function of temperature obtained over different PGMs on TiO_2 support. **(a)** 5 wt% Rh/TiO_2, **(b)** 5 wt% Ru/TiO_2**,(c)**5 wt% Pd/TiO_2 and **(d)** 5 wt% Pt/TiO_2. 90

Figure 4.36: Conversions of CO_2 and CO as a function of temperature. The 5 wt% Rh/TiO_2 catalysts were prepared by the wet-incipient method

and not calcined. **(a)** CO methanation and **(b)** CO_2 methanation. Feed composition: 25 % CO_2 and 75 % H_2. 93

Figure 4.37: Comparison of the R values (R = CO conversion/CO_2 conversion) of the Rh/TiO_2 catalysts as a function of temperature. The Rh/TiO_2 catalysts were prepared by t he wet-incipient method and not calcined.(a) 5wt% Rh/TiO_2 ,(b) 3wt% Rh/TiO_2 and (c) 1wt% Rh/TiO_2. 94

Figure 4.38: Conversions of CO_2 and CO as a function of temperature for 5 wt% Ru/TiO_2 . The catalysts were prepared by a wet-incipient method and not calcined. **(a)**CO methanation and **(b)** CO_2 methanation. Feed composition: 25 %CO_2 and 75%H_2. 95

Figure 4.39: Conversions of CO_2 and CO as a function of temperature for 5 wt%Pd/TiO_2 .The catalysts were prepared by wet-incipient method and not calcined. **(a)** CO methanation and **(b)** CO_2 methanation. Feed composition: 25 %CO_2 and 75 %H_2. 96

Figure 4.40: Conversions of CO_2 and CO as a function of temperature for 5wt%Pt/TiO_2 .The catalysts prepared by wet-incipient method and not calcined. **(a)**CO methanation and **(b)** CO_2 methanation. Feed composition: 25 % CO_2 and 75 % H_2. 97

Figure 4.41: CO_2 methanation results obtained from the 5wt% Pt/TiO_2 catalyst at 480 ^{0}C. 99

Figure 4.42: Percentage yield of CO produced by the RWGS reaction during CO_2 methanation reaction. **(a)** 5 wt% Rh/TiO_2, **(b)** 5 wt% Ru/TiO_2 ,

(c) 5 wt% Pd/TiO_2 and (d) 5 wt% Pt/TiO_2. 100

Figure 4.43: Comparison of the R values (R = CO conversion/CO_2 conversion) of the 5 wt% TiO_2 supported PGM catalysts as a function of temperature. The catalysts were prepared by the wet-incipient method and not calcined.(a) 5 wt% Rh/TiO_2 ,(b) 5 wt% Ru/TiO_2 ,(c) 5 wt% Pd/TiO_2 and (d) 5 wt% Pt/TiO_2. 101

Figure 4.44: Conversions of CO/CO_2 as a function of temperature obtained over 5wt%Rh/TiO_2 catalysts prepared by wet-incipient method and not calcined. **(a)**CO conversion and **(b)** CO_2 conversion.Feed composition: 8%CO,23%CO_2 and 69%H_2. 102

Figure 4.45: Conversions of CO/CO_2 as a function of temperature obtained over 5wt%Ru/TiO_2 catalysts prepared by wet-incipient method and not calcined. **(a)**CO conversion and **(b)** CO_2 conversion. Feed composition: 8%CO,23%CO_2 and 69%H_2. 103

Figure 4.46: Conversions of CO/CO_2 as a function of temperature obtained over 5 wt% Pd/TiO_2 catalysts prepared by wet-incipient method and not calcined . **(a)**CO conversion and **(b)** CO_2 conversion. Feed composition: 8% CO, 23% CO_2 and 69% H_2. 104

Figure 4.47: Conversions of CO/CO_2 as a function of temperature obtained over 5wt%Pt/TiO_2 catalysts prepared by wet-incipient method and then not calcined. **(a)**CO conversion and **(b)** CO_2 conversion. Feed composition: 8%CO,23%CO_2 and 69%H_2. 105

Figure 4.48: CH_4 formation as a function of temperature obtained from the (a) 5 wt% Rh/TiO_2 and (b) 5 wt% Ru/TiO_2 catalysts. 108

List of Tables

Chapter 1

Table 1.1: Different types of fuel cells (taken from Ref 3). 3

Chapter 4

Table 4.1: BET surface area and pore volume of the TiO_2 supported Ru catalysts. 48

Table 4.2: BET surface area and pore volume of the TiO_2 supported Pd catalysts. 62

Table 4.3: BET surface area and pore volume of the TiO_2 supported Rh catalysts. 71

Table 4.4: BET surface area and pore volume of the TiO_2 supported Pt catalysts. 76

Table 4.5: Temperature for 50% and 100% CO conversion in the CO methanation reaction (5 wt% Ru/TiO_2). 81

Table 4.6: Temperature for 50 % and 100 % CO conversion in the CO methanation reaction (1 wt% and 3 wt% Ru/TiO_2). 83

Table 4.7: Temperature for 50 % and 100 % CO conversion in the CO methanation reaction (5 wt% Pd/TiO_2). 85

Table 4.8: Temperature for 50 % and 100 % CO conversion in the CO methanation

reaction (1 wt% , 3 wt% and 5 wt% Rh/TiO_2). 88

Table 4.9: Temperature for 50 % and 100 % CO conversion in the CO methanation reaction (1 wt% , 3 wt% and 5 wt% Pt/TiO_2). 89

Table 4.10: Summary of the 50% and 100% CO conversion in the CO methanation reaction for the 5wt% Rh, Ru, Pd and Pt TiO_2 supported catalysts. 91

Table 4.11: CO_2 conversions at 360 ^{0}C and 480 ^{0}C in the CO_2 methanation reaction for the for the 5 wt% Rh, Ru, Pd and Pt, TiO_2 supported catalysts. 98

Table 4.12: Summary of the selective methanation of CO in CO/CO_2 mixtures over the TiO_2 supported PGMs. 106

Nomenclature

Abbreviation	Description
AFC	Alkaline Fuel Cell
BET	Brunauer-Emmett-Teller
$Conv(CO)_{480}$	CO conversion at 480 ^{0}C
$Conv(CO_2)_{480}$	CO_2 conversion at 480 ^{0}C
EDX	Energy Dispersive X-ray Spectroscopy
FID	Flame Ionisation Detector
GC	Gas Chromatograph
GE	General Electric
Max_{CO}	Maximum CO conversion
Max_{CO2}	CO_2 conversion at maximum CO conversion
MCFC	Molten Carbonate Fuel Cell
PAFC	Phosphoric Acid Fuel Cell

PEMFC	Polymer Electrolyte Membrane Fuel Cell
PGMs	Platinum Group Metals
PSA	Pressure Swing Adsorption
PXRD	Powder X-ray Diffraction
RWGS	Reverse Water Gas Shift
TCD	Thermal Conductivity Detector
TEM	Transmission Electron Microscopy
TPR	Temperature Programmed Reduction
T_{50}	Temperature of 50% CO conversion
T_{100}	Temperature of 100% CO conversion
SMSIs	Strong Metal-Support Interactions
SOFC	Solid Oxide Fuel Cell
WGS	Water Gas Shift
XPS	X-ray Photoelectron Spectroscopy

Chapter 1
Introduction

1.1. Aim of this study

It has become imperative to find alternative methods of generating energy. The Polymer Electrolyte Membrane Fuel Cell is considered to be the energy creator of the future because, unlike the conventional methods of generating energy from fossil fuels, it leads to less environmental pollution and the many other negative outcomes associated with conventional methods. However one of the disadvantages which is hindering global usage of the PEMFC is that the reformate gas used in PEMFCs contains CO which poisons the cell electrodes. This study is focused on reducing the concentration of CO using a selective CO methanation reaction involving TiO_2 supported PGMs. The PEMFC reformate gas also contains CO_2 which can lead to the consumption of significant quantities of H_2 if CO_2 methanation occurs. Due to this an objective was to investigate CO methanation, CO_2 methanation and the selective methanation of CO in CO/CO_2 gas mixtures and to investigate whether a correlation exists in the activity and behavior of the catalysts in the separate reactions.

1.2. Fuel Cells

Fuel cells are electrochemical cells which can convert the chemical energy which is stored in a fuel directly into electricity with very high efficiency.[1] Due to this; fuel cells have attracted a lot of attention over the past decade as an alternative route to traditional energy production routes. Unlike the conventional method of generating energy from fossil fuels which leads to many negative consequences such as environmental pollution, global conflict and fossil fuel depletion, the only by-products produced by fuel cells are water and heat.[2] In addition fuel cells have the ability to power anything from residences to cell phones. Unlike batteries, fuel cells do not need to be recharged as long as they are supplied with fuel. Many energy generating devices require

high maintenance due to their many moveable parts, however with fuel cells there is low maintenance because they do not have many moveable parts. Due to their scaleable design they are very appropriate for use in energy-limited devices such as iPods and laptops. Unlike other energy technologies such as wind or photovoltaics, fuel cells do not have geographic or environmental limitations; they can be located anywhere. Some of the markets in which fuel cells could play a huge role include the transportation, portable and stationary sectors.

Presently there are only five known types of fuel cells which have been described. These are the alkaline fuel cell (AFC), phosphoric acid fuel cell (PAFC), polymer electrolyte membrane fuel cell (PEMFC), molten carbonate fuel cell (MCFC) and solid oxide fuel cell (SOFC).[3]All of these consists of an ion-conducting electrolyte which is placed between two electrodes (anode and cathode) and have the same operating principle, they just differ by the composition of the electrolyte used in the cell.[3] For all of the fuel cells the electrodes have to be porous because the gas has to come into contact with the electrodes and the electrolyte simultaneously.[3] The fuel cells also have common separate reactions that occur on the anode and cathode. The resulting charged species (i.e. protons) have to be transferred through the electrolyte and electrons have to flow through the external circuit in order to generate the DC electricity in the fuel cell. Most of these fuel cells are still being developed and have certain advantages and disadvantages relative to each other.[3] **Table 1.1** list some of the features of the different types of fuel cells.

Table 1.1: Different types of fuel cells (taken from Ref 3).

Types of fuel cells and their features

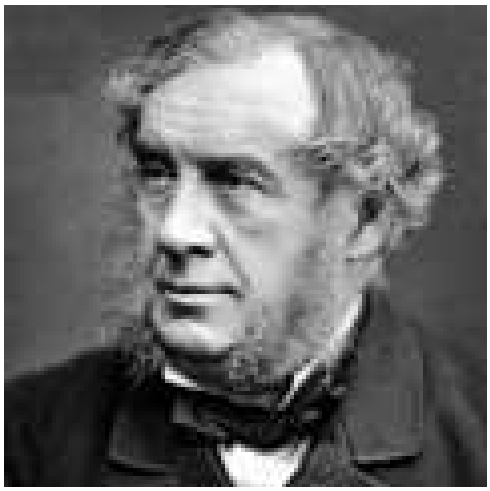
Features	Fuel cell type			
Name	Polymer electrolyte	Phosphoric acid	Molten carbonate	Solid oxide
Electrolyte	Ion exchange membrane	Phosphoric acid	Alkali carbonates mixture	Yttria-stabilized zirconia
Operating temperature (°C)	70–90	180–220	650–700	800–1000
Charge carrier	H^+	H^+	CO_3^{2-}	O^{2-}
Electrolyte state	Solid	Immobilized liquid	Immobilized liquid	Solid
Cell hardware	Carbon- or metal-based	Graphite-based	Stainless steel	Ceramic
Catalyst, anode	Platinum (Pt)	Platinum (Pt)	Nickel (Ni)	Nickel (Ni)
Fuels for cell	H_2	H_2	Reformate or CO/H_2	Reformate or CO/H_2 or CH_4
Reforming	External or direct MeOH	External	External or internal	External or internal, or direct CH_4
Feed for fuel processor	MeOH, natural gas, LPG, gasoline, diesel, jet fuel	Natural gas, MeOH, gasoline, diesel, jet fuel	Gas from coal or biomass, natural gas, gasoline, diesel, jet fuel	Gas from coal or biomass, natural gas, gasoline, diesel, jet fuel
Oxidant for cell	O_2/air	O_2/air	CO_2/O_2/air	O_2/air
Co-generation heat	None	Low quality	High	High
Cell efficiency (% LHV)	40–50	40–50	50–60	50–60

Even though fuel cells have so many advantages they also have a few disadvantages and limitations which inhibit their commercialization, and much research is being conducted in order to solve these problems. The limitations include:

- The requirement of reforming the fuel
- The cost of materials with specific properties such as platinum and Nafion materials.
- The decrease in performance due to the degradation of the catalyst when a fuel source other than hydrogen is used.

1.3. History of Fuel Cells

Even though there has been some controversy as to who came up with the idea of the fuel cell, Sir William Robert Grove (**Figure 1.1**) is credited with the invention of the first fuel cell in 1839.[4] He managed to come up with this idea by using the inverse of a process which was formulated by William Nicholson and Anthony Carlisle in 1800.[4] In this process William Nicholson and Anthony Carlisle used electricity to decompose water into hydrogen and oxygen. This was the first chemical reaction which used electricity and it became to be known as electrolysis. In order to perform this procedure Nicholson and Carlisle used a Volta battery and connected the ends of two conducting wires to the electrodes of the battery.[4] The other ends of the wires were allowed to come into contact with an aqueous solution of sodium chloride. When this occurred hydrogen and oxygen began to form on the electrodes.[4] So in 1839 William Grove took the inverse of this idea by forming water from hydrogen and oxygen instead of decomposing it. He performed this by using two platinum electrodes which were submerged in a solution of dilute sulfuric acid.[4] The other ends of the electrodes were then enclosed in two containers.[4] The one container had oxygen and the other had hydrogen.[4] Water was also present in both containers and this allowed Grove to observe current flow because the water level in the containers began to rise.[4] Grove connected 50 more pairs of such electrodes in series in order to obtain more current. He named his gas battery invention the Grove cell and this technically became the first fuel cell. There has been much disagreement about who presented the fuel cell idea first, William Grove or Christian Friedrich Schönbein. However letters written by Schönbein to his friend Faraday indicate that Grove is the inventor.[4] In one of the letters Schönbein disagrees with Grove's concept of oxidation occurring on the anode electrode.[4] However this is exactly what happens in fuel cells.



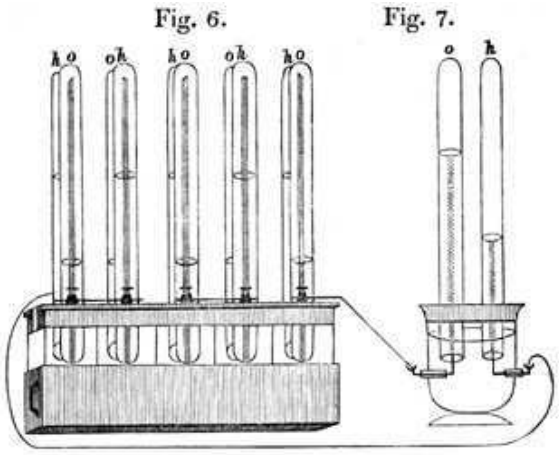


Figure 1.1: Picture of William Grove the inventor of the first fuel cell and the set-up he used to come up with his invention (taken from Ref 4).

After Grove's discovery many other researchers contributed to the development of the fuel cell. In 1889 Ludwig Mond and his assistant Carl Langer performed a lot of fuel cell experiments. In these experiments they would use gas (CO_x and H_2) which was produced from coal. This was contrary to what Groves believed i.e. that only pure hydrogen could be used with electrodes coated with a thin layer of perforated platinum.[5] During the experiments they encountered many setbacks which were caused by the liquid electrolytes.[5] As a result they could only achieve 6 amps per square foot at 0.3 volts.[5] One of the realizations that Grove made about his electrodes was that there was a need for a larger area of contact between the electrolyte, the gaseous reagent and the electrode, he referred to this as the "notable surface of action".[6] Mond and Langer were the first researchers who used this concept and tried to modify Grove's electrodes by making the electrode structure porous and thus giving it a three dimensional form.[6] This form of electrode has been incorporated into modern fuel cells today. At about the same time a separate team which consisted of Charles R. Alder Wright and C. Thompson conducted similar experiments. The cell that they constructed could not reach voltages higher than 1 volt because the gases that they used i.e. hydrogen and oxygen would mix in their separate chambers, an effect caused by leaks in the cell.[4] Louis Joseph Colardeau and Louis Paul Cailleteton had similar difficulties and later became discouraged because they believed that the process was not practical as it required the use of precious metals.[4] In addition it was reported in many publications around this period

that coal was the appropriate source of energy because of its low price and any other more efficient source would not lower the price of electricity below that produced from coal.[4]

Despite all of these difficulties, many researchers still continued with their work on fuel cells. These included Friedrich Wilhelm Ostwald who is known as one of the founders of physical chemistry. In 1893 Ostwald contributed to the development of fuel cells by describing the roles which are played by the different components in the fuel cell.[7] In the early 1900s Emil Baur and his students conducted experiments on different types of fuel cells. Of particular importance is the experiment in which they used high-temperature devices and a unit which used an electrolyte made out of clay and metal oxides.[8] Not much fuel cell research was conducted during most of the 1900s. It was only in the 1950s that Thomas Grubb and Leonard Niedrach (**Figure 1.2**) created a very important invention which was called the PEM fuel cell because they used a sulphonated polystyrene ion-exchange membrane as the electrolyte.[4] Both Grubbs and Niedrach worked for a company called General Electric (GE).[4] This company supplied the U.S. Navy and the U.S. Army with a small fuel cell where hydrogen was made by combining water and lithium hydride. GE also supplied NASA with their fuel cell technology for use in their Gemini program.[4] In 1959 Harry Ihrig and his team made a fuel cell for a tractor which belonged to a company called Allis Chalmer.[4] This was the first fuel cell powered tractor.



Figure 1.2: Picture of Thomas Grubb and Leonard Niedrach who were the inventors of the first PEM fuel cell (taken from Ref.4).

Since the 1970s fuel cell research has been focused on the following areas:

- Reforming the fuel used in fuel cells.
- Decreasing the diffusion limitations in the electrodes in order to get a larger area of action.
- Obtaining longer lifetime and greater performance.
- Reducing the cost of the fuel cell catalysts.

Nowadays many companies and governments are trying to develop fuel cells which can be used in applications such as fuel cell powered cars, bikes, tractors and even mobile phones. Even banks, police stations and hospitals are trying to incorporate fuel cells in their energy generation units. So there is an enormous variety of fuel cell applications.

1.4. Polymer electrolyte membrane fuel cell (PEMFC).

Of the different types of fuel cells, the polymer electrolyte membrane fuel cell (PEMFC) is by far the most promising candidate for transportation (e.g. fuel cell vehicles), stationary (e.g. fuel cell generators) and portable (e.g. fuel cell powered cell phones) applications due to its light weight, compactness, low operating temperature (~80^0C) and its ability to sustain operation at high current density compared to the other types of fuel cells.[1]

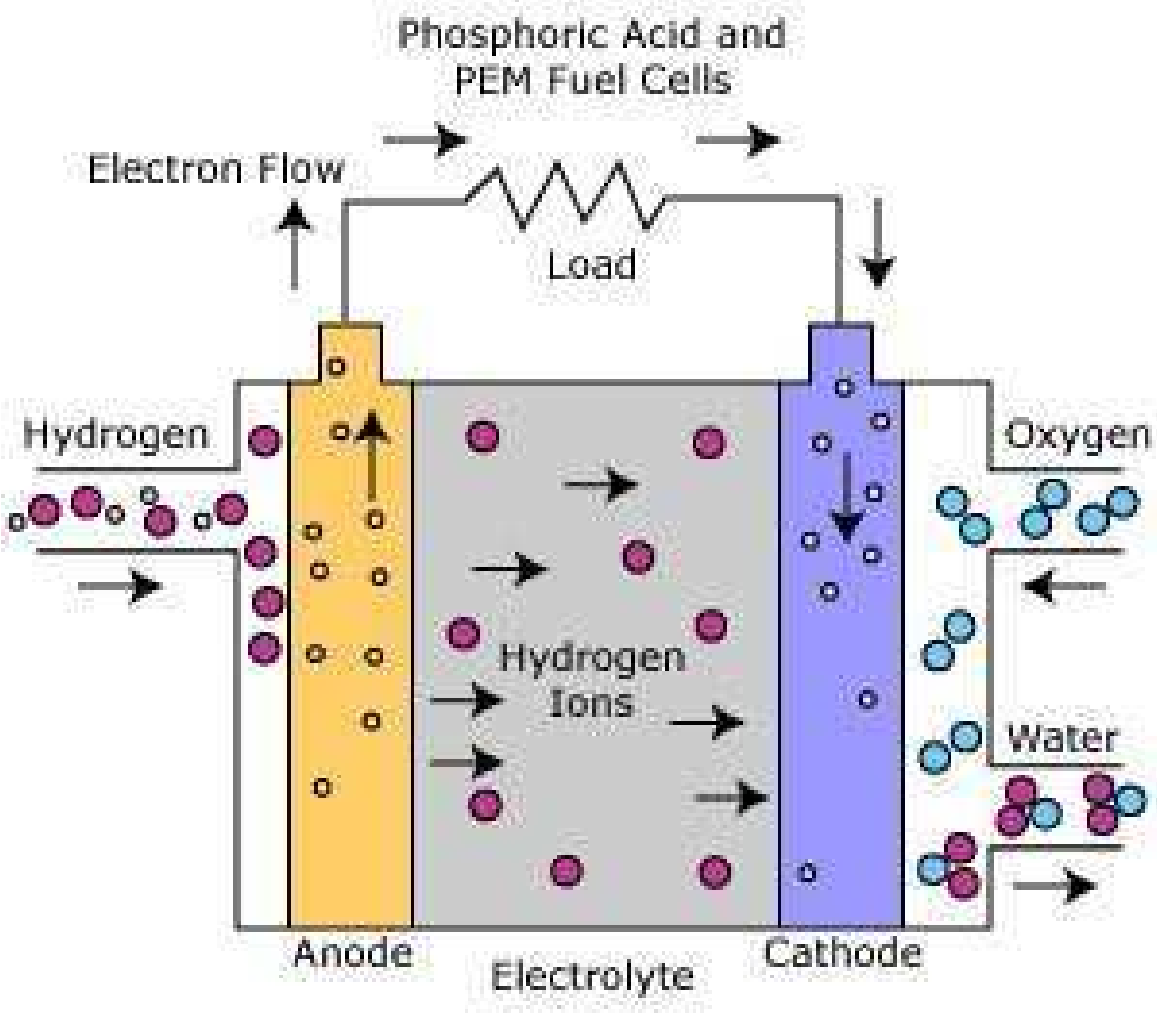


Figure 1.3: Illustration of how a typical PEMFC operates.

Taken from: www.fctec.com/images/fctype.PEMFC.jpg

As can be noted from **Figure 1.3** a typical PEMFC consists of an anode electrode, cathode electrode and a solid polymer electrolyte membrane. The membrane is typically a fluorinated sulfonic acid polymer such as Teflon which consists of a fluorocarbon polymer backbone with sulfonic acid groups.[3] This polymer electrolyte membrane is an electronic insulator but also a good conductor of protons.[3] Unlike liquid electrolytes the solid polymer electrolyte does not leak over time and it serves as a good barrier for gases (hydrogen and oxygen) thus preventing them from mixing in their separate compartments.[3] Both electrodes are normally coated with a platinum on carbon support catalyst but more advanced electrodes are coated with a Pt-Ru /C binary catalyst and with the help of this catalyst, hydrogen is oxidized on the anode electrode into protons and electrons (Equation **(1.1)**).[1] The electrons move towards the cathode electrode through the external circuit and this leads to the generation of the current output of the fuel cell. The resulting protons are transferred to the cathode through the polymer electrolyte membrane because the sulfonic acid groups are stationary, but the protons attached to them can migrate through the membrane. [3] The protons and electrons react with oxygen on the cathode to form water (Equation **(1.2)**). The overall reaction in the PEMFC leads to the production of heat and electrical energy (Equation **(1.3)**). One of the reasons why the PEMFC has such low operating temperatures, between 70 ^{0}C and 90 ^{0}C which provide instant start-up and no need for insulation to protect the user from being burnt is because the water which is produced as a by-product needs to hydrate the membrane before it evaporates.[3]

$$\text{Anode: } H_2(g) \rightarrow 2H^+(aq) + 2e^- \qquad (1.1)$$

$$\text{Cathode: } 1/2O_2\,(g) + 2H^+(aq) + 2e^- \rightarrow H_2O(l) \qquad (1.2)$$

$$\text{Overall: } H_2\,(g) + 1/2O_2\,(g) \rightarrow H_2O(l) + \text{electric energy} + \text{heat} \qquad (1.3)$$

Even though the PEMFC might be a solution to energy production, several drawbacks still exist which are hindering its commercialization (e.g. hydrogen storage, cost and the appropriate infrastructure).[2] One of these important drawbacks is the poisoning (deactivation) of the platinum catalyst on the anode electrode by carbon monoxide (CO). CO is one of the most well

known poisons of industrial Pt catalysts and it deactivates the Pt catalyst by forming stronger interactions with the catalyst than those of the feed. Thus CO blocks the active sites of the catalyst.[9] The CO is present in the hydrogen rich feed because hydrogen is commonly produced by the steam reforming or partial oxidation of hydrocarbons such as methane.[10] (See Equation **(1.4))** represents steam reforming and Equation **(1.5)** which represents partial oxidation).

$$CH_4 + H_2O \leftrightarrow CO + 3H_2 \qquad \Delta_R H^0_{298K} = 206 \text{ kJ/mol} \quad (1.4)$$

$$CH_4 + 1/2\ O_2 \leftrightarrow CO + 2H_2 \qquad \Delta_R H^0_{298K} = -36 \text{ kJ/mol} \quad (1.5)$$

Both the steam reforming and partial oxidation of hydrogen can lead to the production of about 1 vol % of CO. Due to this the gas produced from these reactions has to be subjected to a set of purification steps which are shown in **Figure 1.4**. As noted from **Figure 1.4**, the sulfur which is found in hydrocarbon fuels has to be removed and then this desulfurised gas is subjected to reforming either by steam reforming or partial oxidation in order to produce H_2 and CO.[3] This reformate gas is then passed on to the water gas shift reaction which reduces the concentration of CO. However at this stage the concentration of CO is still too high (typically 1-3%) . The Pt catalyst is easily deactivated by even small concentrations of CO, [11] so the CO content has to be lower than 10 ppm.[12] Due to this, an additional purification step is required which reduces the CO concentration. The syngas gas produced from natural gas can be used to produce ultra clean gas by the Fischer-Tropsch synthesis or methanol synthesis reactions. However this would lead to high costs and an additional clean up step would still be required.[3] Even if the methanol were converted to H_2 by electrochemical means by the use of the direct methanol fuel cell this would lead to difficulties these include the lack of infrastructure and environmental concerns,[3] so an additional cleanup step would still be the more favorable option.

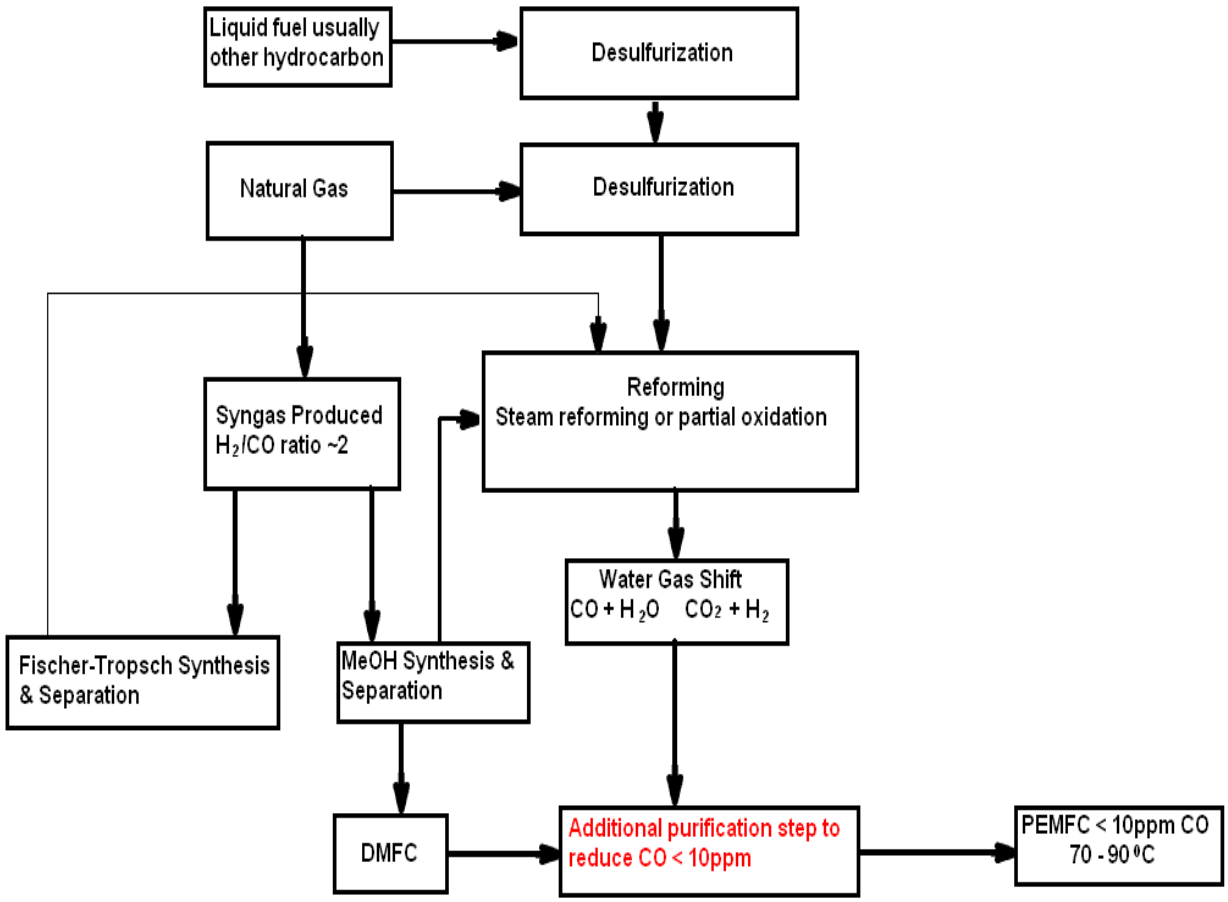


Figure 1.4: Flow diagram of the purification of the PEMFC fuel (modified from Ref. 3).

In theory there are many processes that could be used to reduce the CO concentration in the hydrogen-rich gas feed. Of these a notable approach involves membrane separation. In this process a Pd-Ag membrane is used to separate the H_2 from the CO by allowing the H_2 to permeate through the membrane under the influence of a high differential pressure across the sides of the membrane, and high temperatures.[13] Obtaining this differential pressure is not an issue for a process which utilizes liquid fuels as a pump can be used to provide the differential pressure.[13] The disadvantages associated with this process include the high cost of the Pd-Ag membrane and the requirement to provide the differential pressure.[13]

Another process that could be used is the pressure swing adsorption (PSA) process, in which materials which are known to be highly absorptive such as zeolites are used as molecular sieves.[13] These materials act as molecular sieves by absorbing the unwanted CO at high pressures and then a highly reliable control system is used to swing the pressure to low pressures so that the absorbed CO can be desorbed.[13] Just like the membrane separation process, the PSA method is very costly and complicated since a control system to swing the pressure is required.

With chemical purification methods a choice is usually made between the preferential CO oxidation (PROX) (Equation **(1.6)**) and the selective CO methanation (Equation **(1.7)**) reactions. They have been widely reported to be the most viable methods for CO removal in H_2 rich gases as they do not require too much space and they have low operating temperatures.[14] The PROX requires the addition of oxygen which may lead to a reduced hydrogen yield due to the oxidation of H_2,[12] safety related problems and loss of energy due to the combustion of hydrogen to form water.[11] In addition the PROX is known to have a very narrow temperature window of operation and in order to avoid H_2 oxidation a low supply of O_2 would have to be controlled by means of very expensive flow meters. So the PROX reaction can be complicated and is a very costly method which would have limitations for use in low-power PEFCs. Here the supply of oxidant needs to be very tightly controlled.[13] Unlike PROX, the selective methanation of CO does not require an additional reactant and both the CO methanation and CO_2 methanation (Equation **(1.8)**) reactions are less exothermic than the CO oxidation and H_2 oxidation (Equation **(1.9)**) reactions. Due to this the methanation reaction is easier to control than the PROX reaction. In addition, the methane which is produced from this reaction is not wasted as it can be re-used by passing the cells off-gas into a cell reformer for use as feedstock or it can be used as a fuel which can be burnt for heating purposes.[14] Even though the methanation reaction uses 3 moles of hydrogen for 1 mole of CO, only 1 mol of H_2 is lost to water if methane selectivity is 100%. The 2 mols which are lost to CH_4 are recycled back into the cell. The requirements of a PEMFC is that it should have a gas line which re-circulates any unreacted H_2.[13] Even if the H_2 were to be significantly consumed, the consumed amount would be acceptable since the CO content is low. Theoretically the PROX reaction does not consume any H_2. However, this is practically impossible because the oxidation of H_2 can also be favoured.[13] Due to these advantages it would

seem that the selective CO methanation reaction might be the better alternative to reformate gas purification, but obviously high selectivity for CO (as opposed to CO_2) methanation is to be sought.

CO oxidation:	$CO + 1/2O_2 \leftrightarrow CO_2$	$\Delta_R H^0_{298K} = -284kJ/mol$ (1.6)
CO methanation:	$CO + 3H_2 \leftrightarrow CH_4 + H_2O$	$\Delta_R H^0_{298K} = -206kJ/mol$ (1.7)
CO_2 methanation:	$CO_2 + 4H_2 \leftrightarrow CH_4 + 2H_2O$	$\Delta_R H^0_{298K} = -165kJ/mol$ (1.8)
H_2 oxidation:	$H_2 + 1/2O_2 \leftrightarrow H_2O$	$\Delta_R H^0_{298K} = -244kJ/mol$ (1.9)

1.5: The methanation reaction.

The methanation reaction (Equation **(1.7)**) was discovered by Sabatier and Senderens in 1902 making them the first scientists to produce methane catalytically by passing carbon oxide and hydrogen over a nickel catalyst.[15] As noted in **Figure 1.5** the methanation reaction is one of the simplest catalytic reactions. Its mechanism involves the dissociation of CO into C^- and H^- ions, followed by the hydrogenation of these species into methane and water. Besides being an alternative to the PROX reaction, the methanation reaction is also used in various industrials processes. As an example, the removal of carbon oxides (COx) in the feed gas in the ammonia synthesis which would otherwise poison the ammonium synthesis catalysts, in the gasification of coal, where it is used to produce methane from synthesis gas, and in the Fischer-Tropsch synthesis.[15] The use of the methanation reaction for the removal of carbon monoxide actually dates to the early 1920s where George Claude from France and Casales from Italy both conducted the reaction at high pressures.[15] In the 1930s scientists in the USA also used this reaction in ammonia and hydrogen plants.[9] Some old coal-based plants used methanators that contained iron catalysts which were later discovered to have disadvantages when compared to nickel catalysts but were able to operate in the presence of large amounts of poisons.[9] It was not until the 1950s that a process step which utilized a nickel-based catalyst that operated at low

pressures was incorporated into the ammonia process flowsheets.[9] In the 1970s the methanation reaction attracted a lot of attention for the production of substitute natural gas due to a shortage of the natural gas at that time.[9] In this process coal was partially reduced to form CO and this CO was reacted with H_2 to form methane and water. Nowadays the selective methanation reaction is an important topic of study for the cleanup of reformate gas for PEMFC applications.

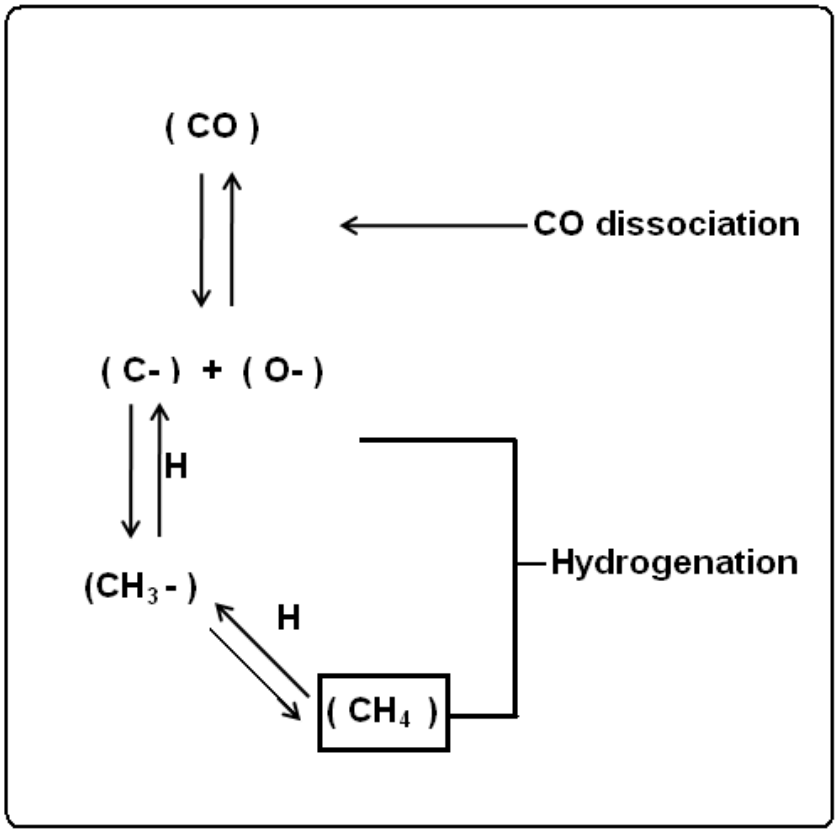


Figure 1.5: Mechanism of CO methanation to form methane and water.

Compared to other catalysts Ni and Ru based catalysts are the most intensively investigated and used for the selective methanation of CO for PEMFC purposes. Ni supported on aluminum oxide is known as a traditional catalyst for methanation. Even though Ru is relatively expensive, it is believed to be more active in CO methanation than nickel.[16] Unlike Ni which is easily deactivated at low temperatures as a result of the interaction of the metal particles with carbon monoxide and the formation of mobile nickel subcarbonyls, Ru is known to be stable when used over a wide range of temperatures.[16] Hence Ru catalysts for low-temperature hydrogenation of

carbon oxides to methane are commercially available from companies such as Alvigo (RKM-3) and Süd Chemie (METH 150).[16] Fe catalysts have some potential for the methanation reaction however, Fe is also much less active than Ru catalysts and more prone to carbon deposition.

Many researchers such as Bligaard et al.[17] and Norskov et al.[18] have reported that the activity of a catalyst for the methanation reaction is influenced or determined by two properties on the catalysts surface, which are the breaking up of CO and the stability of the C and O species on the catalyst surface (Figure 1.5**)**. By relating a catalyst's activity with its ability to form chemical bonds with the reactants, the intermediates or the products, a volcano curve can be obtained. A volcano curve is a very important tool in heterogeneous catalysis and has been created by Bligaard et al.[17] (**Figure 1.6**) where he used the chemisorptions energy on metal surfaces to describe their catalytic activity. From this volcano curve it was noted that for the transition metals located more to the right of the curve, with high dissociative CO adsorption energies, the rate of the methanation reaction was limited by the high resistance for CO dissociation.[17] Those metals did not form good catalysts. However for the metals found to the left of the curve, with low dissociative CO adsorption energies, the rate of the reaction was limited by the high binding energy of the absorbed C and O species and these metals did not form good catalysts.[17] The most active catalysts would be the catalysts found in the middle of the curve (e.g. Ru) as they would have optimum chemisorption energy of about -150 kJ/mol.[17] This explains why many researchers have found Ru catalysts to have a very high activity for the methanation reaction. The next best catalysts were Rh and Ni catalysts.

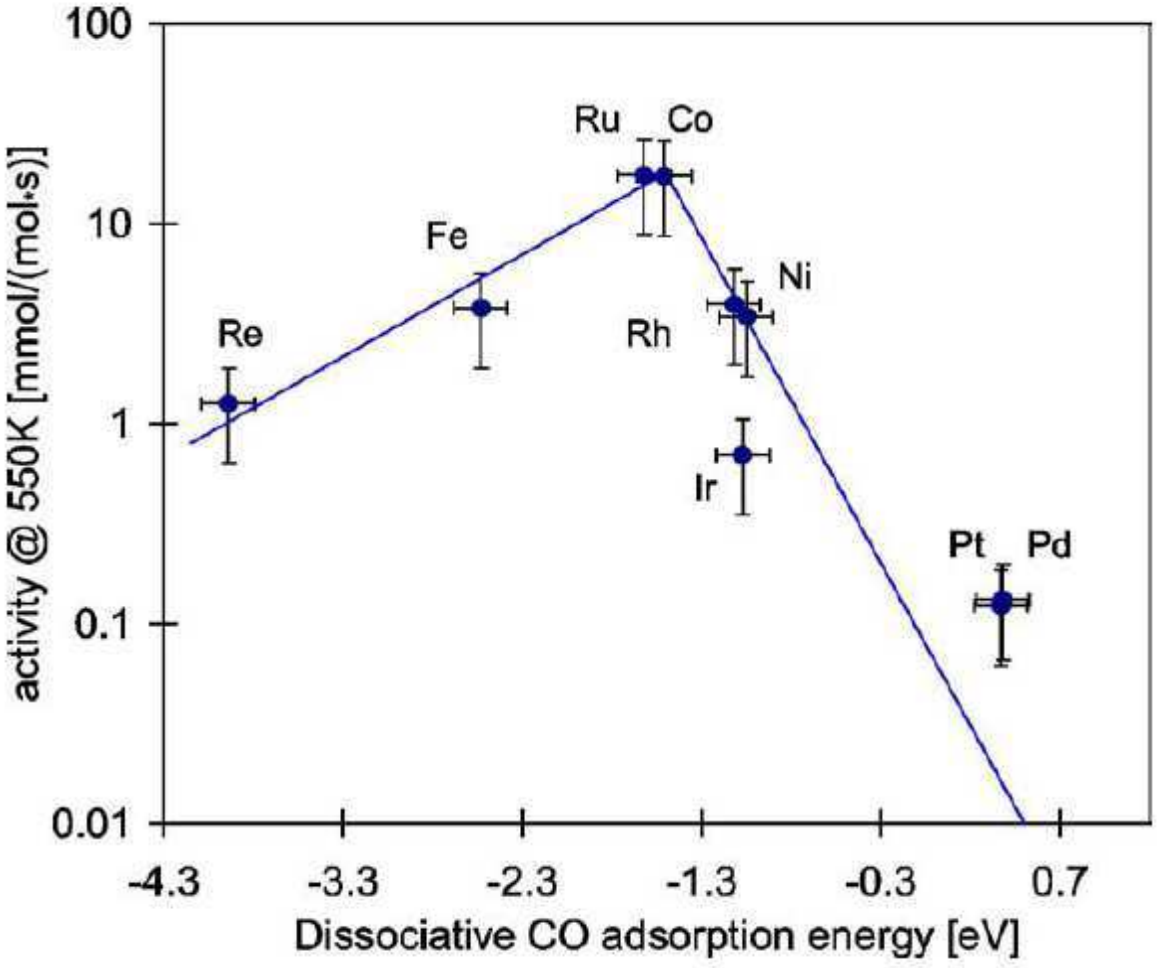


Figure 1.6: Volcano curve which was obtained by Bligaard et al. where he measured CO methanation activities against the calculated dissociative CO adsorption energies.(taken from Ref.17)

One of the disadvantages of the selective methanation of CO is that steam reforming and partial oxidation of hydrocarbons also results in the production of CO_2 (Equations **(1.9) & (1.10)** respectively). Due to this the reformate gas contains more than 20 vol% of CO_2 which can be co-methanated with CO.[19] If CO_2 methanation (Equation **(1.8)**) occurs, significant quantities of H_2 will be consumed. So in order for the selective methanation reaction of CO to be effective a suitable catalyst, which promotes the selective methanation of CO and not the methanation of CO_2, has to be used.

$CH_4 + 2H_2O \leftrightarrow CO_2 + 4H_2$ $\Delta_R H^0_{298K} = 165$ kJ/mol (1.9)

$CH_4 + O_2 \leftrightarrow CO_2 + 2H_2$ $\Delta_R H^0_{298K} = -319$kJ/mol (1.10)

1.6: Justification.

With the high demands for energy, as well as the issue of fossil fuel depletion and environmental pollution, it has become crucial to find alternative sources for energy production. One such source is the PEMFC because it can provide electrical energy with high efficiency and zero production of pollutants. However, the poisoning of the anode electrode by CO (found in the reformate gas), is one of the problems which is preventing commercialization, it has become imperative to find a process which can reduce the concentration of CO in the reformate gas. The selective methanation of CO with the aid of a catalyst has been reported to have the potential for being such a process. The effectiveness of this process could be enhanced by the use of a very active and selective catalyst for the selective methanation of CO into methane.

In this study we intend to determine whether a useful catalyst for this reaction can be found. Several studies have reported the advantageous effects that the reducible TiO_2 metal oxide support has on the activity and selectivity of PGMs for the selective methanation of CO and this aspect will be investigated. Attention will be focused on Ru/TiO_2, Pd/TiO_2, Pt/TiO_2 and Rh/TiO_2 catalysts for the methanation of CO and CO_2 (separately) and CO/CO_2 mixture.

1.7. References

1. C. Spielgel, 2008, PEM fuel cell modeling and simulation using Matlab, Academic Press, Amsterdam.
2. J. Wee, Renewable and Sustainable Energy Reviews, 2007, 11, 1720-1738.
3. C. Song, Catalysis Today, 2002, 77, 17-49.
4. J. M. Andújar and F. Segura, Renewable and Sustainable Energy Reviews, 2009, 13, 2309-2322.
5. P.B.L. Chaurasia, Y. Ando and T. Tanaka, Energy Conversion and Management, 2003, 44, 611-28.
6. A. J. Appleby, Journal of Power Sources, 1990, 29, 3-11.
7. A. B. Stambouli and E. Traversa, Renewable and Sustainable Energy Reviews, 2002, 6,433-55.
8. C. Stone, A.E. Morrison, Solid State Ionics, 2002, 152, 1-13.
9. B. B. Pearce, M. V. Twigg and C. Woodward, 1989, Methanation. In: Catalyst handbook (ed. M.V. Twigg) second edition, 340-378. Wolfe Publishing Ltd, London.
10. A. Heinzel, B. Vogel, P. Hübner, Journal of Power Sources, 2002, 105, 202-207.
11. M. B. I. Choudhury, S. Ahmed, M. A. Shalabi and T. Inui, Applied Catalysis A: General, 2006, 314, 47-53.
12. P.Panagiotopoulou, D.I. Kondarides, X.E. Verykios, Applied Catalysis B: Environmental, 2009, 88,470-478.
13. C. Galletti, S. Specchia, G. Saracco and V. Specchia, Chemical Engineering Science, 2010, 590-596.
14. G. Xu, X. Chen and Z. Zhang, Chemical Engineering Journal, 2006, 121, 97-107.

15. M. P. Andersson, F. Abild-Pedersen, I. N. Remediakis, T. Bligaard, G. Jones, J. Engbaek, O. Lytken, S. Horch, J. H. Nielsen, J. Sehested, J. R. Rostrup-Nielsen and J. K. Norskov, Journal of Catalysis, 2008, 255, 6-19.

16. Z. Kowalczyk, K. Stolecki, W. Rarog-Pilecko, E. Miskiewicz, E. Wilczkowska and Z. Karpinski, Applied Catalysis A: General, 2008, 342, 35-39.

17. T.Bligaard, J.K. Norskovs, S. Dahl, J.Matthiesen, C.H. Christensen and J. Sehested, Journal of Catalysis, 2004, 224, 206-217.

18. J.K. Norskov, T. Bligaard, A. Logadottir, S. Bahn, L.B. Hansen, M. Bollinger, H. Bengaard, B. Hammer, Z. Sljivancanin, M. Mavrikakis, Y. Xu, S. Dahl and C.J.H. Jacobsen, Journal of Catalysis, 2002,209,275-278.

19. Q. Liu, X. Dong, X. Mo and W. Lin, Journal of Natural Gas Chemistry, 2008, 17, 268-272.

Chapter 2
Literature review

2.1. CO methanation studies with PGMs

In order to find an effective catalyst for the selective methanation of CO in reformate gas, a number of studies have been conducted by various research groups. The platinum-group metal (PGM) catalysts which have been investigated include Ru,[1,2,3] Rh,[4-6] Pd,[7,8], Ir,[9] Os and Pt.[10,11] The PGMs are well known for their superior catalytic properties in this reaction. All of the PGMs have displayed activity for hydrogenation-dehydrogenation reactions and they differ in their ability to catalyze various reactions involving CO and H_2.[11] McKee investigated the co-adsorption and interaction of CO and H_2 using unsupported PGMs.[12] In order to measure the composition of the gas he used a volumetric apparatus which was connected to a mass spectrometer. For Pt it was noted that CO is absorbed more strongly than H_2 and thus an interaction between the two gases does not occur as the latter can be displaced by the former.[12] Due to this the production of methane was not favored. However for Rh and Ir catalysts strong absorption of CO still occurred but an interaction between the two gases was noted as detected by the formation of methane.[12] Compared to the other PGMs Ru was noted to behave quite differently as half of the absorbed CO could be removed by evacuation and the other half was completely removed by H_2 reduction and further evacuation.[12] This showed that CO was not strongly absorbed on the Ru surface and an interaction between the two gases occurred. By observing the interaction of the two gases with time it was noted that the production of methane and water was favoured and no CO_2 was produced.[3] The order of activity of the catalysts was found to be Ru >> Rh ~ Ir > Pt ~Pd.[12]

2.2. CO methanation studies with supported PGMs

Vannice investigated the activity of the PGMs (except Os) supported on alumina for the methanation of CO in H_2 and CO gas mixtures.[13] He noted that the Ru/Al_2O_3 catalyst was the most active and the order of activity was found to decrease : $Ru/Al_2O_3 > Rh/Al_2O_3 > Pd/Al_2O_3 > Pt/Al_2O_3 > Ir/Al_2O_3$.[13] In terms of product distribution the Ru catalyst gave about 60% methane with the rest being higher molecular weight hydrocarbons.[13] However the Pd/Al_2O_3 catalysts produced 100% methane meaning that, even though it was less active than the Ru catalyst, it was more selective for the production of methane.

Panagiotopoulou et al.[14] conducted the same study but also investigated the CO_2 methanation and the selective methanation of CO in both CO_2 and H_2/CO gas mixtures. He studied with four of the PGMs , Ru, Rh, Pd and Pt on an alumina support (**Figure 2.1**). Like Vannice, the Ru/Al_2O_3 catalyst was found to be the most active with activity varying in the order of $Ru/Al_2O_3 \sim Rh/Al_2O_3 > Pt/Al_2O_3 > Pd/Al_2O_3$.[14] A finding that did not correspond with Vannice's study was the observation that is the Pd/Al_2O_3 catalyst did not display high selectivity for methane production. Instead it led to the production of CO_2 through the reverse water gas shift (RWGS) reaction.[14] The Rh/Al_2O_3 catalyst which was ranked as the second most active was found to have a higher selectivity for methane production than the Ru/Al_2O_3 catalyst.[14] In CO_2 methanation the Ru/Al_2O_3 catalyst was reported to be the most active with the Pd/Al_2O_3 catalyst being the least active catalyst. One of the interesting findings from this study is that in CO_2, H_2 and CO gas mixtures the methanation of CO_2 is retarded until CO methanation is complete.[14]

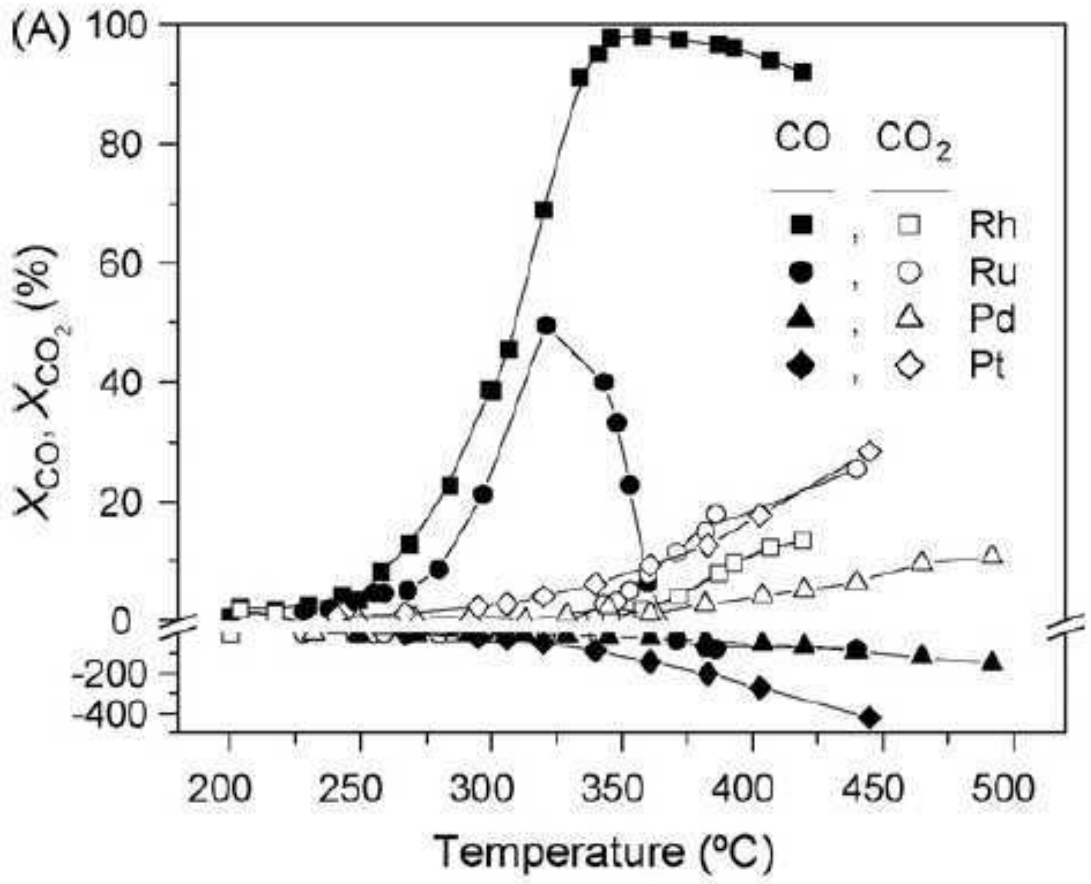


Figure 2.1: Selective methanation of CO in CO_2 and H_2 gas mixtures which was performed by Panagiotopoulou et al. (Taken from Ref. 14)

Due to the reported literature results on the effectiveness of the Ru/Al_2O_3 catalysts in the selective methanation of CO, Galletti et.al.[15] decided to investigate the effect of metal loading on CO selective methanation. The authors also investigated the temperature range at which CO methanation is at a maximum and CO_2 methanation is at a minimum. They studied Ru/Al_2O_3 catalysts with metal loadings of 3 %, 4 % and 5 % which were prepared with high surface areas as compared to other studies.[15] From chemisorption studies the 4% Ru/Al_2O_3 catalyst had the highest dispersion.[15] CO conversion studies were conducted (**Figure 2.2**) with a gas mixture with composition 0.5 % CO, 40 % H_2, 18% CO_2 and 15 % H_2O in He. It was noted that all catalysts led to complete CO conversion. The drop in CO conversion around 340 ^{0}C was assumed to be due to the energetics of the RWGS reaction.[15]

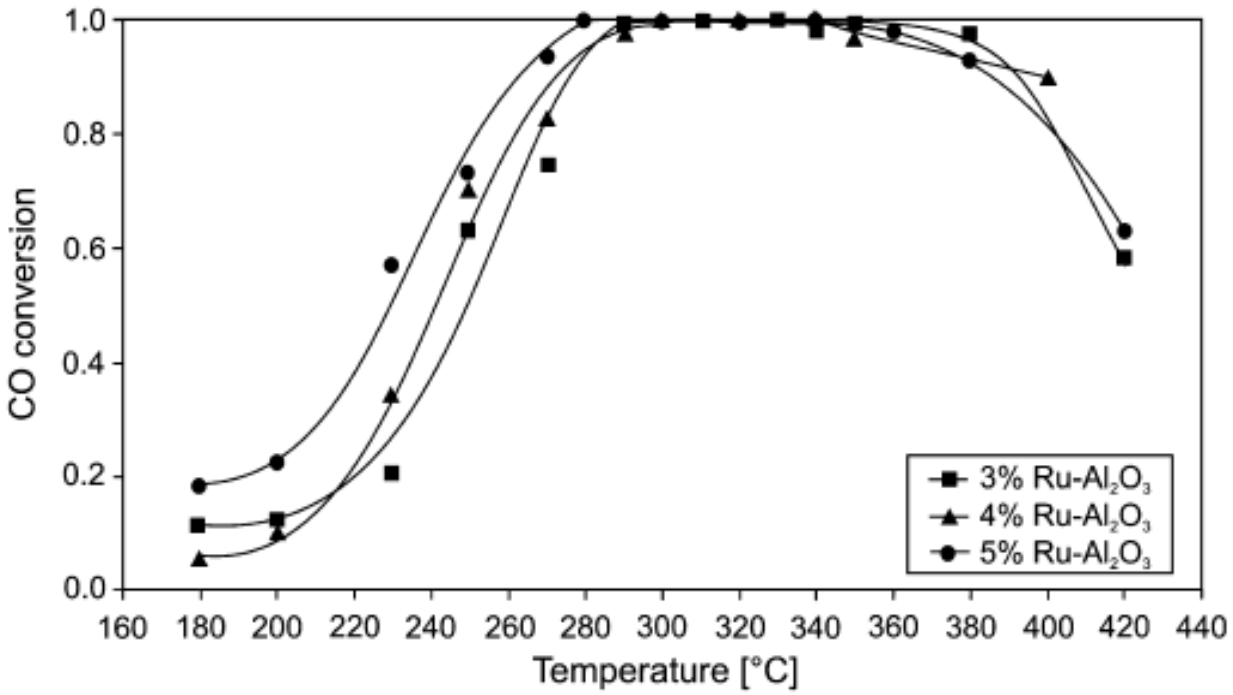


Figure 2.2: CO conversion results which were reported by Galletti et.al.(Taken from Ref.15)

The formation of CH_4 was also reported in order to determine whether CO_2 methanation was occurring.[15] These results showed that CO_2 methanation was favored at higher temperatures as the mole ratio of CH_4 to CO in the reaction was 1:1 and more CH_4 was produced than expected from the available CO present at higher temperatures. This effect was most pronounced for the 5% Ru/Al_2O_3 catalyst as methane formation was significantly higher at high temperatures.[15] To determine the selectivity of CO methanation, and not CO_2, of the catalysts, R ratios were calculated where R= mol formed CH_4/mol reacted CO.[15] From these results it was noted that the 4% Ru/Al_2O_3 catalyst had the largest temperature range in which CO methanation was at a maximum conversion level while CO_2 methanation was at a minimum.[15]

Many studies have been conducted which focused on the influence of the support on the activity of a catalyst. As known, the support prevents the agglomeration of metal particles under temperatures relevant to most reactions and it aids in the appropriate dispersion of the metal particles. But there is evidence which suggests that the support performs other functions.[11] In

another study Panagiotopoulou et al.[1] studied the performance of Ru on different supports which were Al_2O_3, TiO_2, YSZ, CeO_2 and SiO_2 with respect to the metal loading, mean crystallite size of the supported metals and the nature of the support (**Figure 2.3**). From this study it was noted that Ru/TiO_2 displayed the highest activity for the selective methanation of CO with the order of increasing activity being Ru/TiO_2>Ru/Al_2O_3, Ru/CeO_2>Ru/YSZ>Ru/SiO_2.[1] The authors pointed out that the selectivity to CH_4 at a given temperature did not depend significantly on the nature of the support but the activation energies of the CO and CO_2 hydrogenation reactions and the activities of the catalysts were dependent on the nature of the support.[1] They also noted that activity increased with increasing metal loading and the temperature at which CO methanation occurred was shifted to lower temperatures by the use of higher metal loadings (5 wt%).[1] In addition they reported that the Ru/TiO_2 catalysts with larger crystallite sizes displayed higher turnover frequencies.[1] A conclusion was reached that the high activity of the Ru/TiO_2 catalysts was not due to strong metal-support interactions (SMSIs) which alter the catalytic behavior of the metal by electron transfer between the metal and support. Rather the high activity was due to the formation of new active sites on the surface of the highly reducible TiO_2 support which had extraordinary electron donating properties and which were found at the metal-support interface.[1]

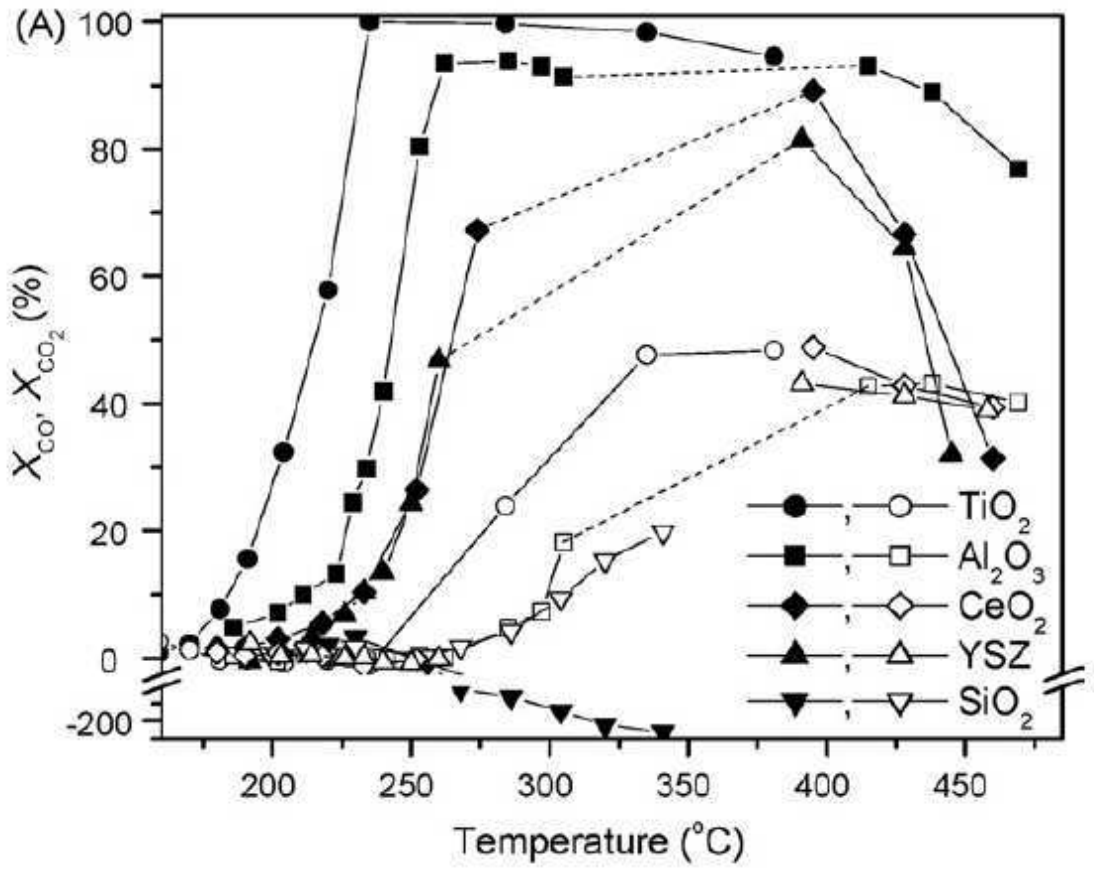


Figure 2.3: Selective methanation of CO in CO_2 and H_2 gas mixture with the use of Ru on different supports performed by Panagiotopoulou et al. (Taken from Ref.1)

Panagiotopoulou et al.[1] reached the above conclusion which was consistent with previous studies. For instance, Tauster et al. examined the absorption of H_2 and CO on PGM supported on TiO_2 and noted that reduction of these catalysts at low temperatures (200 ^{0}C) produced well dispersed metals with the ability to absorb both H_2 and CO.[11] In contrast, when these metals were reduced at higher temperatures (500 ^{0}C) they did not absorb H_2 and CO. According to the authors this was due to metal-support interactions which existed between the support and the metal.[1] Shen et al.[16] investigated the activity and selectivity of Pd supported on Al_2O_3, SiO_2, TiO_2 and ZrO_3 and concluded that the high activity and selectivity of Pd/ZrO_3 for methanol production and that of Pd/TiO_2 for methane was due to the metal-support interactions. This led to the creation of cationic palladium (Pd^+) species which were principally present when the

catalysts were prepared by the deposition-precipitation method and not by the wet-incipient method. The low activity of the Pd/SiO_2 and Pd/Al_2O_3 catalysts was proposed to be as a result of the absence of the metal-support interactions.[16] Bracey and Burch's proposal differed in that they reported that the Pd/TiO_2 catalysts had high activity even when strong metal-support interactions were not present.[17] They anticipated that the high activity of the Pd/TiO_2 catalyst was not due to metal-support interactions but due to the formation of new active sites at the interface between the metal and the support which have the ability to be of assistance in the adsorption of CO.[17] These findings agreed with those noted by Panagiotopoulou et al.[1] In another study in which Panagiotopoulou et al. studied the activity of PGMs supported on reducible (TiO_2,CeO_2,YSZ and La_2O_3) and irreducible (Al_2O_3,MgO and SiO_2) supports for the water gas shift (WGS) reaction and also noted that the enhanced activity of Pt on the reducible TiO_2 and CeO_2 support was due to the formation of new active sites.[18]

This present study is concerned with examining the activity of PGMs on a TiO_2 support with the main focus being on Ru, Rh, Pt and Pd metals, for the CO methanation reaction,CO_2 methanation reaction and the selective methanation of CO in CO/CO_2 gas mixtures. Ir normally displays poor performance for the selective methanation of CO and Os is commonly excluded from the studies due to its low activity.[9, 12, 13] The performance of these catalysts will be investigated in relation to metal loading (1 wt%, 3 wt% and 5 wt %) and metal crystallite size by investigating both calcined and uncalcined catalysts. In addition the activity of Pd/TiO_2 catalysts prepared by the deposition-precipitation method will be compared to the activity of Pd/TiO_2 catalysts prepared by the wet-incipient method. It is hoped that different catalyst preparation methods will have an effect on catalyst activity. In addition the performance of the catalysts will be investigated in terms of temperature by conducting the reactions at different temperatures. As can be noted from the above review, the performance of the PGMs on Al_2O_3 has been thoroughly investigated. [1, 13 & 14] However no comparative comprehensive study which examines the activity of PGMs on TiO_2 for the selective methanation of CO has as yet been reported.

2.3: Objectives of the project:

Objectives of the current project are the following:

- Investigate the activity of TiO_2 supported Ru, Rh, Pd and Pt catalysts with varying loadings (1 wt%, 3 wt% and 5 wt%) for CO, CO_2 and CO/CO_2 methanation reactions as a function of temperature.
- To compare the behavior and activity of the catalysts for the CO methanation, CO_2 methanation and CO/CO_2 methanation reactions in order to establish whether a correlation exists in the three reactions.
- To plot the conversions for the CO and the CO_2 methanation reaction in one plot so that the temperature window of operation at which CO methanation is at a maximum and CO_2 is at a minimum can be determined.
- To compare the selectivity of the prepared catalysts for the CO methanation and the CO_2 methanation reaction by determining R values.
- To find the catalyst that displays the highest activity for the CO, CO_2 and CO/CO_2 methanation reactions. To determine the selectivity of the catalyst for the selective methanation of CO in CO/CO_2 gas mixtures by determining the formation of CH_4.

2.4. References

1. P. Panagiotopoulou, D.I. Kondarides, X.E. Verykios, Applied Catalysis B: Environmental, 2009, 88,470-478.
2. Z. Kowalczyk, K. Stolecki, W. Rarog-Pilecko, E. Miskiewicz, E. Wilczkowska and Z. Karpinski, Applied Catalysis A: General, 2008, 342, 35-39.
3. O. Görke, P. Pfeifer and K. Schubert, Catalysis Today, 2005, 110, 132-139.
4. M. Ojeda, S. Rojas, M. Boutonnet, F. J. Perez-Alonso, F. J. Garcia-Garcia and J. L. G. Fierro, Applied Catalysis A:General, 2004, 274, 33-41.
5. M. Ojeda, S. Rojas, F. J. Garcia-Garcia, M. L. Granados, P. Terreros and J. L. G. Fierro, Catalysis Communications, 2004, 5, 703-707.
6. T. Hanaoka, H. Arakawa, T. Matsuzaki, Y. Sugi, K. Kanno and Y. Abe, Catalysis Today, 2000, 58, 271-280.
7. M. A. Vannice, S. Y. Wang and S. H. Moon, Journal of Catalysis, 1981, 71, 152-166.
8. F. Solymosi, A. Erdohelyi and M. Lancz, Journal of Catalysis, 1985, 95, 567-577.
9. M. A. Vannice, Journal of Catalysis, 1977, 50, 228-236.
10. M. A. Vannice, Journal of Catalysis, 1975, 40,129-134.
11. S. J. Tauster, S. C. Fung and R. L. Garten, Journal of the American Chemical Society, 1978, 100, 170-175.
12. D.W. McKee, Journal of Catalysis, 1967, 8, 240-249
13. M.A. Vannice, Journal of Catalysis, 1975, 37, 449-461.
14. P. Panagiotopoulou, D. I. Kondarides and X. E. Verykios, Applied Catalysis A: General, 2008, 344, 45-54.

15. C. Galletti, S. Specchia, G. Saracco and V. Specchia, Chemical Engineering Science, 2010, 590-596.

16. W. Shen, M. Okumura, Y. Matsumura and M. Haruta, Applied Catalysis A: General, 2001, 213, 225-232.

17. J. D. Bracey and R. Burch, Journal of Catalysis, 1984, 86, 384-391.

18. P. Panagiotopoulou and D. I. Kondarides, Catalysis Today, 2006, 112, 49-52.

Chapter 3
Experimental

3.1. Introduction

This chapter describes the experimental procedures which were used in this study. In the first section the catalysts preparation is discussed while in the second section the characterization methods used and the catalyst performance test are described.

3.2. Catalyst preparation

3.2.1. Preparation of the uncalcined TiO_2 supported Ru,Rh,Pt and Pd catalysts by the wet-incipient method

In order to prepare the Pd/TiO_2 and Ru/TiO_2 catalysts with metal loadings of 1wt%, 3wt% and 5wt%, an aqueous solution of the corresponding $RuCl_3.3H_2O$, $Pd(NO_3)_2.2H_2O$, $RhCl_3.2H_2O$ and $H_2PtCl_6.3H_2O$ hydrated salts was prepared. This was done by dissolving the salts in a calculated volume of distilled water. In order to calculate the volume of distilled water required a small amount of the titania (P25-Degussa) powder support was subjected to Brunauer-Emmett-Teller (BET) analysis in order to determine the pore volume, which was found to be 0.5ml/g. A solution containing this metal salt was then added to a calculated mass of titanium oxide in increments of a few drops with sufficient mixing between drops. This resulted in the formation of slurry which was dried in an oven at 110^0C for 24 hours in order to evaporate the water.[1] After 24 hours the catalysts were allowed to cool down to room temperature and ground until fine with

a pestle and mortar and stored in sample vials. The scheme below (**Figure 3.1**) illustrates the catalyst preparation method.

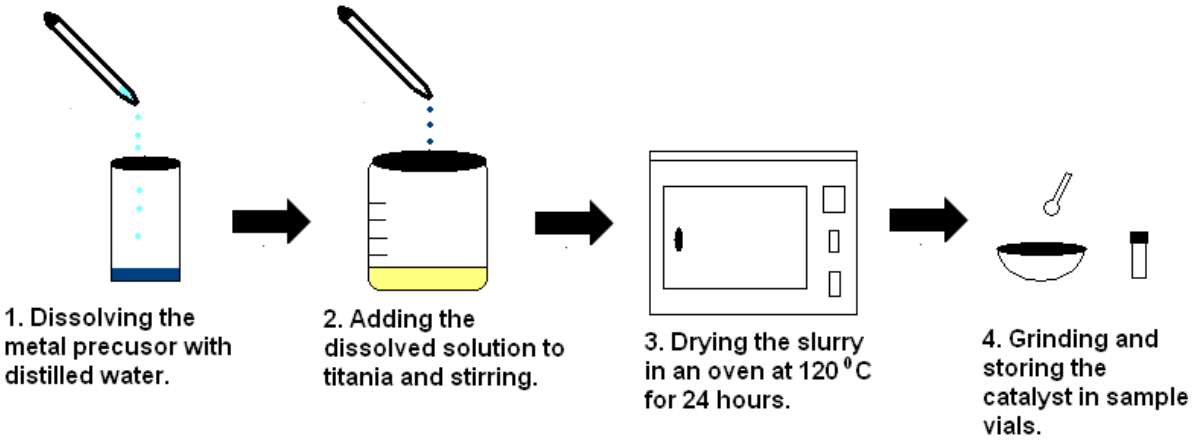


Figure 3.1: Flow diagram illustrating how the uncalcined catalysts were prepared.

3.2.2. Preparation of the Ru/TiO_2 and Pd/TiO_2 catalysts by the deposition-precipitation method.

To prepare the Ru/TiO_2 and Pd/TiO_2 catalysts with metal loadings of 1wt%, 3wt% and 5wt% by the deposition-precipitation method, the corresponding $RuCl_3.3H_2O$ and $Pd(NO_3)_2.2H_2O$ precursor salts were dissolved in a calculated volume of distilled water in order to obtain a 0.005 M aqueous solution. A calculated amount of titania (P25-Degussa) was added to the 0.005 M aqueous solution which contained the required metal percentage with respect to the support.[2] The resulting solution (**Figure 3.2**) was heated to 70^0C under stirring and maintained at this temperature while a 0.25 M Na_2CO_3 solution was added drop wise until a pH of 10 was reached.[2] This solution was further maintained at this temperature (70^0C) for 1 hour under stirring in order to precipitate the metal hydroxide on the surface of the support.[2]

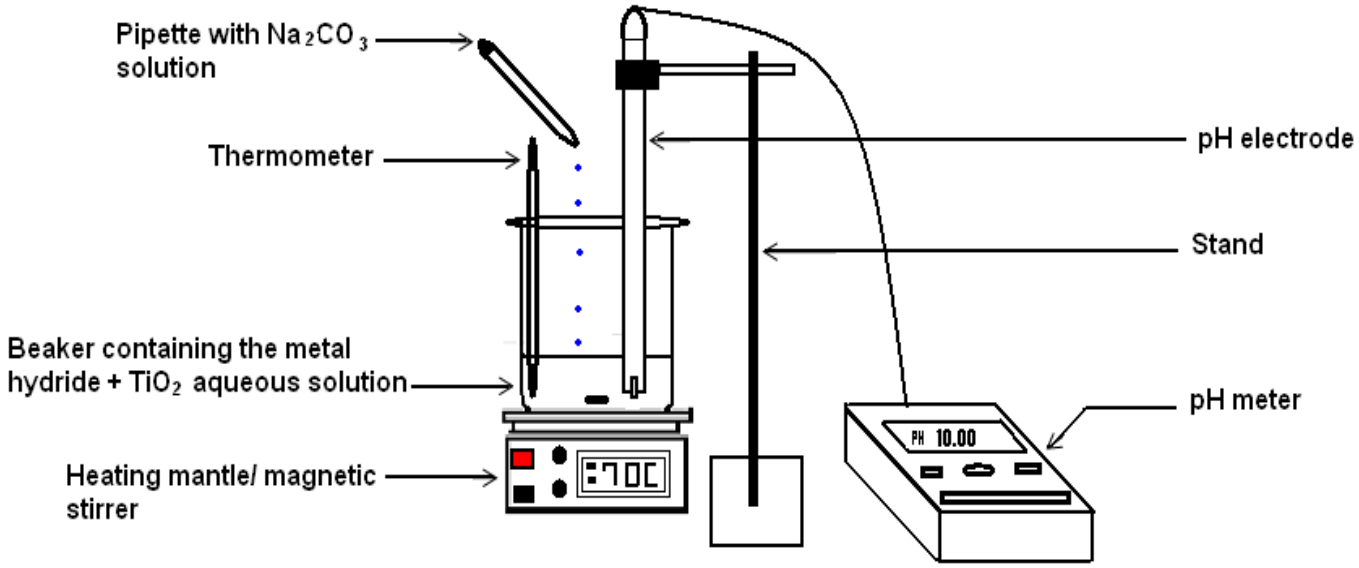


Figure 3.2: Set-up used for the preparation of the Ru/TiO_2 and Pd/TiO_2 catalysts by the deposition-precipitation method.

The resulting solid was separated by filtration and washed four times with distilled water. Then the filtered and washed solid was placed into a round bottom flask which was connected to a high vacuum system.[2] The solid was then vacuum-dried for 20 hours at room temperature.[2] After 20 hours the dried solid was transferred to a crucible and ground until fine. The crucible which contained the fine powder was placed into a calcination oven and calcined. The calcination oven was set to ramp at a heating rate of 10 ^{0}C/min until 400 ^{0}C and then held at this temperature for 5 hours. The sample was then allowed to cool down to room temperature. The final products were stored in sample vials and subjected to different characterization methods.

3.2.3. Preparation of the catalysts by the wet-incipient method followed by calcination.

The preparation of the calcined Ru/TiO_2 and Pd/TiO_2 catalysts is similar to the one used in section **3.3.1.** with the only difference being that the catalyst were calcined at 400 ^{0}C for 5 hours

after they were dried in the oven.[3] The scheme (**Figure 3.3**) below aims to illustrates the preparation method.

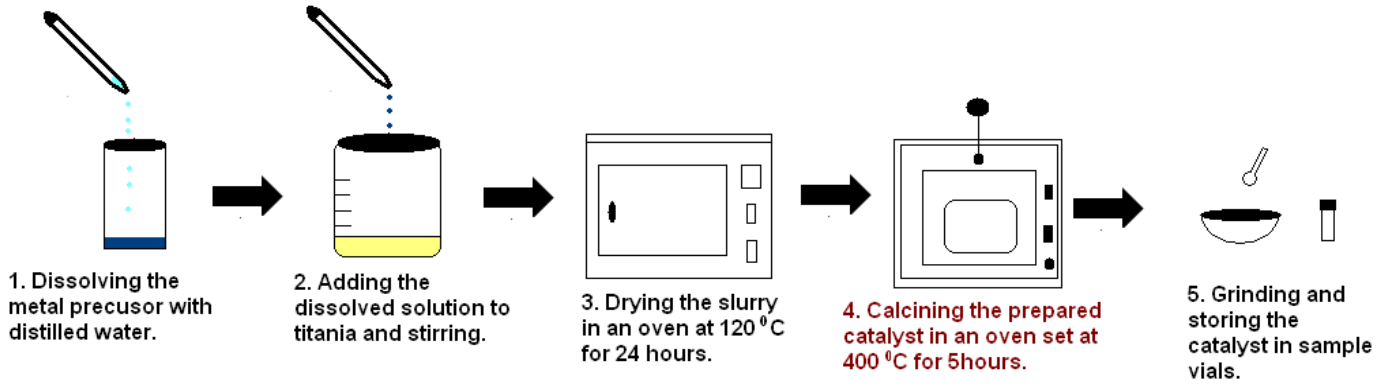


Figure 3.3: Schematic of the preparation of the calcined catalysts.

3.2.4. Preparation of the 5wt% Ru/TiO_2 uncalcined catalyst with 1/2wt% of the Cl^- ion.

A calculated amount of $RuCl_3.3H_2O$ which would correspond to 5wt% with respect to the support was dissolved in the calculated volume of distilled water. To this solution was added NH_4Cl (0.5wt% with respect to the support) and the solution was stirred. This solution was then added to a weighed amount of the titania powder with thorough mixing. The dark green slurry which was obtained was dried in an oven set at 110^0C for 24 hours.[1] After drying the catalyst was not calcined but was finely ground and subjected to Temperature Programmed Reduction (TPR) analysis.

3.3. Catalyst characterization procedures

3.3.1. Brunauer-Emmett-Teller (BET) analysis:

The BET analysis is a very important technique for determining the physicochemical properties of catalysts such as pore volume, pore diameter and the very important surface area of a catalyst. In order to understand the behavior of a catalyst one needs to know these physicochemical properties. During the BET analysis approximately 0.2 g samples were degassed in a Micromeritics Flow Prep 060 sample degas system (**Figure 3.4**), under nitrogen for 4 hours at 150 ^{0}C.The samples were then cooled to room temperature under a flow of nitrogen.



Figure 3.4: Picture of the Micromeritics Flow Prep 060 sample degas system.

The physicochemical properties such as the BET surface area, pore volume and the pore size distribution of the sample were then determined by the N_2 adsorption/desorption according to the BET method using a Micromeritics Tristar, surface area and porosity analyzer (**Figure 3.5**).



Figure 3.5: Picture of the Micromeritics Tristar surface area and porosity analyzer.

3.3.2. Temperature Programmed Reduction (TPR) analysis:

In order to establish the reducibility of the catalyst, TPR analysis was performed. About 0.1 g of sample was loaded into a U-shaped quartz tube. This tube was then connected to the Micromeritics Autochem II chemisorption analyzer system (**Figure 3.6**) and a reducing gas containing 5% H_2 in argon was passed over the sample at a flow rate of 50ml/min. A heating rate of 10^0C/min was used to raise the temperature to 800^0C.The TPR profile was collected from a PC program (Clarity) and the reduction temperature determined.



Figure 3.6: Picture of the Micromeritics Autochem II chemisorptions analyzer system.

The TPR profile of the Rh/TiO_2 and Pt/TiO_2 catalysts could not be obtained by this procedure. The two catalysts had to be degassed in argon for 2 hours at 150 ^{0}C in order to remove any moisture that might have been present in the catalysts. Then they were allowed to cool to room temperature and reduced with the 5% H_2 in argon reducing gas. However this also did not lead to

useful TPR profiles so the degassing temperature was raised to 200 ^{0}C. Again this did not prove to be successful. As a last attempt the catalysts were first oxidized in air at 150 ^{0}C for 2 hours, then cooled and reduced. This attempt was also unsuccessful.

3.3.3. Transmission Electron Microscopy (TEM):

In order to determine the particle sizes, catalyst morphology, catalyst microstructure and distribution of particles on a support the Tecnai G^2 Spirit TEM (**Figure 3.7)** was used. Prior to TEM analysis the samples were prepared by dissolving them in methanol and ultrasonically mixing them in a warm bath for about 10 minutes. A drop of the sample was then transferred to a carbon coated copper grid on a sheet of filter paper. The sample was allowed to dry after which the copper grid was loaded on to a single tilt holder which was thoroughly checked for any debris under a microscope. The holder was then inserted into the Tecnai G^2 spirit TEM and the instrument corrected for astigmatism and the eucentric height position. Due to the small size of the particles, analysis was conducted between magnifications of 23,000 X to about 110,000 X.



Figure 3.7: Picture of the Tecnai G^2 spirit TEM instrument.

3.3.4. Powder Powder X-ray diffraction (PXRD):

In order to determine the phase of the support and the crystallite sizes of the metals PXRD was used. This was performed on all of the prepared catalysts. During the analysis about 1 g of sample was compressed in a sample holder and then inserted into the instrument. The PXRD instrument that was for analyzing the samples and to obtain the patterns was the D2 Bruker Phaser (**Figure 3.8**) instrument.

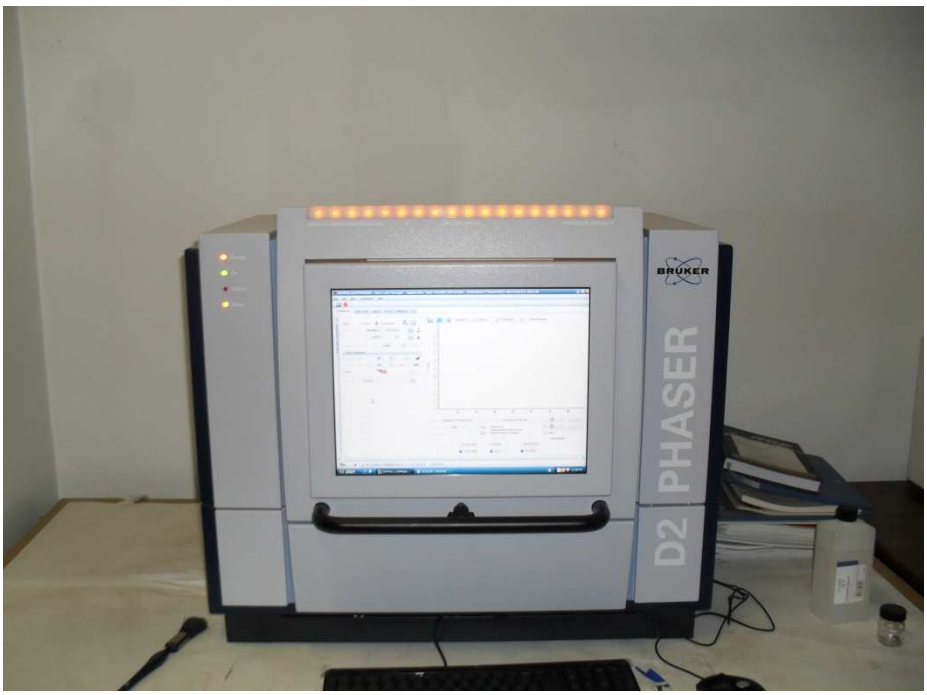


Figure 3.8: Picture of the D2 Bruker Phaser Powder X-ray diffraction instrument.

3.4. Catalysts performance test

3.4.1: Set up for the catalyst performance test.

The catalytic performance of the catalysts was analyzed with the use of the set up which is illustrated in **Figure 3.9.** Assembling the test unit was part of the project requirement. As can be noted from **Figure 3.9** the catalyst analysis system consists of two gas cylinders with one of them being H_2 and the other being either a mixture of CO and H_2, CO_2 and H_2 or a mixture of CO, CO_2 and H_2 depending on the analysis objective of the reaction. All of the cylinders were purchased from AFROX and were of ultra high purity. A two way valve was connected to the stainless steel tubing coming from the two cylinders in order to make it possible to switch between the gas cylinders. Thus if only hydrogen was required then the two way valve would be switched towards the hydrogen cylinder and the contents of the other cylinder would not be allowed to flow. In order to permit or prevent gas flow a shut-off valve was connected to the stainless steel tubing coming from the two way valve. This valve would be used if leaks were to occur in the test unit. The flow controlling valve was used to adjust the flow rate as the flow would be different for reduction and for the actual catalytic run. The thermocouple, temperature controller and furnace were employed to control the reaction temperature in the reactor. A steel reactor which was 25 cm in length and 0.6 cm in diameter was used and a small steel rod (14 cm in length and 0.4 cm in diameter) was inserted into the reactor to ensure that the catalyst rested in the center of the reactor. During the loading of the catalyst the rod was inserted first into the reactor then quartz wool was placed on top followed by the catalyst. The thermocouple was then inserted in such a way that its tip was located in the center of the reactor. This ensured that only the center temperature where the catalyst rested was measured. A knock-out point was connected to trap all of the water produced in the methanation reaction. Condensation of water still occurred in the stainless steel tubing which interfered with the Gas Chromatograph (GC) detectors; so heating tapes set to 150^0C and covered with quartz wool for insulation were used to prevent this. A gas chromatograph operating with a thermal conductivity detector (TCD-GC) with argon as carrier gas was used to detect H_2, CO, CO_2 and CH_4. A gas chromatograph with a

flame ionization detector (FID-GC) and nitrogen as carrier gas was used to detect CH_4 and any other higher hydrocarbons that might have formed. The gas flow rate was measured with the use of the flow meter.

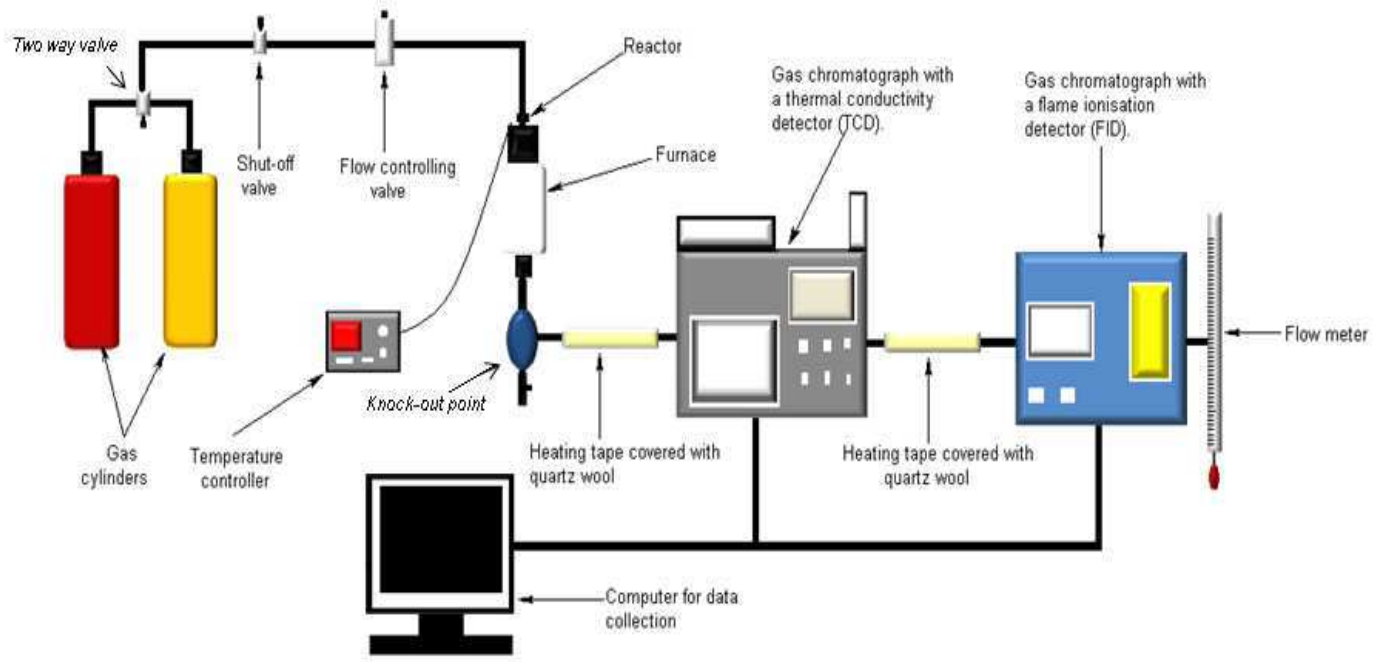


Figure 3.9: Schematic representation of the set-up used for the catalytic performance tests.

3.4.2: Catalyst performance test.

3.4.2.1. Blank runs

Prior to every set of catalytic runs a blank run was performed. In this run the gas was passed through the catalytic test unit without any catalyst present to convert any gas, which was then detected with the TCD-GC. This would aid in the calculations of the conversions of CO and CO_2. For the CO methanation reaction the 8% CO and 92% H_2 composition gas (**Figure 3.10**) was used and for the methanation of CO_2 the 25% CO_2 and 75% H_2 gas (**Figure 3.11**) mixture was used. The selective methanation of CO in a CO_2 and H_2 gas mixture (8% CO, 23% CO_2 and

69% H_2) (**Figure 3.12**) was also determined. In order to determine the yield of methane from the proposed reactions a calibration gas composed of 20% CO, 20% CO_2, 20% N_2, 20% H_2 and 20% CH_4 was passed through the FID-GC.

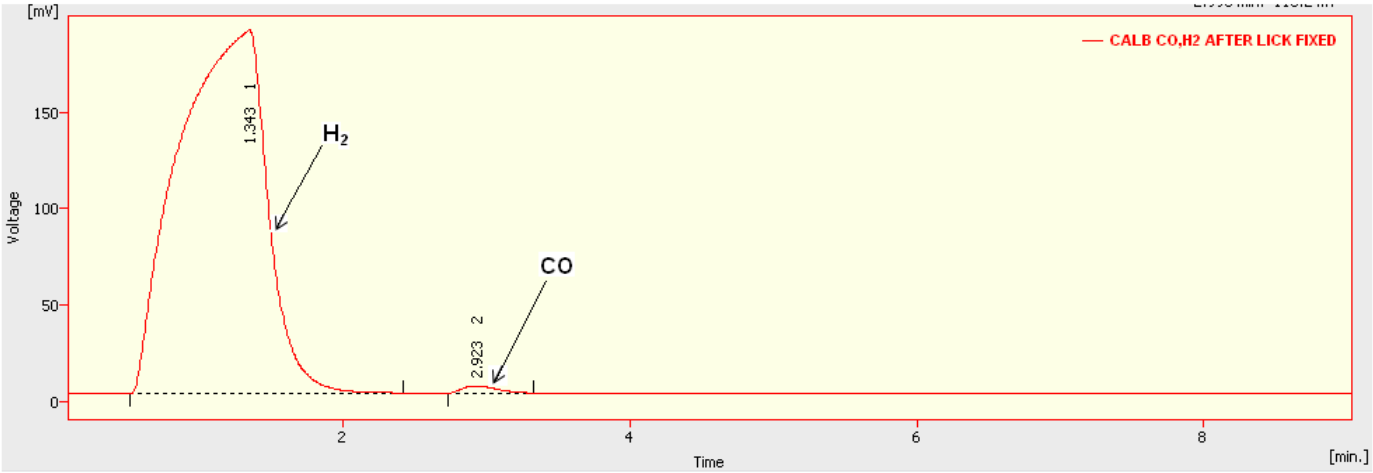


Figure 3.10: Blank run for the CO methanation reaction.

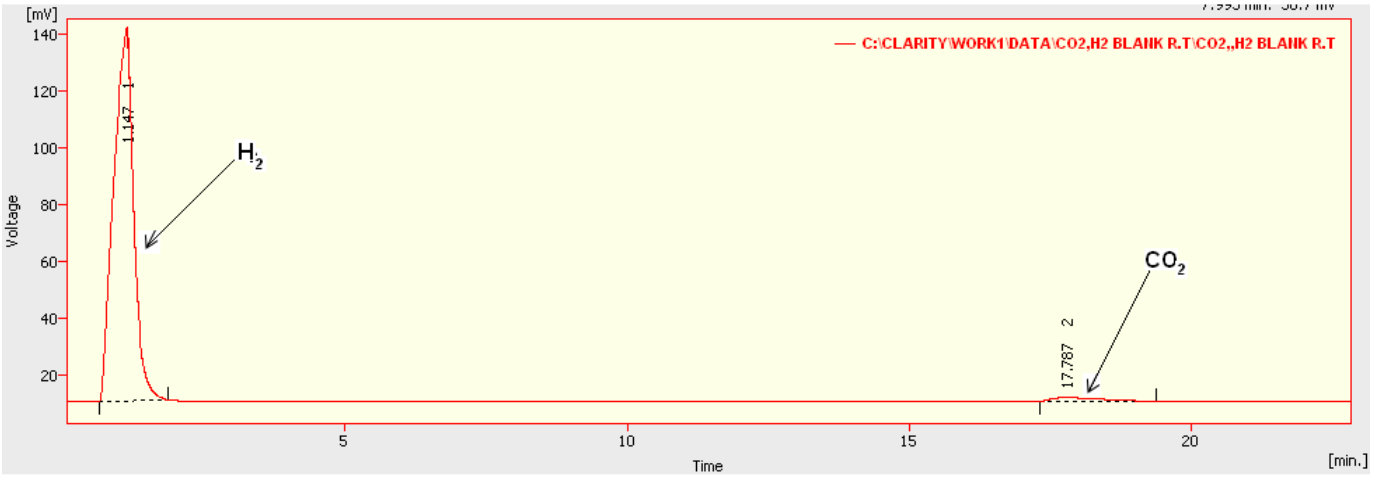


Figure 3.11: Blank run for the CO_2 methanation reaction.

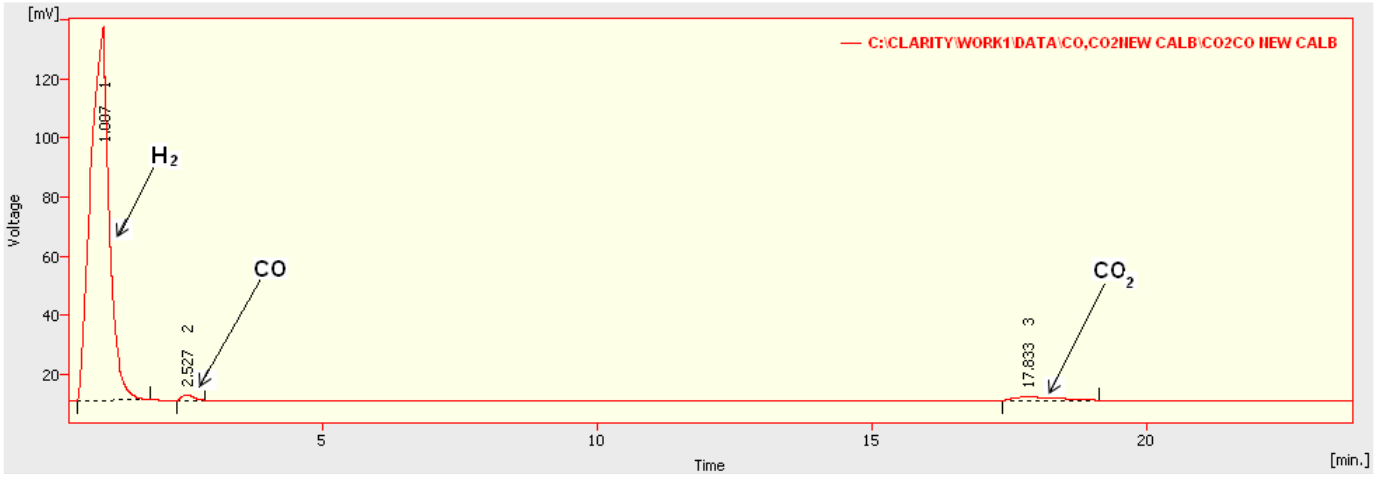


Figure 3.12: Blank run for the selective methanation of CO in a CO_2 and H_2 gas mixture.

3.4.2.2. Actual catalytic runs

In the actual experiment 0.15 g of fresh catalyst was placed into a steel reactor and reduced in situ with H_2 at a flow rate of 60 ml/min for a period of 2 hours at 400^0C.[4] The reactor was then set to 480 ^{0}C under a flow of H_2 and when it reached and stabilized at this temperature the flow was switched to the reaction mixture with the various composition described above. The gases were used at a flow rate of 200 ml/min for 8 hours.[4] This procedure was repeated at different temperatures (180 ^{0}C, 240 ^{0}C , 300 ^{0}C, 360 ^{0}C, and 420 ^{0}C) with fresh catalyst each time. All of the prepared catalysts were analysed using this procedure.

3.4.2.3. Calculations used to determine conversions and yields

Using the data obtained from the blank runs and the actual catalytic runs, CO conversions in the CO methanation reaction, CO_2 conversions in the CO_2 reaction and CO conversion in the selective methanation of CO were calculated.

Conversions of CO in the CO methanation reaction and CO/CO_2 methanation reaction:

$$= (((\%CO\ (in) - \%\ CO\ (out))/(\%\ CO\ (in))) \times 100\%$$

Conversions of CO_2 in the CO methanation reaction and CO/CO2 methanation reaction:

$$= \left(\frac{([(\%CO]_2\ (in) - \%CO_2(out))}{\%CO_2\ (in)}\right) \times 100\%$$

Percentage yield of CO from the CO_2 methanation reaction

$$= \left(\frac{\%CO\ (out)}{\%CO_2(in)}\right) \times 100\%$$

R value to compare the selectivity of CO methanation with CO_2 methanation

$$\mathbf{R} = \frac{\%CO\ conversion}{\%CO_2\ conversion} \rightarrow \infty$$

Formation of CH_4 from the CO/CO_2 methanation reaction

$$= \left(\frac{\%\ CH_4\ (out)}{\%CO\ (in)}\right) \times 100\%$$

3.5. References

1. P. Panagiotopoulou, D. I. Kondarides and X. E. Verykios, Applied Catalysis A: General, 2008, 344, 45-54.
2. W. Shen,M. Okumura, Y. Matsumura, M. Haruta, Applied Catalysis A: General, 2001, 213,225-232.
3. S. Corradini, G.G. Lenzi, M.K. Lenzi, C.M.F. Soares and O.A.A. Santos, Journal of Non-crystalline solids, 354, 4865-4870.
4. P. Panagiotopoulou, D.I. Kondarides, X.E. Verykios, Applied Catalysis B: Environmental, 2009, 88,470-478.
5. Y.H. Kim, E. D. Park, H.C. Lee and D. Lee, Applied Catalysis A: General, 2009, 366, 363-369.

Chapter 4
Results and discussion

4.1. Introduction

This chapter deals with the results which were obtained in this study. The results which were obtained from the characterization of the prepared catalysts are reported first, followed by the results obtained from the catalytic performance tests.

4.2. Catalyst characterization results

4.2.1. Powder X-ray diffraction (PXRD) analysis of the Ru/TiO_2 catalysts.

In order to determine the crystalline phases of the synthesized Ru catalysts they were studied by the PXRD technique. The PXRD pattern which was obtained for the 5 wt% Ru/TiO_2 catalysts is displayed in **Figure 4.1**. The PXRD pattern revealed the presence of both anatase and rutile phases with the anatase phase being the prevailing crystallographic phase. The RuO_2 phase was detected at $2\theta = 28^o$ and 35^o and these peaks have been indexed to the RuO_2 (110) and RuO_2 (101) planes respectively in accordance with the literature.[1] This means that both after drying and calcination the $RuCl_3.3H_2O$ precursor decomposes into RuO_2. The addition of ruthenium did not alter the PXRD pattern of the TiO_2 support .The RuO_2 peaks which occurs as shoulders at 28^o and 35^o give some indication of the particle sizes for the three catalysts since the peak widths vary for the three different samples. However the particle sizes of the calcined catalyst and the deposition-precipitation catalysts could not be determined from the PXRD patterns due to the overlapping of the peaks. The Ru/TiO_2 uncalcined catalyst seems to have very small particles

because the RuO_2 peak cannot be observed for this catalyst. Thus the RuO_2 on the uncalcined Ru/TiO_2 catalyst is well dispersed on the TiO_2 support.[2]

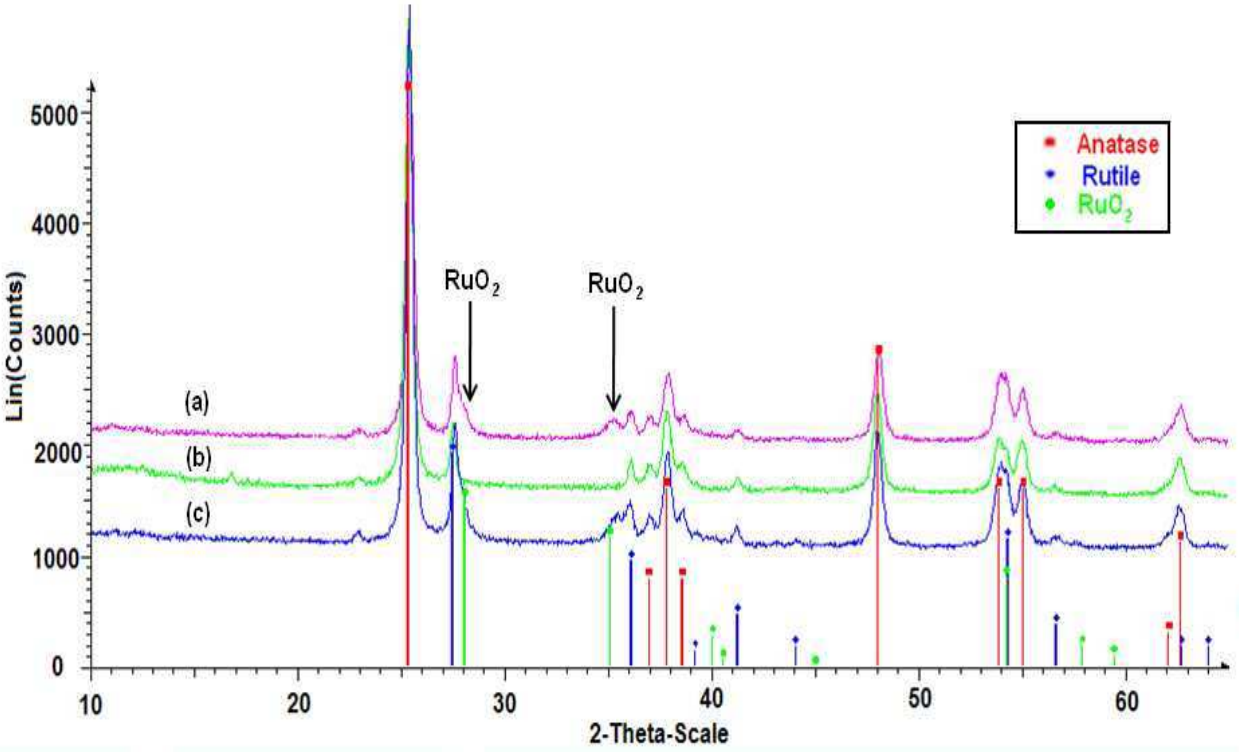


Figure 4.1: PXRD pattern of the three 5 wt% Ru/TiO_2 catalysts. **(a)** Prepared by wetness-incipient method, dried at 110 ^{0}C and calcined at 400 ^{0}C for 5 hours **(b)** Prepared by wetness-incipient method, dried at 110 ^{0}C and not calcined **(c)** prepared by deposition-precipitation method and calcined at 400 ^{0}C for 5 hours.

Since the RuO_2 peaks overlapped with the rutile peak an attempt was made to reduce the Ru/TiO_2 catalysts in hydrogen so that the RuO_2 could be converted into Ru metal. The PXRD patterns which were obtained are presented in **Figure 4.2**. The RuO_2 peaks are no longer present at at $2\theta = 28^o$ and 35^o but have been converted into Ru peaks which are present at $2\theta = 38^o$ and 43^o. These PXRD peaks were used to determine the average crystallite size (d) of the Ru catalysts with the use of the Scherrer equation (Equation (**4.1**)):

$$d = \frac{0.9\lambda}{\sqrt{Bm^2 - Bs^2}\cos\theta}, \qquad (4.1)$$

where λ is the wavelength of X-ray sources, θ is the Bragg angle and Bm,Bs represent the peak widths of sample and standard in radians. Bs also compensates for instrumental broadening. The Ru crystallite size of the calcined catalyst was found to be 6 nm, the deposition-precipitation catalyst had a Ru crystallite size of 9 nm and the uncalcined catalysts crystallite size could not be determined by PXRD as the particles were too small.

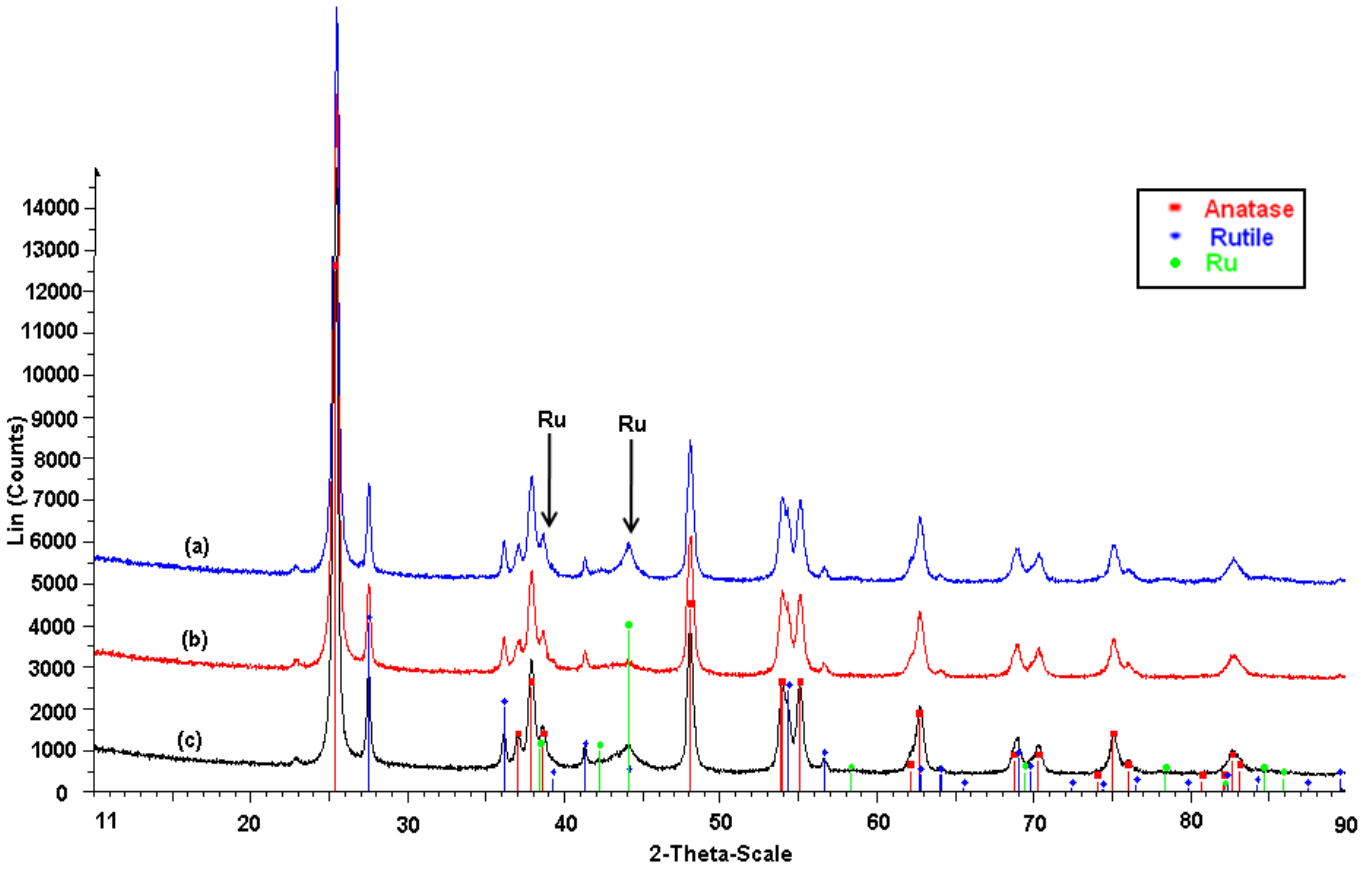


Figure 4.2: PXRD pattern of the reduced 5 wt% Ru/TiO_2 catalysts. **(a)** Prepared by wetness-incipient method, dried at 110 ^{0}C and calcined at 400 ^{0}C for 5 hours **(b)** Prepared by wetness-incipient method, dried at 110 ^{0}C and not calcined **(c)** prepared by deposition-precipitation method and calcined at 400 ^{0}C for 5 hours.

4.2.2. Brunauer-Emmett-Teller (BET) analysis of the Ru/TiO_2 catalysts

In order to obtain the surface area and pore sizes of the TiO_2 supported Ru catalysts, the BET technique was employed. The results are tabulated in **Table 4.1** below. The BET surface area and pore volume of the TiO_2 support was measured to be 49 m^2/g and 0.20 cm^3/g respectively. This was used as a reference to compare the increase or decrease in surface area and pore volume of the Ru/TiO_2 catalysts.

Table 4.1: BET surface area and pore volume of the TiO_2 supported Ru catalysts.

	BET surface area (m^2/g)	Pore volume (cm^3/g)
TiO_2(Degussa,P-25)	49	0.20
$1\%Ru/TiO_2$ [a]	44	0.34
$1\%Ru/TiO_2$ [b]	47	0.33
$1\%Ru/TiO_2$ [c]	45	0.49
$3\%Ru/TiO_2$ [a]	44	0.34
$3\%Ru/TiO_2$ [b]	49	0.31
$3\%Ru/TiO_2$ [c]	42	0.34
$5\%Ru/TiO_2$ [a]	43	0.27
$5\%Ru/TiO_2$ [b]	43	0.29
$5\%Ru/TiO_2$ [c]	41	0.44

[a] Prepared by wetness-incipient method dried at 110^0C for 24 hours and calcined at 400^0C for 5 hours , [b] prepared by wetness-incipient method dried at 110^0C for 24 hours, [c] prepared by deposition-precipitation method, vacuum dried for 20 hours and calcined at 400^0C for 5 hours.

From **Table 4.1** it can be noted that the catalysts display a decrease in surface area and an increase in pore volume as compared to the untreated TiO_2 support. According to Babu *et. al.*[3] this could be due to the occupation of the TiO_2 pores by larger Ru particles. The untreated TiO_2

displays a slightly lower pore volume because the pores are unoccupied and after metal loading some of the pores become occupied, preferably the smaller pores, and this leads to an average increase in pore volume since the smaller pores are unoccupied as compared to the untreated TiO_2. In terms of particle size, sufficient information could not be extracted from the BET results and thus Transmission Electron Microscopy was used for this purpose (**Section 4.2.3**).

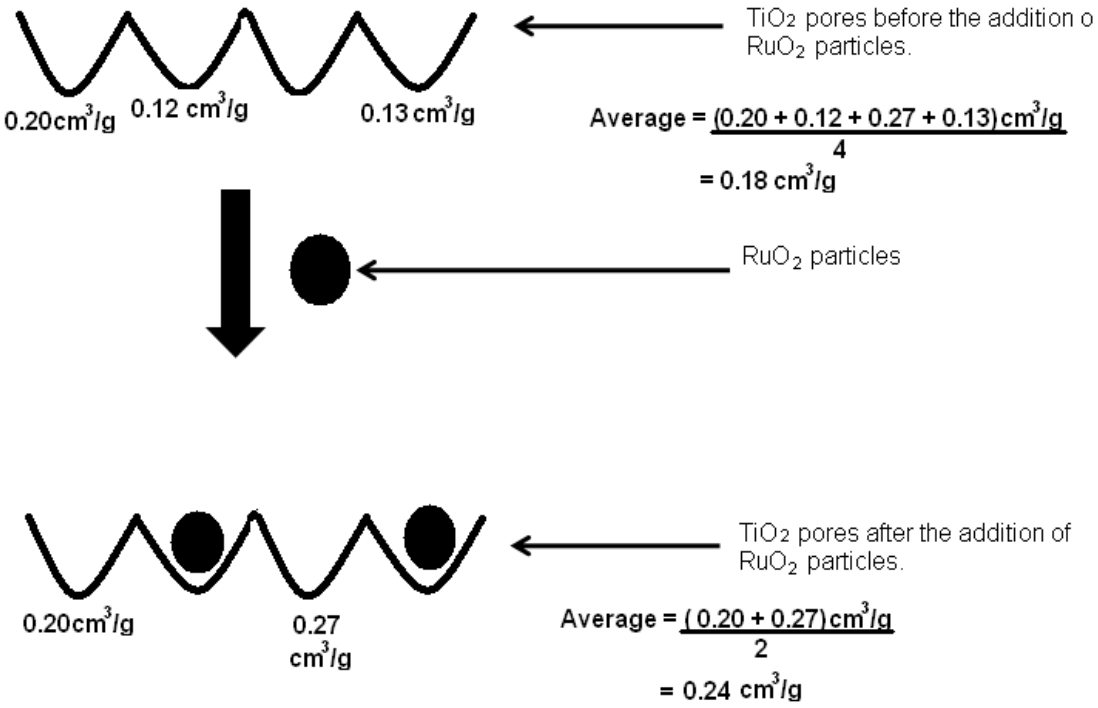


Figure 4.3: Example of how the pore volume increases.

4.2.3. Transmission Electron Microscopy (TEM) analysis of the Ru/TiO_2 catalysts

After the Ru/TiO_2 catalysts were prepared they were analysed using TEM and **Figure 4.4** displays the TEM images which were obtained. It can be noted that only TiO_2 particles can be seen and the Ru clusters cannot be observed. In order to obtain the size of Ru metal particles the catalysts were reduced in hydrogen and then analysed with TEM. The images are presented in **Figure 4.5, 4.6** and **4.7**.

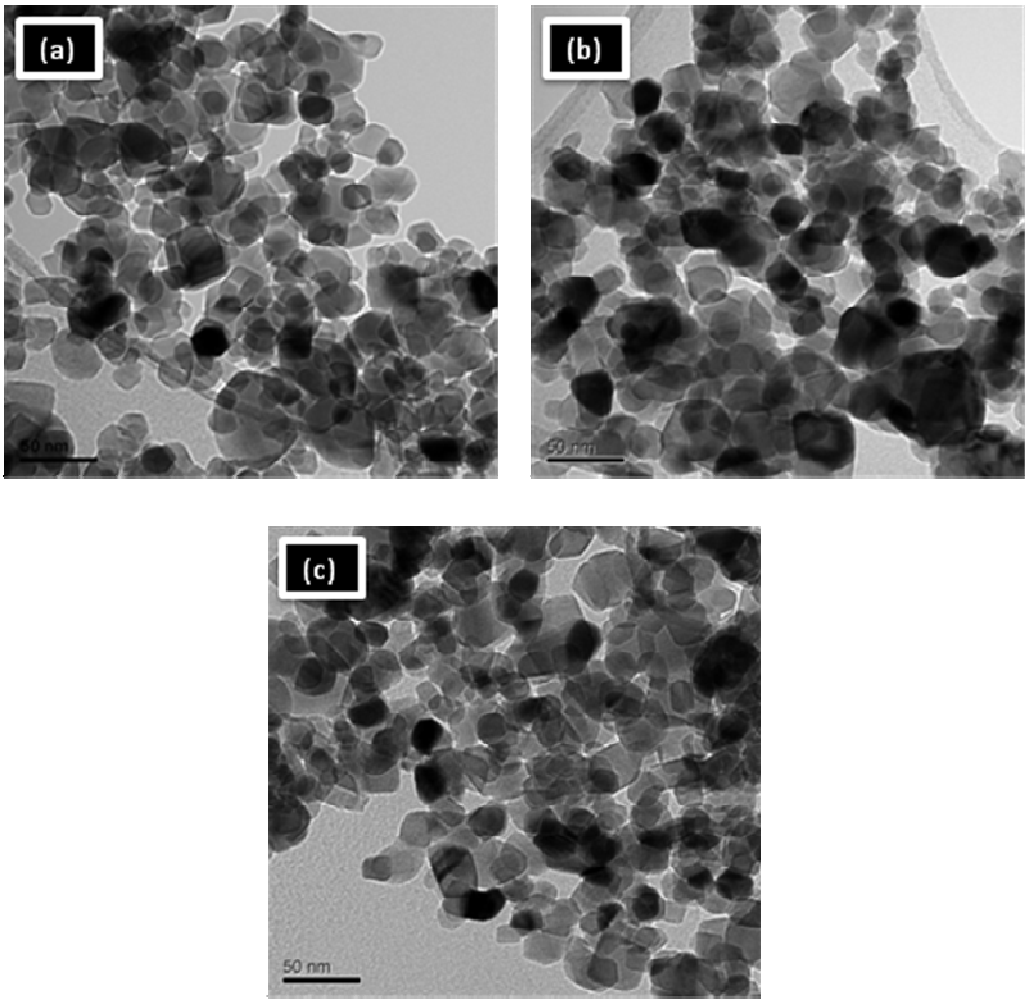


Figure 4.4: TEM images of the 5wt% Ru/TiO_2 catalysts before they were reduced.**(a)** dried at 110^{0}C for 24 hours and calcined at 400 ^{0}C for 5 hours,**(b)** prepared by deposition-precipitation method, vacuum dried for 20 hours and calcined at 400 ^{0}C for 5 hours and **(c)** dried at 110 ^{0}C for 24 hours.

4.2.3.1. TEM analysis of the calcined 5% Ru/TiO_2 catalyst

The TEM image which was obtained for the calcined 5 wt% Ru/TiO_2 catalyst after it was reduced is presented in **Figure 4.5a** below. From this image it can be noted that the TiO_2 support is made up of aggregates of three dimensional particles of TiO_2. The Ru particles appear to be deposited on these TiO_2 particles. Due to the heat effect caused by calcination some of the Ru particles seem to form agglomerates however individual Ru can still be identified. **Figure 4.5b** shows the particle size distribution which was obtained by analyzing 100 particles. From this it was noted that the particles vary in width from 1 nm to 7 nm with most of the particles having a width between 2 nm and 5 nm with the average particle width being 4 nm. This corresponds to the calculated crystallite size from PXRD. Shen et. al.,[4] found the particles to vary in width from 1 nm to 14 nm with the majority being between 1 nm and 6 nm leading to an average particle size of 4,1 nm. They looked at a 5wt% Ru/TiO_2 catalyst which was calcined at 350 ^{0}C and reduced in hydrogen before TEM analysis. Streethawong et.al. [1] found the particle size of RuO_2 particles to be between 2-3 nm, studying a 1 wt% Ru/TiO_2 catalyst which was dried at 80 ^{0}C and calcined at 500 ^{0}C.

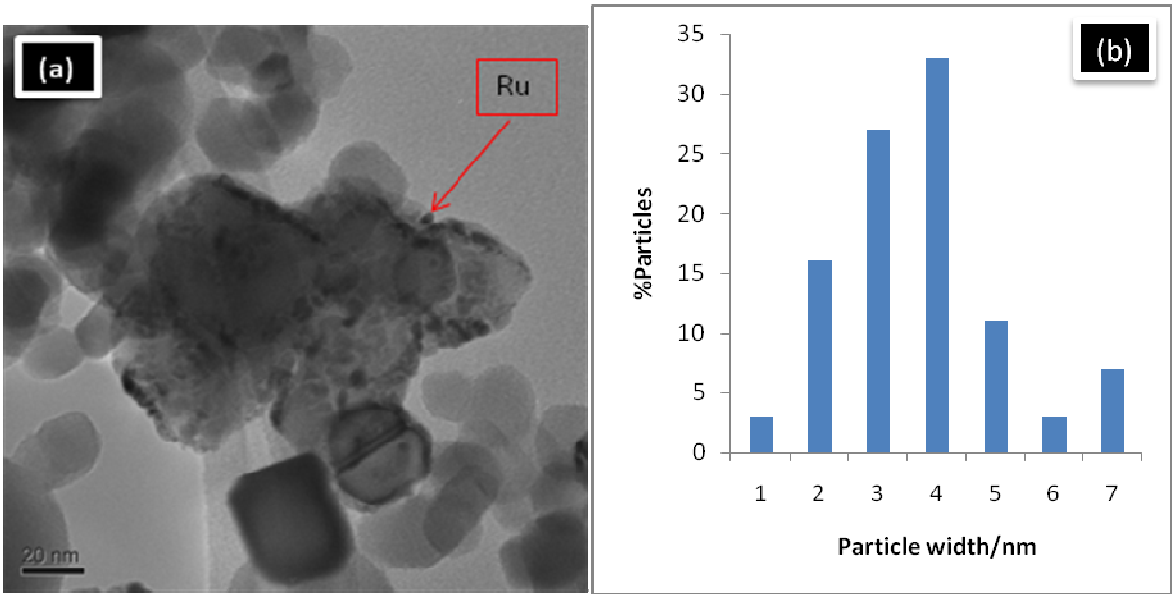


Figure 4.5: TEM image of the 5 wt% Ru/TiO_2 catalyst which was calcined at 400 ^{0}C for 5 hours.

4.2.3.2. TEM analysis of the deposition-precipitation 5% Ru/TiO_2 catalyst.

TEM was also used to analyze the 5% Ru/TiO_2 catalyst which was prepared by the deposition-precipitation method and reduced prior to TEM analysis. **Figure 4.6a** illustrates that most of the particles form aggregates on the transparent TiO_2 support. **Figure 4.6b** represents the particle width distribution of the particles. From this it can be noted that the particles range in width from 2 nm to 9 nm. The majority of the particles have a particle width between 4 nm to 6 nm and the average particle width was found to be 6 nm. This is consistent with the crystallite size calculated from PXRD analysis. V. Balek et al.,[5] examined a 75% Ru metal and 25% TiO_2 catalyst which was prepared by deposition-precipitation method and subjected to heat treatment until 800 ^{0}C and found particles with an average size of 30-50 nm. So this could mean that preparation methods have a huge effect on the characteristics of a catalyst such as particle size and microstructure as this catalyst has slightly larger particles as compared with the calcined 5 wt% calcined and uncalcined Ru/TiO_2 catalysts.

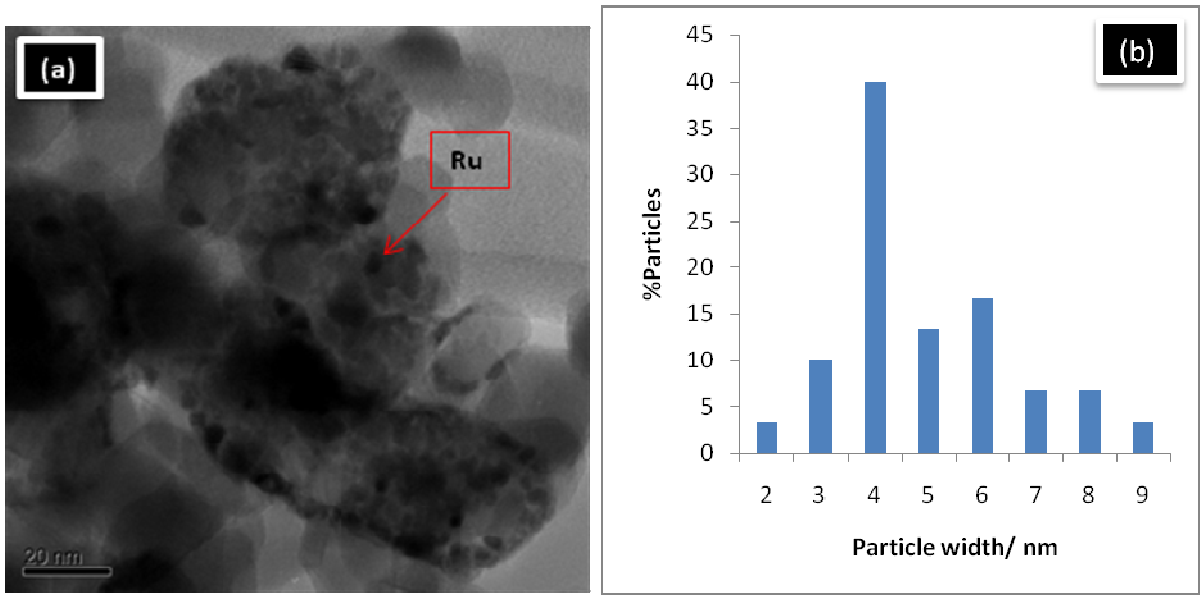


Figure 4.6: TEM image of the 5 wt% Ru/TiO_2 catalyst which was prepared by the deposition-precipitation method and calcined at 400 ^{0}C for 5 hours.

4.2.3.3. TEM analysis of the uncalcined 5%Ru/TiO_2 catalyst.

The TEM image which was obtained from the analysis of the 5wt% Ru/TiO_2 catalyst previously dried at 110 ^{0}C and not calcined is presented in **Figure 4.7a** below. This image illustrates that after reduction the particles of the uncalcined 5wt% Ru/TiO_2 catalyst are very small as compared with those found with the other two differently prepared catalysts. In order to obtain **Figure 4.7b,** 100 particles were analyzed and the analysis shows the particle size distribution of the particles and from this it can be observed that most of the particles vary in width between 1.0 and 4.8 nm. The majority of the particles vary in width between 2.2 and 2.8 nm giving an average particle size of 2.9 nm. This corresponds to the particle size reported by Streethawong et.al,[1] even though they calcined their catalyst at 500 ^{0}C and analysed a 1wt% Ru/TiO_2 catalyst. This implies that drying the catalyst at 110 ^{0}C and not subjecting it to calcination could have led to smaller particles.

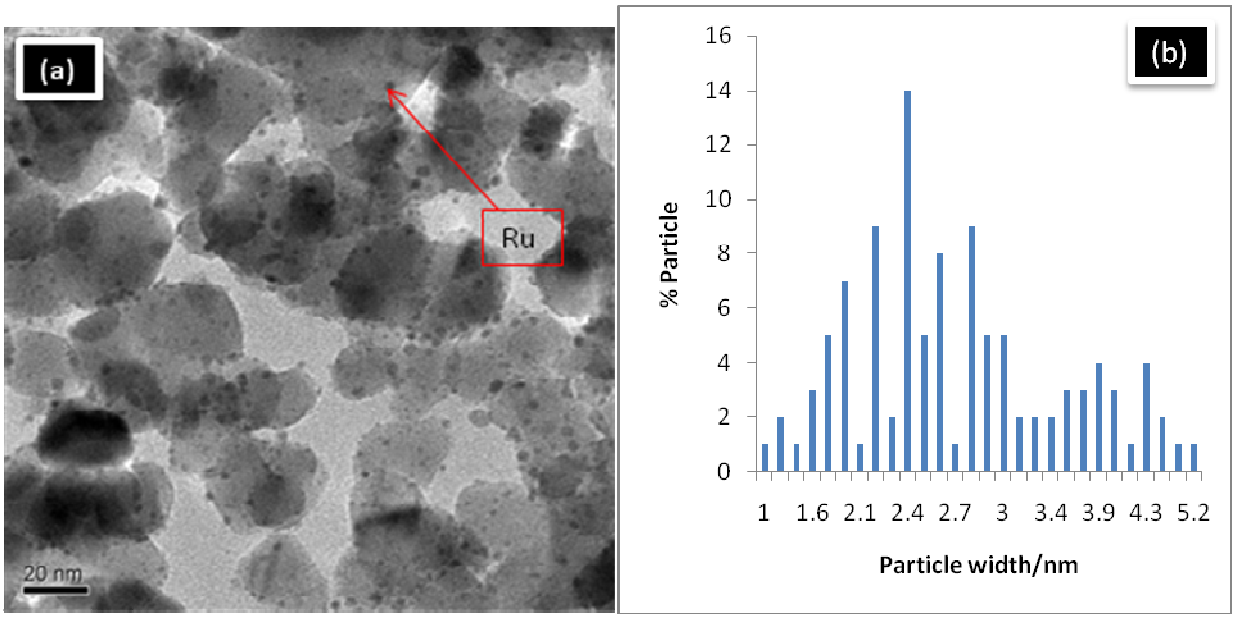


Figure 4.7: TEM image of the 5wt% Ru/TiO_2 catalyst which was dried at 110 ^{0}C and not subjected to calcination.

4.2.4. Temperature Programmed Reduction (TPR) analysis of the Ru/TiO_2 catalysts

4.2.4.1. TPR of the calcined Ru/TiO_2 catalysts

The TPR method allows one to study the reducibility of a catalyst. The results which were obtained from the TPR analysis of the calcined 1 wt%, 3 wt% and 5 wt% Ru/TiO_2 catalysts are presented in **Figure 4.8** below. The TPR profile shows a reduction peak with a maximum at about 220 ^{0}C which is due to the reduction of RuO_2 to Ru (Equation **(4.2)**).[2&6] According to Jinxiang et.al.,[7] alumina supported RuO_2 is reduced between 178-265 ^{0}C with a maximum at around 200 ^{0}C.This maximum can be shifted to higher temperatures depending on the amount of Ru used.

$$RuO_2 \longrightarrow Ru \qquad (4.2)$$

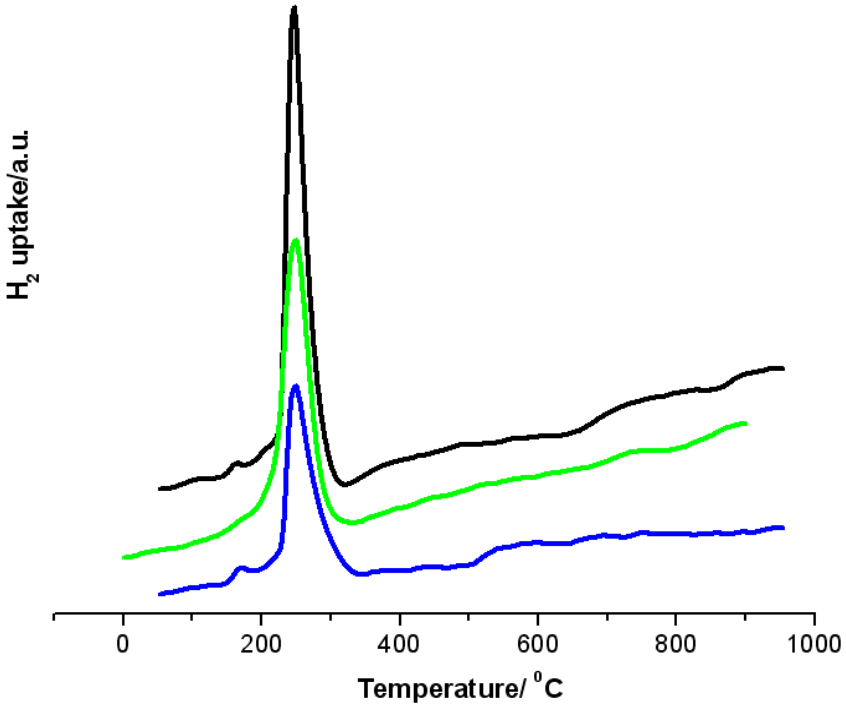


Figure 4.8: TPR profile of the Ru/TiO_2 catalysts calcined at 400 ^{0}C for 5 hours. **(a)** 5 wt% Ru/TiO_2,**(b)** 3 wt% Ru/TiO_2 and **(c)** 1 wt% Ru/TiO_2.

4.2.4.2. TPR of the Ru/TiO_2 catalysts which were prepared by the deposition-precipitation method.

The reducibility of the deposition-precipitation catalysts was also investigated by the TPR method and the TPR profiles are presented in **Figure 4.9**. This TPR profile is quite similar to the TPR profile in **Figure 4.8** implying that the two sets of catalyst prepared by different methods do not vary that much in reducibility. The reduction peak with a maximum at about 220 ^{0}C also represents the reduction of the RuO_2 oxides on the TiO_2 surface to the Ru metallic form. Just as in **Figure 4.8**, the extent of H_2 consumption decreases with decreasing metal loading.

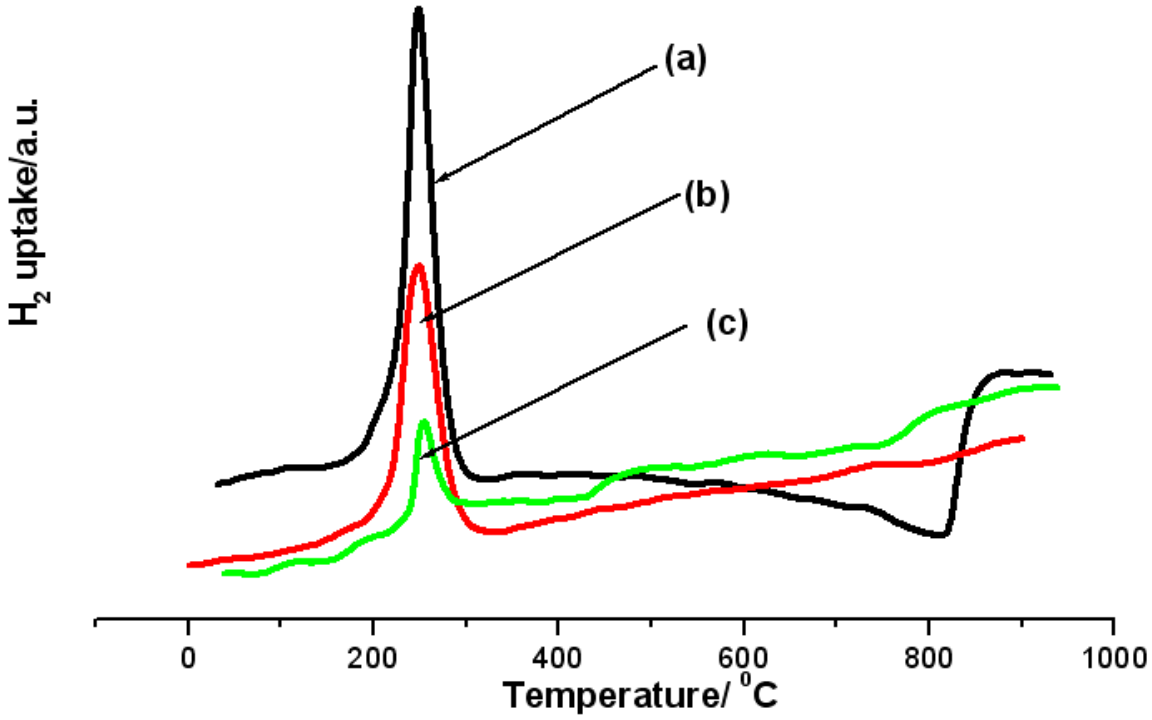


Figure 4.9: TPR profile of the Ru/TiO_2 catalysts prepared by the deposition-precipitation method and calcined at 400 ^{0}C for 5 hours. **(a)** 5 wt% Ru/TiO_2,**(b)** 3 wt% Ru/TiO_2 and **(c)** 1 wt% Ru/TiO_2.

4.2.4.3. TPR of the uncalcined Ru/TiO_2 catalysts

Figure 4.10 represents the TPR profile for the uncalcined Ru/TiO_2 catalysts. This TPR profile is quite different compared to the as it has a reduction peak with maximum at about 120 ^{0}C and not at 220 ^{0}C. This peak at 120 ^{0}C can be attributed to the reduction of $RuCl_3$ and not to the reduction of RuO_2 like the calcined and deposition-precipitation Ru/TiO_2 catalysts.[9] According to Pintar et.al. the $RuCl_3$ reduction peak occurs within the range of 0 – 200 ^{0}C. Pintar et.al., [9] investigated 1 wt% and 3 wt% Ru/TiO_2 catalysts which were prepared by the incipient-wetness impregnation method and not subjected to calcination. The TPR results in **Figure 4.10** also agree with the TPR results from Bond et.al.,[10] who investigated the reduction behavior of TiO_2 supported $RuCl_3$ catalysts which had not been calcined and found that the reduction of $RuCl_3$ begins at about 57 ^{0}C and the size of the TPR peak increases with increasing metal loading and thus the peak maxima also increases with increasing metal loading. The TPR profiles of the 3 wt% and 5 wt% uncalcined Ru/TiO_2 catalysts in **Figure 4.10** have slight shoulders. According to Bond et.al.,[10] this could mean that more than one type of $RuCl_3$ species are present i.e. automically dispersed micro-crystals might be present on the TiO_2 surface. In **Figure 4.10** another reduction peak with a maximum at about 330 ^{0}C is noted. Pintar *et.al.*[9] suggested that this peak could be due to the partial reduction of the TiO_2 support which is promoted by the presence of the Ru particles. The reason for this assumption is that they performed TPR analysis of the unloaded TiO_2 support and it revealed a reduction peak at about 300 ^{0}C which they assigned to the partial reduction of TiO_2. TPR analysis of the unloaded TiO_2 was conducted (not shown), however we did not observe a TiO_2 reduction peak. Due to this it was assumed that it is very unlikely that the 330 ^{0}C reduction peak could be due to TiO_2 reduction in our case.

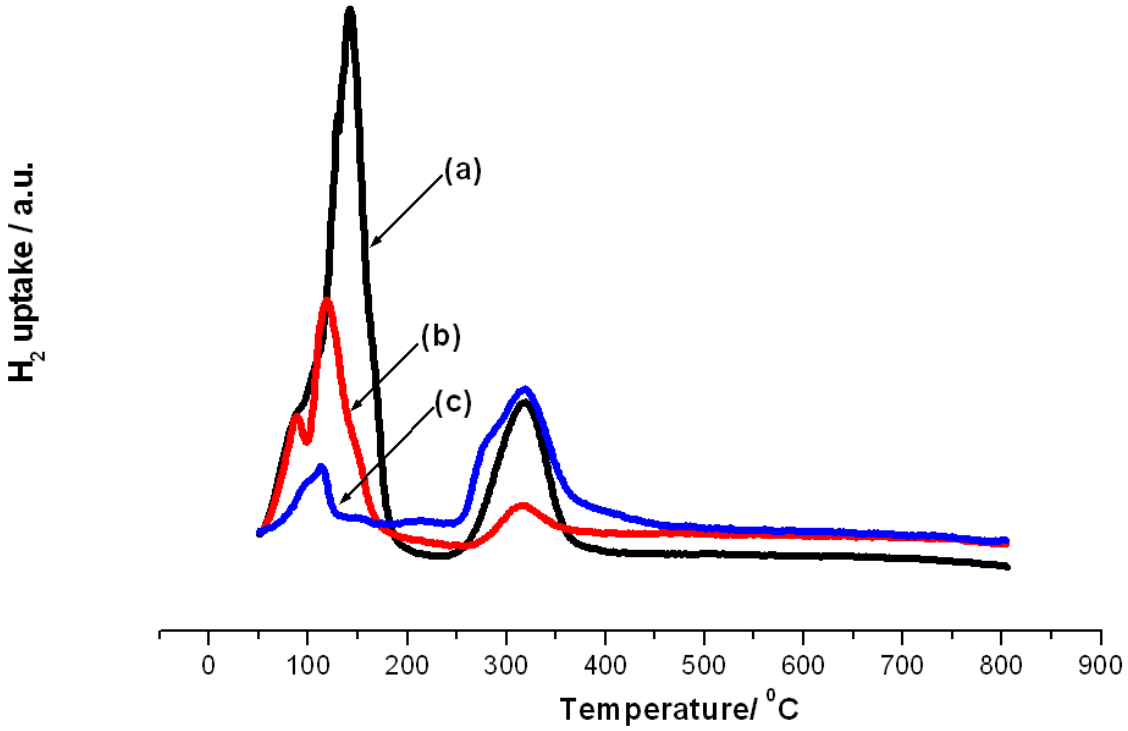


Figure 4.10: TPR profile of the Ru/TiO_2 catalysts prepared by the incipient wetness impregnation and not subjected to calcination.**(a)** 5 wt% Ru/TiO_2, **(b)** 3 wt% Ru/TiO_2 and **(c)** 1 wt% Ru/TiO_2.

We made another assumption that this peak could be due to the reduction of chlorine species. In order to test this assumption, a sample of the 5 wt% Ru/TiO_2 catalyst was prepared and 0.5 wt% of Cl^- from NH_4Cl was added to the sample. This sample was then calcined to remove the NH_3 and subjected to TPR analysis. The TPR profiles of the two catalysts i.e. the original 5 wt% Ru/TiO_2 catalyst which had not been calcined and the 5 wt% Ru/TiO_2 which contained 0.5 wt% Cl^- were compared (**Figure 4.11**). In **Figure 4.11** it was noted that the intensity of the peak at 330 ^0C for both catalysts was the same and due to this it was established that the peak at 330 ^0C was not due to the reduction of chlorine species because the intensity of the 5 wt% Ru/TiO_2 which contained 0.5 wt% Cl^- would have been slightly greater than that of the original 5 wt% Ru/TiO_2 catalyst which had not been calcined.

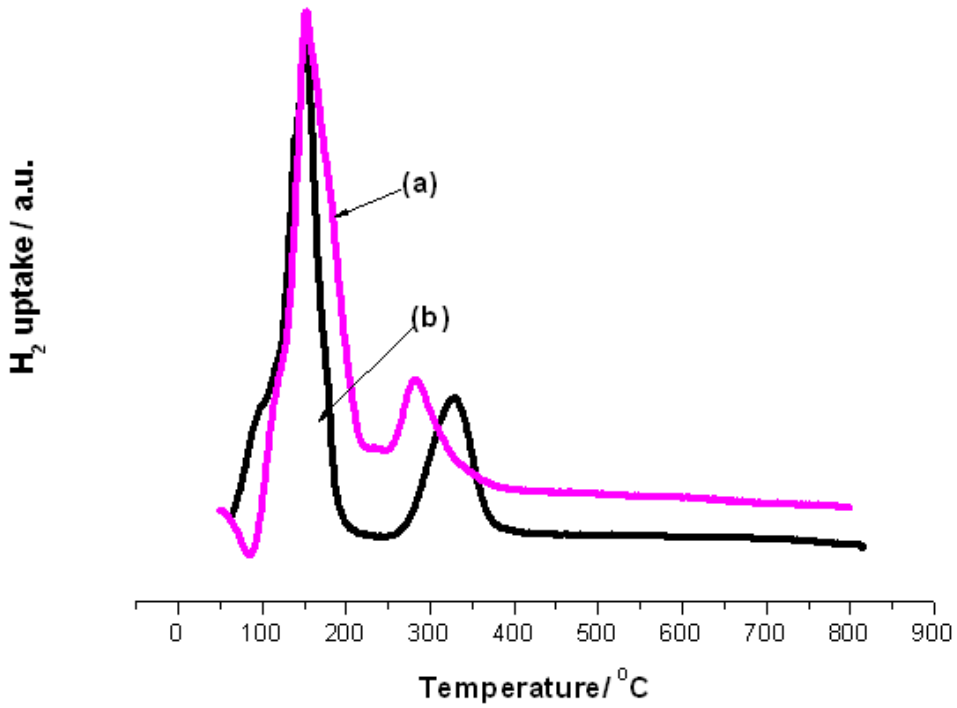


Figure 4.11: TPR profiles of the **(a)** 5 wt% Ru/TiO_2 with 0.5 wt% Cl^- and the **(b)** 5 wt% Ru/TiO_2 uncalcined catalyst.

An alternative reason for the reduction peak at 300 ^{0}C in **Figure 4.10** may be that the Ru forms a complex that interacts with the TiO_2. Due to this a metal-support interaction occurs between the oxygen of the TiO_2 support and the Ru resulting in the formation of the Ru ___O bond as illustrated in **Figure 4.12**.This interaction is known as strong metal support interaction (SMSI) and it might be the cause of the reduction peak observed at 330 ^{0}C. This could explain why the intensity of the 330 ^{0}C peak is higher for the 1 wt% Ru/TiO_2 catalyst than the 3 wt% and 5 wt% catalysts because according to Li et.al.,[2] a catalyst with a low Ru content usually succumbs to an SMSI state more easily than a catalyst with a high Ru contents.

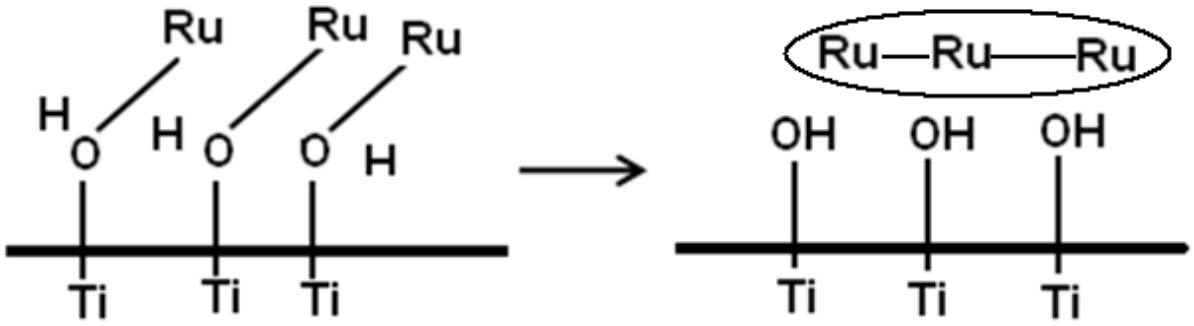


Figure 4.12: Proposed mechanism of how the 330 ^{0}C reduction peak might arise in the TPR profile of the uncalcined catalysts.

4.2.5. Powder X-ray diffraction (PXRD) analysis of the Pd/TiO_2 catalysts.

The crystalline phases of the Pd/TiO_2 catalysts were studied by PXRD analysis and the patterns are displayed in **Figure 4.13**.The TiO_2 support consists of the anatase and rutile crystalline phases and the anatase phase is the more prevalent crystallographic phase as compared to the rutile phase. There is an indication of the formation of the PdO phase in all of the catalysts with a peak at $2\theta = 34^{o}$.This peak is clearly visible for all catalysts, it does not overlap with the rutile or anatase peaks. This means that the $Pd(NO_3)_2.2H_2O$ precursor decomposes into PdO after catalyst preparation. The catalyst prepared by the deposition-precipitation method has the largest peak. The calcined Pd/TiO_2 catalyst has the second largest peak and the uncalcined catalyst reveals the smallest broad peak. This means that the deposition-precipitation catalyst has the largest PdO particles. The calcined Pd/TiO_2 catalyst has the second largest peak and the uncalcined catalyst has the smallest particles. The Scherrer equation was used to determine the crystallite size. The calcined Pd/TiO_2 catalyst had a crystallite size of 4.2 nm, uncalcined had a crystallite size of 4.1 nm and the deposition-precipitation catalyst had a crystallite size of 9.6 nm.

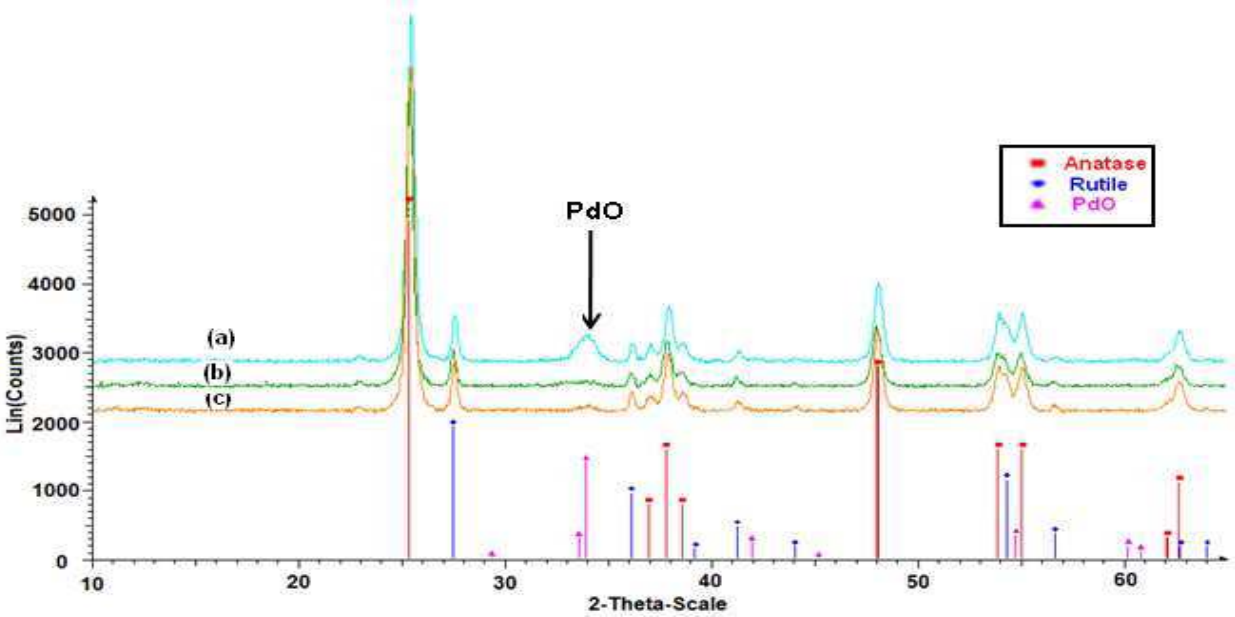


Figure 4.13: PXRD pattern of the three 5 wt% Pd/TiO_2 catalysts. **(a)** Prepared by deposition-precipitation method and calcined at 400 ^{0}C for 5 hours,**(b)** dried at 110 ^{0}C and not calcined and **(c)** calcined at 400 ^{0}C for 5 hours.

The prepared catalysts were subjected to reduction under a flow of hydrogen. As can be noted from **Figure 4.14** which represents the PXRD patterns of the reduced catalysts, the PdO peak displays a shift from $2\theta = 34^{o}$ and reappears as the Pd peak at $2\theta = 40^{o}$ and 47^{o} . This shows that the PdO was successfully reduced to its active Pd metallic form.

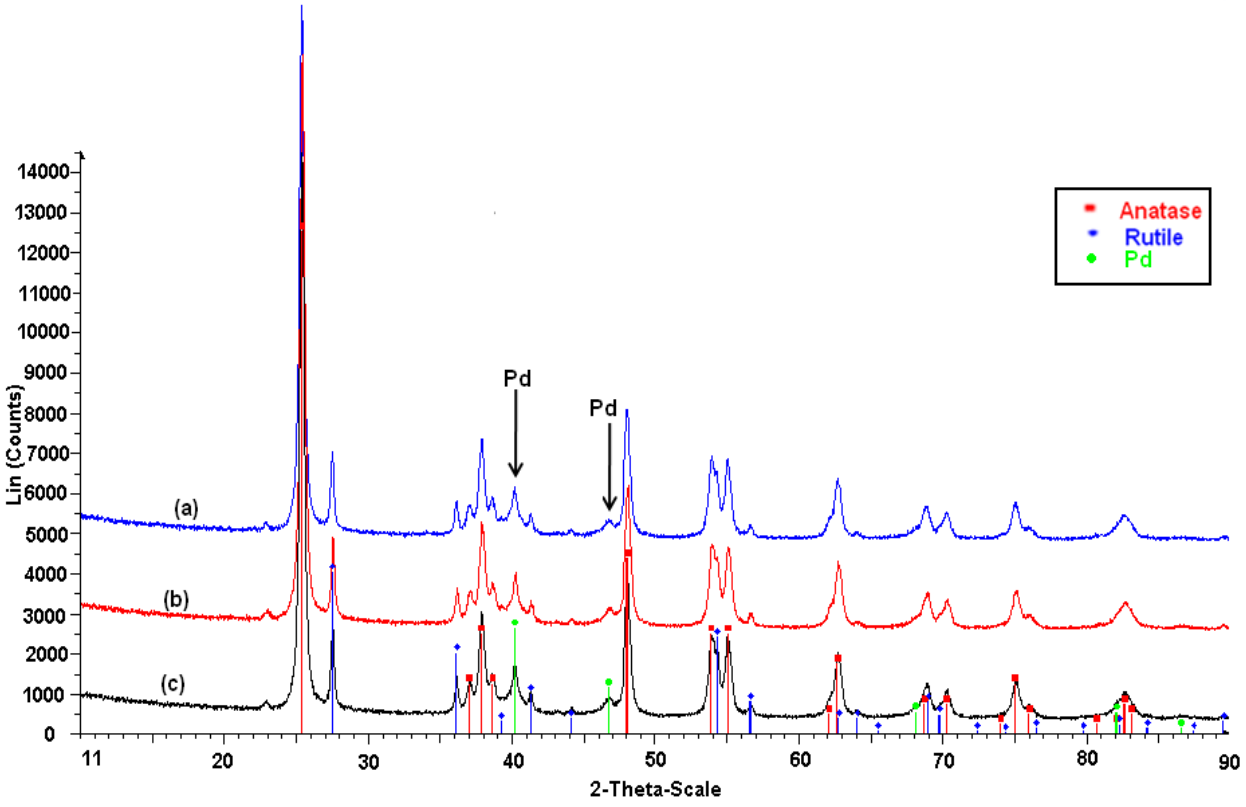


Figure 4.14: PXRD patterns of the reduced Pd/TiO_2 catalysts, **(a)** Prepared by deposition-precipitation method and calcined at 400 ^{0}C for 5 hours,**(b)** dried at 110 ^{0}C and not calcined and **(c)** calcined at 400 ^{0}C for 5 hours.

4.2.6. BET analysis of the Pd/TiO_2 catalysts

In order to study the physicochemical properties of the prepared catalysts BET analysis was performed. The results which were obtained are presented in **Table 4.2**. The general trend is that the surface area decreases and the pore volume increases as the catalysts became loaded. This makes sense as the support becomes loaded the surface area should decrease and the average pore volume should increase as the pores became occupied.

Table 4.2: BET surface area and pore volume of the TiO_2 supported Pd catalysts.

	BET surface area (m^2/g)	Pore volume (cm^3/g)
TiO_2(Degussa,P-25)	49	0.20
1%Pd/TiO_2[a]	47	0.32
1%Pd/TiO_2[b]	49	0.26
1%Pd/TiO_2[c]	43	0.44
3%Pd/TiO_2[a]	43	0.45
3%Pd/TiO_2[b]	49	0.32
3%Pd/TiO_2[c]	47	0.46
5%Pd/TiO_2[a]	46	0.34
5%Pd/TiO_2[b]	48	0.32
5%Pd/TiO_2[c]	45	0.44

[a] Prepared by wetness-incipient method dried at 110 ^{0}C for 24 hours and calcined at 400 ^{0}C for 5 hours , [b] prepared by wetness-incipient method dried at 110 ^{0}C for 24 hours, [c] prepared by deposition-precipitation method, vacuum dried for 20 hours and calcined at 400 ^{0}C for 5 hours.

4.2.7. Transmission Electron Microscopy (TEM) analysis of the Pd/TiO_2 catalysts

The Pd/TiO_2 catalysts were subjected to TEM analysis before being reduced (**Figure 4.15**). The TEM images showed only TiO_2 particles which could not be used to calculate the Pd particle sizes. EDX analysis (not shown) gave an indication that Pd was present. The catalysts were reduced in order to convert them to the metallic form. The TEM images of these reduced catalysts are presented in **Figure 4.16**, **4.17** and **4.18**. These images show that reducing the catalysts leads to a significant change in morphology of the Pd.

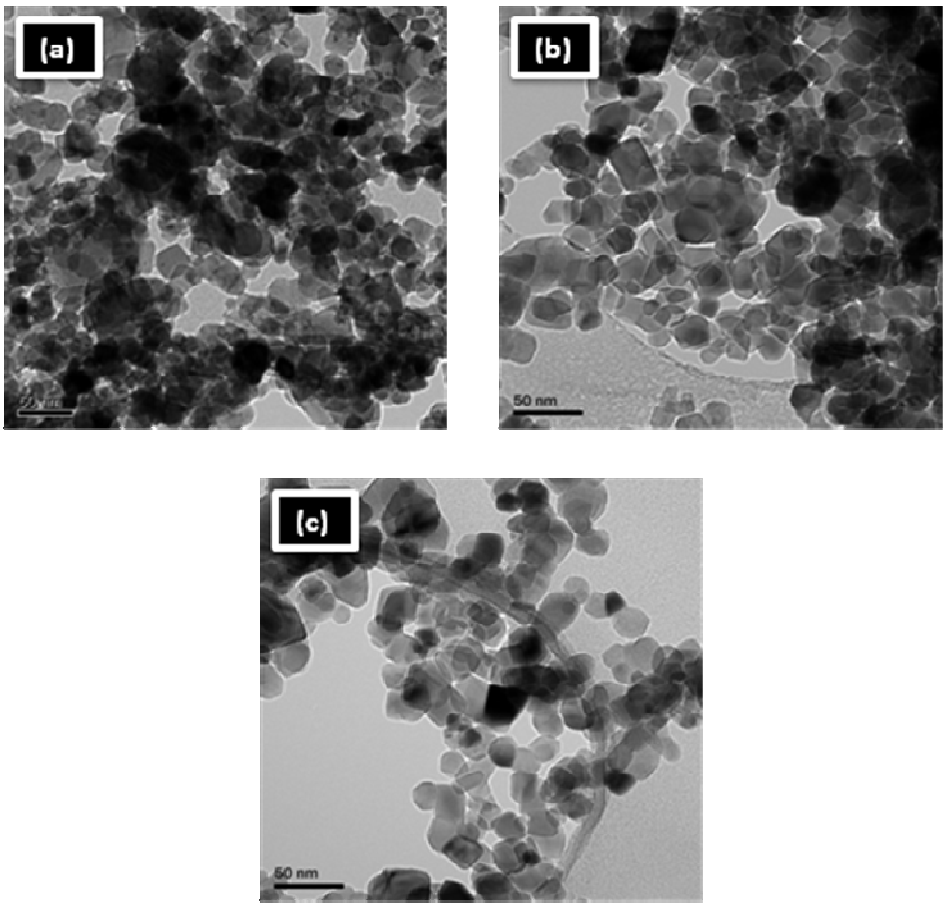


Figure 4.15: TEM images of the 5 wt% Pd/TiO_2 catalysts before they were reduced. **(a)** Dried at 110 ^{0}C for 24 hours and calcined at 400 ^{0}C for 5 hours, **(b)** prepared by deposition-precipitation method, vacuum dried for 20 hours and calcined at 400 ^{0}C for 5 hours and **(c)** dried at 110 ^{0}C for 24 hours

4.2.7.1. TEM analysis of the calcined 5 wt% Pd/TiO_2 catalyst

Figure 4.16a shows the TEM image of the calcined 5 wt% Pd/TiO_2 catalyst which was reduced prior to TEM analysis. This image shows that the particles are well distributed with some clusters over the TiO_2 support. The TiO_2 particles seem to form cube like three dimensional aggregates like the Ru/TiO_2 catalysts. In order to obtain **Figure 4.16b** 100 particles were analysed and it could be noted that the particles vary in width from 2 nm to 11 nm and most of the particles are between 3 nm and 4 nm in width and have an average width of 7 nm. This is in agreement with the crystallite size determined from PXRD.

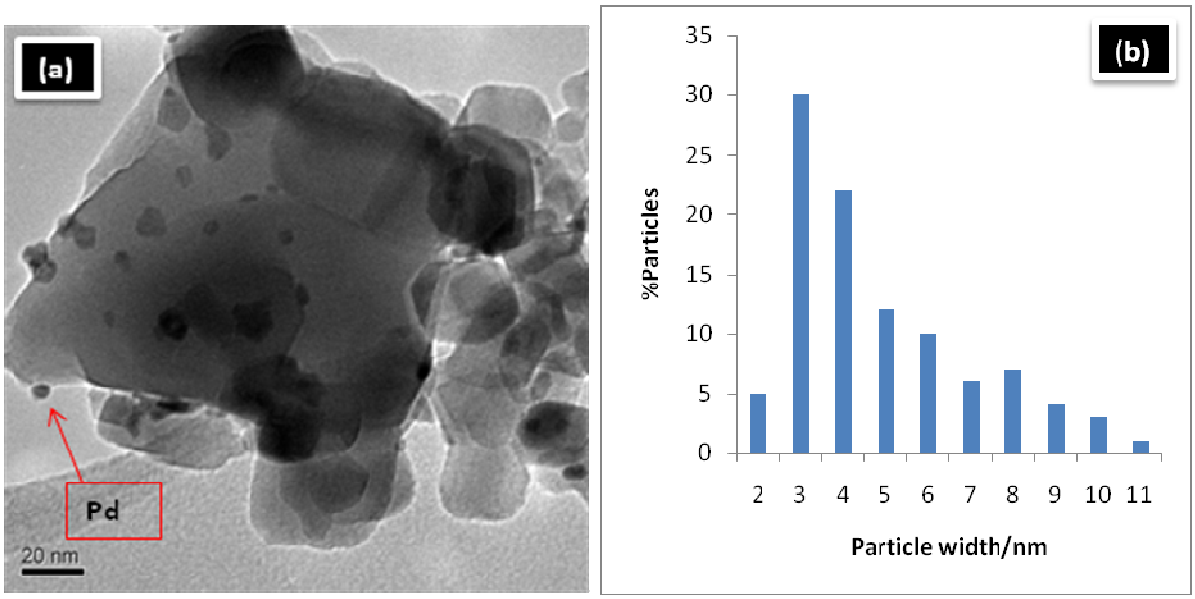


Figure 4.16: TEM image of the 5wt% Pd/TiO_2 catalyst which was calcined at 400 ^{0}C for 5 hours.

4.2.7.2. TEM analysis of the deposition-precipitation 5%Pd/TiO_2 catalyst.

Figure 4.17a represents the TEM image of the 5wt% Pd/TiO_2 catalyst which was prepared by the deposition-precipitation method and reduced prior to TEM analysis. The TiO_2 support seems to be forming cluster and the Pd metal particles can be observed on these TiO_2 clusters. About 100 Pd clusters were analysed and these lead to a very narrow particle width distribution which is illustrated in **Figure 4.17b**. Most of the particles are between 3 and 6 nm in width and average particle width was found to be 6nm. This particle width slightly differs from that of the crystallite size which was determined from PXRD. However this average particle size agrees with the one which was reported by Shen et al,[11] for a catalyst which he prepared by the deposition-precipitation method. Shen et.al.,[11] found the particle size distribution of a 3 wt% Pd/TiO_2 catalyst prepared by the deposition-precipitation method ranges between 4 and 20 nm with most of the particles having a particle width of 10 nm. Shen et.al.,[11] analyzed a 3 wt% Pd/TiO_2 catalyst which was prepared from a $PdCl_2$ solution and calcined at 500 ^{0}C for 5 hours.

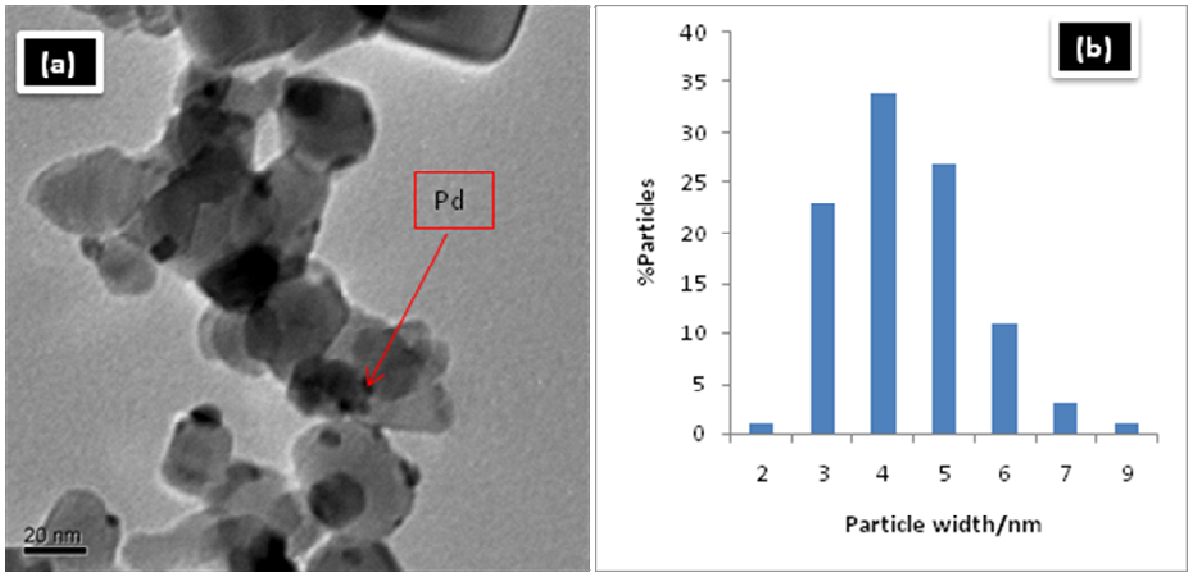


Figure 4.17: TEM image of the 5 wt% Pd/TiO_2 catalyst which was prepared by the deposition-precipitation method and calcined at 400 ^{0}C for 5 hours.

4.2.7.3. TEM analysis of the uncalcined Pd/TiO_2 catalysts

Figure 4.18a represents the TEM image of the uncalcined Pd/TiO_2 particles. The particles appear to be uniformly distributed on the TiO_2 support. The interface between the particles and the TiO_2 support can be observed. **Figure 4.18b** shows the particle width distribution which is narrow and ranges between 2 and 8nm. The average particle size of the 100 analysed particles was found to be 5nm. This agrees with the crystallite size determined in PXRD. This is also comparable with what the particle size reported by Shen et al.[11] for the deposition-precipitation catalyst but does not agree that well to what was reported by Babu et al.[3] who used CO chemisorption for a 1 wt% uncalcined Pd/TiO_2 catalyst and found an average particle size of 26nm.

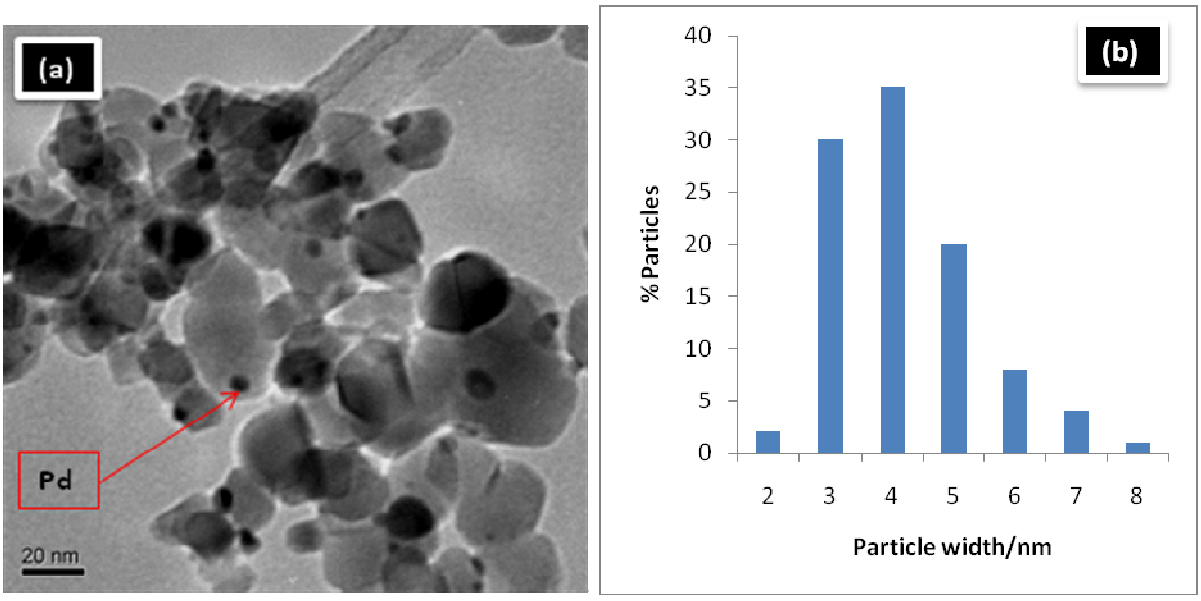


Figure 4.18: TEM image of the 5 wt% Pd/TiO_2 catalyst which was dried at 110 ^{0}C and uncalcined.

4.2.8. Temperature Programmed Reduction (TPR) analysis of the Pd/TiO_2 catalysts

4.2.8.1. TPR of the calcined 5 wt% Pd/TiO_2 catalyst and the TPR of the Pd/TiO_2 catalyst which was prepared by the deposition-precipitation method.

Figure 4.19 illustrates the TPR profile of the 5 wt% Pd/TiO_2 catalyst which was prepared by the incipient wetness impregnation method and calcined at 400 ^{0}C for 5 hours and the 5wt% Pd/TiO_2 catalyst which was prepared by the deposition - precipitation method and calcined at 400 ^{0}C for 5 hours. The TPR profiles display negative reduction peaks at about 55 ^{0}C. This means that the H_2 is not being consumed by the catalyst but instead it is being evolved. According to other researchers, [3, 12 &13] this negative reduction peak is a common feature of Pd catalysts which is caused by the decomposition of β-PdH which is a common feature of Pd catalysts associated with large particles. This means that the PdO is reduced to PdH which then decomposes in Pd and H_2 as illustrated in (Equation **(4.3)**):

$$PdO + H_2 \longrightarrow PdH \longrightarrow Pd + H_2 \qquad \textbf{(4.3)}$$

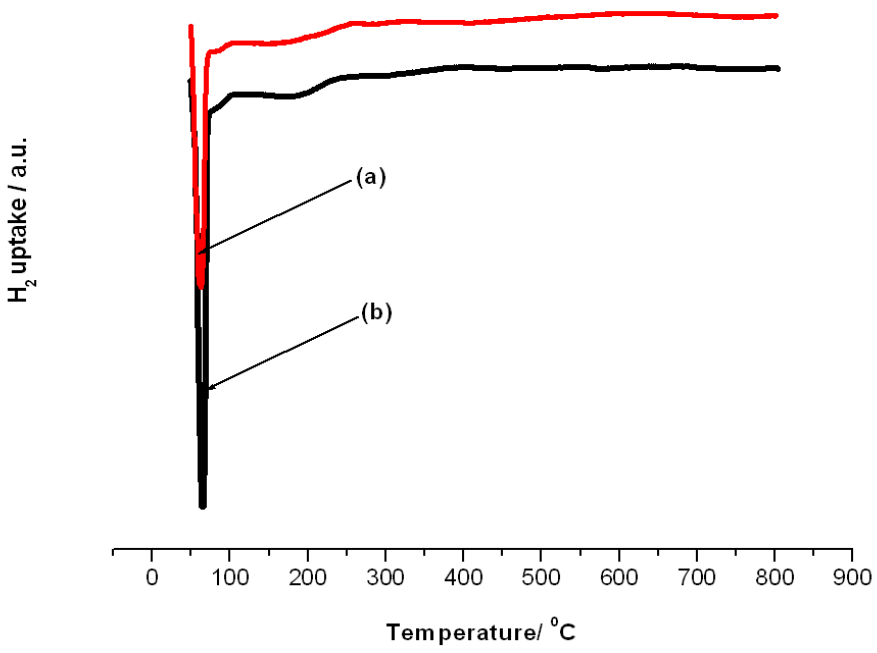


Figure 4.19: TPR profiles of the **(a)** 5wt% Pd/TiO_2 catalyst which was calcined and the **(b)** 5wt% Pd/TiO_2 catalyst prepared by the deposition-precipitation method.

4.2.8.2. TPR of the uncalcined 1 wt% and 5 wt% Pd/TiO_2 catalysts.

Figure 4.20 shows that the TPR profile of the 1 wt% and 5 wt% Pd/TiO_2 catalysts which were prepared by the wetness-incipient method and left uncalcined. Just like the profiles in **Figure 4.19** these profiles display a negative reduction peak at about 55 ^{0}C which is not due to the consumption of H_2 but due to the production of H_2 .This is also due to the decomposition of the β-PdH hydride. **Figure 4.20** also has a second reduction peak at about 300 ^{0}C this phenomenon is quite similar to that displayed by the uncalcined Ru/TiO_2 catalysts in **Figure 4.10**. This could mean that the Pd also forms a complex with TiO_2 which results in the formation of a metal-support interaction. This interaction occurs through the oxygen of TiO_2 and Pd and when this interaction is reduced this could result in the occurrence of the reduction peak at 300 ^{0}C.The intensity of the 300 ^{0}C reduction peak is greater for the 1 wt% Pd/TiO_2 than it is for the 5 wt% Pd/TiO_2 because catalysts with lower loadings succumb more easily to the SMSI state.[2]

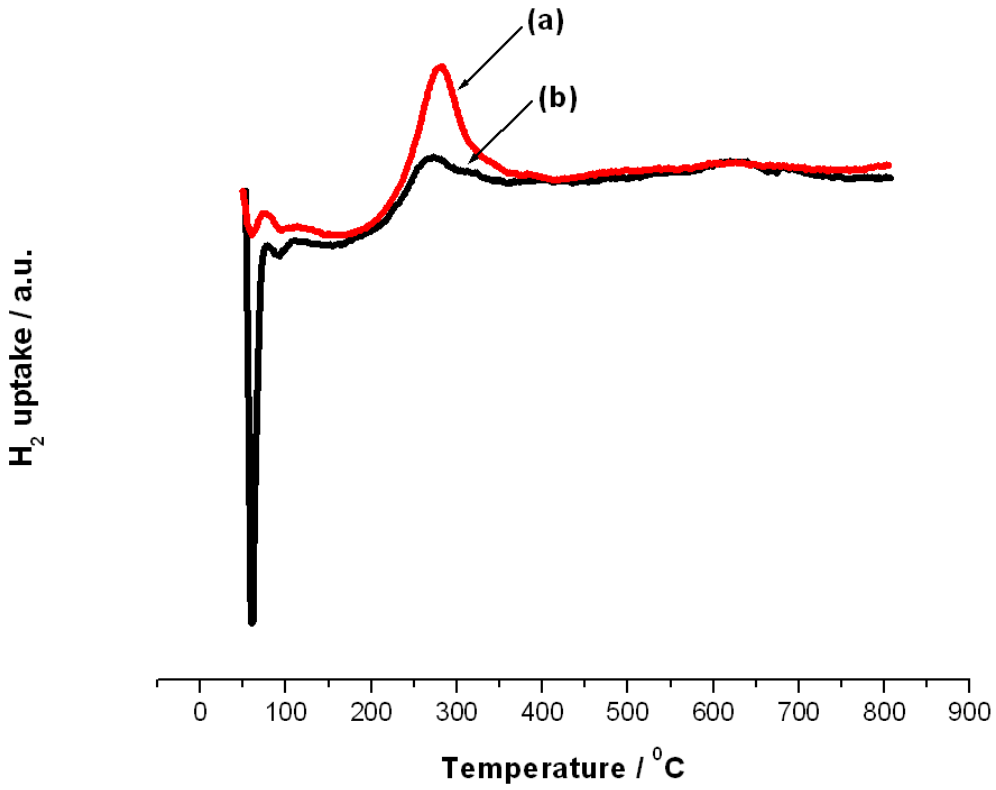


Figure 4.20: The TPR profile of the **(a)** 1 wt% and **(b)** 5 wt% Pd/TiO_2 catalysts which were prepared by the wet-incipient method and left uncalcined.

4.2.9. Powder X-ray diffraction PXRD analysis of the 1 wt%, 3 wt% and 5 wt% Rh/TiO_2 catalysts.

In order to study the crystalline phases of the prepared 1 wt**%,** 3 wt% and 5 wt% Rh/TiO_2 catalysts PXRD analysis was performed and the patterns which were obtained are displayed in **Figure 4.21**. The TiO_2 support consists of the anatase and rutile phases. With the use of a program called EVA the Rh_2O_3 phase of the Rh/TiO_2 catalysts was searched but could not be found in the prepared catalysts. So as an alternative the Rh metallic phase of the catalysts was searched and it was noted that the peak at $2\theta = 41^0$ could represent the presence of the Rh phase. However this peak is overlapping with the rutile peak. So this could mean that after calcination the $RhCl_3.xH_2O$ precursor decomposes into Rh. The particle size of the Rh particles could not be calculated as the peak overlaps with the rutile peak.

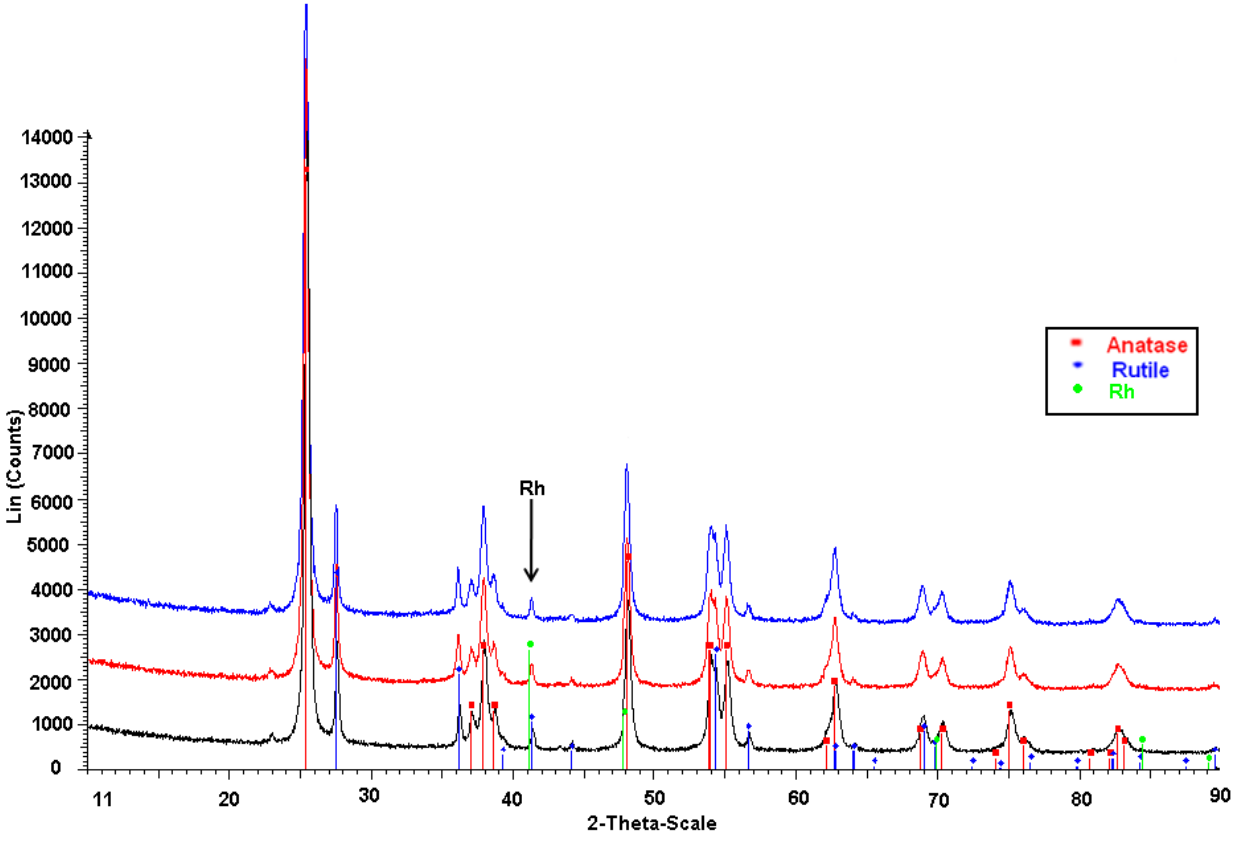


Figure 4.21: PXRD pattern of the Rh/TiO_2 catalysts with different metal loadings **(a)** 5 wt% **(b)** 3 wt% and **(c)** 1 wt%.

In order to verify if the Rh phase was present in the prepared 5 wt% Rh/TiO_2 catalyst it was reduced under hydrogen and subjected to PXRD analysis. This PXRD pattern was compared to that of the original unreduced Rh/TiO_2 catalyst. It was hoped that if the Rh/TiO_2 catalyst exists in the Rh_2O_3 phase and the above assumption is wrong then there would be a difference between the PXRD patterns of the as prepared Rh/TiO_2 catalyst and the reduced catalyst. However by looking at **Figure 4.22** it can be noted that there is no difference between the two catalysts. If the Rh_2O_3 phase was present then there would be a shift in the peak position of Rh_2O_3 whose position is illustrated by the pink lines as it would be found at this position if it was present. Another reason that could have lead to the absence of the Rh_2O_3 peak could be that the particles are well dispersed on the TiO_2 support and could not be identified by PXRD as it depends on the scattering of X-rays on particles which are then detected by detectors to form a signal. Larichev et.al.,[14] reported that they could not observe the Rh reflexes in PXRD because the particles were very small. Larichev et.al.,[14] examined a 6 wt% Rh/TiO_2 catalyst which was prepared by the wetness-incipient method and calcined at 800 ^{0}C.

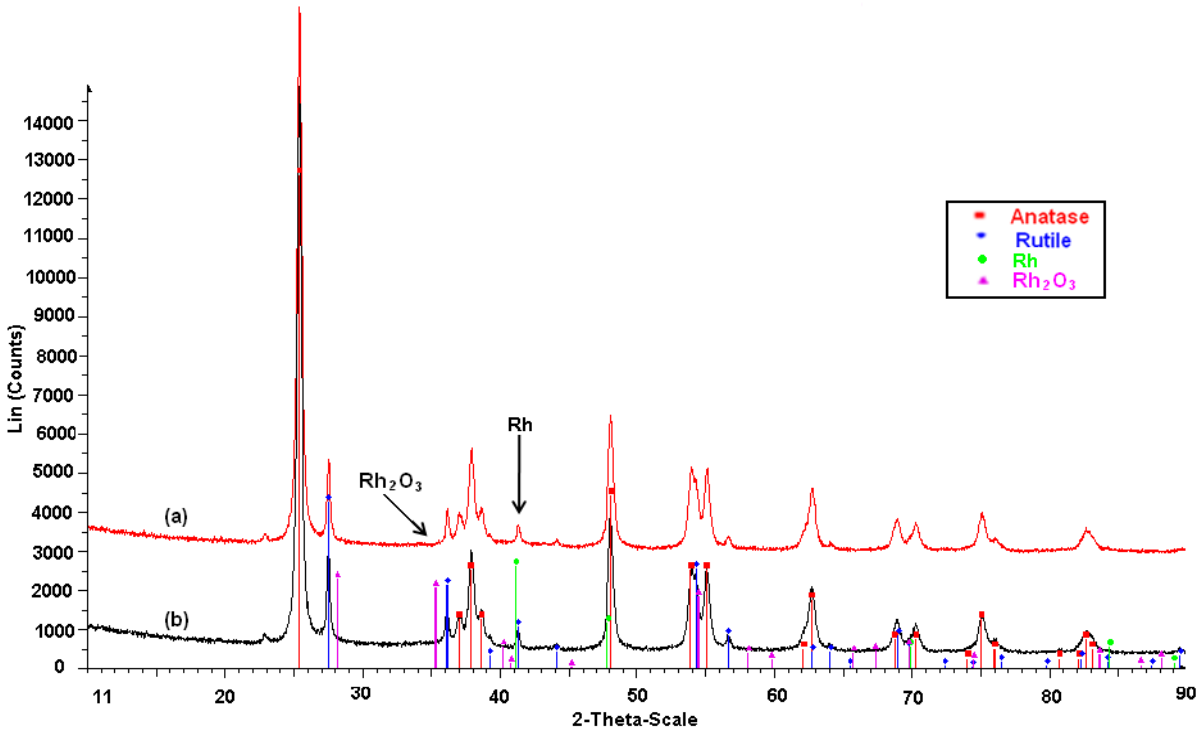


Figure 4.22: PXRD pattern of the 5 wt% Rh/TiO_2 catalysts **(a)** 5 wt% Rh/TiO_2 not reduced and **(b)** 5 wt% Rh/TiO_2 reduced.

4.2.10. BET analysis of the 1 wt%, 3 wt% and 5 wt% Rh/TiO_2 catalysts.

The prepared catalysts were subjected to BET analysis and the results are presented in **Table 4.3**. As it can be noted the surface area of the 5 wt% Rh/TiO_2 has decreased as compared to the unoccupied TiO_2 support. This just shows that the TiO_2 pores are occupied by Rh particles. However the surface area of the 1 wt% Rh/TiO_2 catalyst has not changed as compared to the TiO_2 support.

Table 4.3: BET surface area and pore volume of the TiO_2 supported Rh catalysts.

	BET surface area (m^2/g)	Pore volume (cm^3/g)
TiO_2(Degussa,P-25)	49	0.20
1%Rh/TiO_2	49	0.23
3%Rh/TiO_2	46	0.35
5%Rh/TiO_2	45	0.43

4.2.11. TEM analysis of the 5 wt% Rh/TiO_2 catalysts.

Figure 4.23a shows the TEM image of the 5 wt% Rh/TiO_2 catalyst. This image illustrates that the Rh particles are very small and appear to be well dispersed with a small amount of clusters on the TiO_2 support. This could be one of the reasons why the Rh peaks could not be observed in the PXRD pattern of the Rh/TiO_2 catalysts. **Figure 4.23b** shows the particle width distribution which indicates that the particle width ranges from 1.0 to 2.6 nm and the average particle width was found to be 1.8 nm. This agrees with the average particle width reported by Larichev et.al.,[14] who found the particle width of a 6 wt% Rh/TiO_2 catalyst to be 2.0 nm. Ekou et.al.,[15] also reported a mean particle width of 2.4 nm for a Rh/TiO_2 which is also comparable to 1.8 nm. Unlike the other catalysts the 5wt% Rh/TiO_2 catalyst was not reduced prior to PXRD analysis

because it was established from Energy Dispersive X-ray spectroscopy (EDX) analysis (**Figure 4.23c**) that the catalysts was in its metallic Rh form.

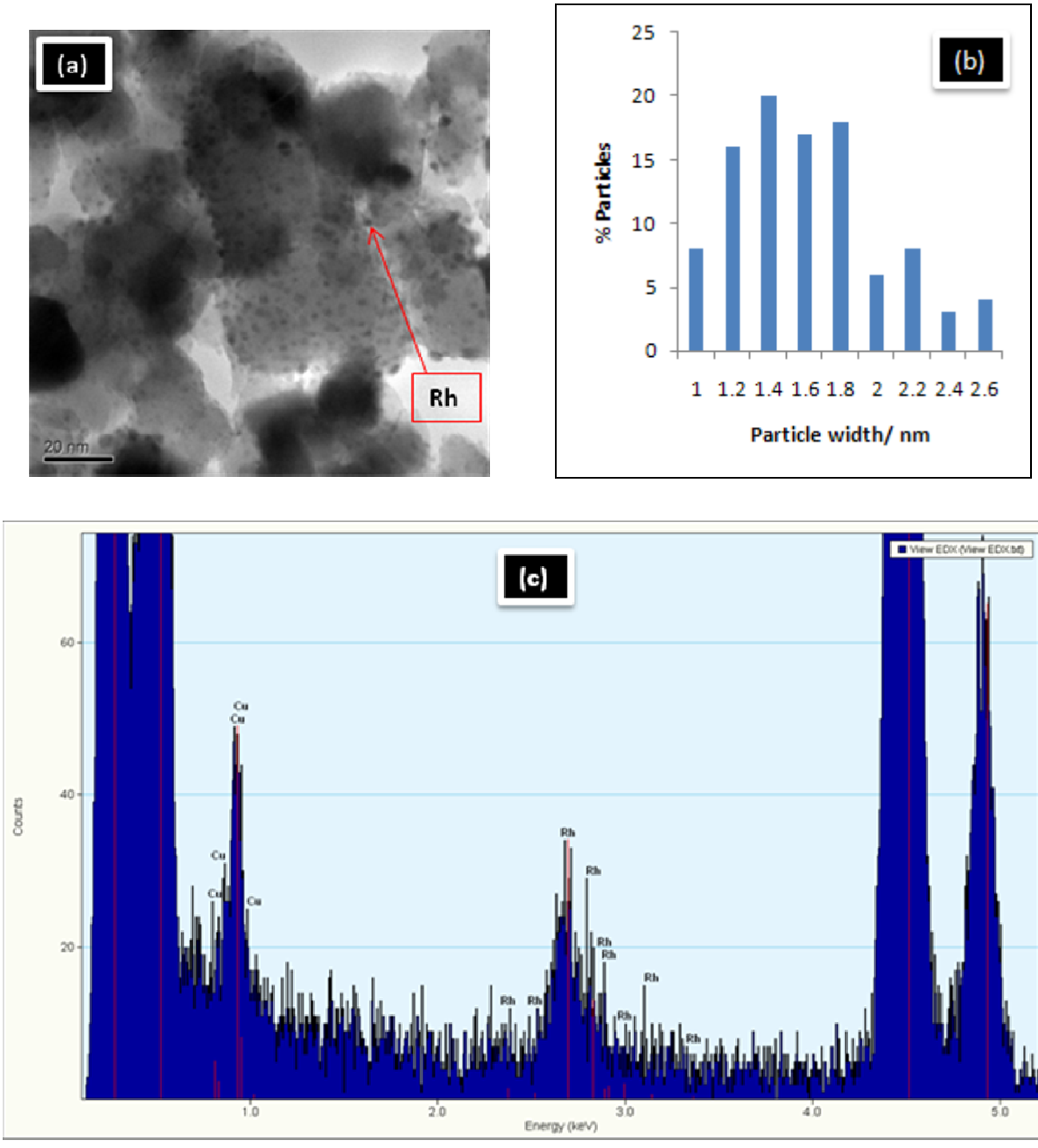


Figure 4.23: TEM image of the 5 wt% Rh/TiO_2 catalyst **(a)** TEM image and **(b)** Particle distribution,**(c)** EDX results.

4.2.12. TPR of the calcined 1 wt%, 3 wt% and 5 wt% Rh/TiO_2 catalysts.

In order to determine the reducibility of the prepared 1 wt%, 3 wt% and 5 wt% Rh/TiO_2 catalysts TPR analysis was performed and the profiles are displayed in **Figure 4.24** below. Before TPR analysis the catalysts were pretreated in situ under oxygen for 2 hours at 300 ^{0}C and then cooled to room temperature. This was done in order to try and convert Rh metal into the Rh_2O_3 oxide so that it could be reduced. In **Figure 4.24** the TPR profiles show a reduction peak at about 100 ^{0}C. According to Ekou et al., [16] this reduction peak is due to the reduction of Rh_2O_3 to the metallic form Rh and this occurs according to Equation **(4.4)**:

$$Rh_2O_3 \longrightarrow Rh \qquad (4.4)$$

According to Ekou et al.,[16] the other reduction peaks which are located at about 200 ^{0}C and about 300 ^{0}C for 5 wt% Rh/TiO_2 catalyst could be due to the partial reduction of the TiO_2 support which is caused by the SMSI which leads to the production of TiO_2−x species (x < 2). However we believe that these peaks could be due to the formation of an interaction between Rh and the oxygen of TiO_2 as was previously explained for Ru/TiO_2 and Pd/TiO_2 catalysts.

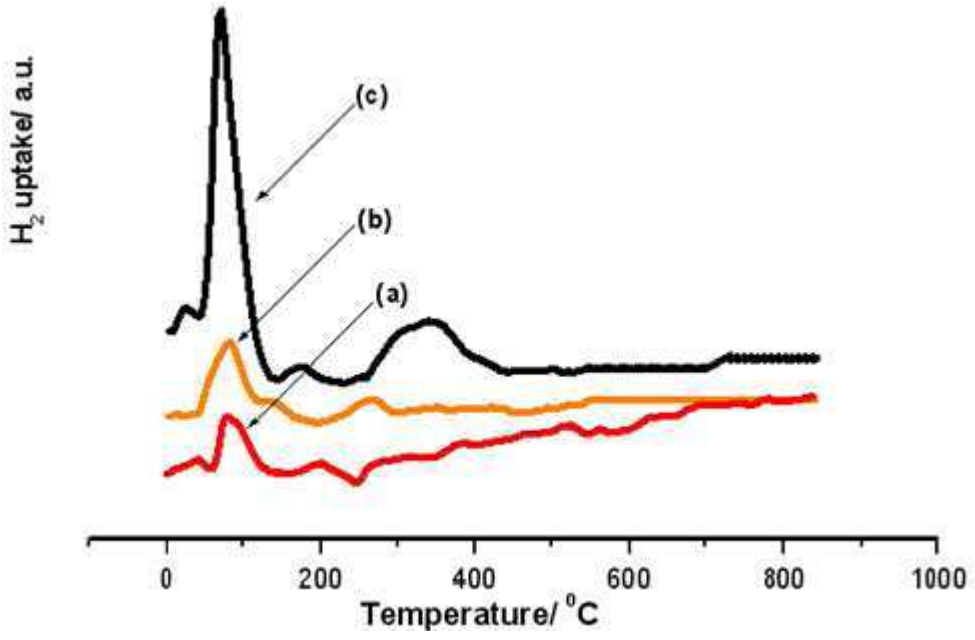


Figure 4.24: TPR profile of the Rh/TiO_2 catalysts with different metal loadings (a) 1 wt% Rh/TiO_2, (b) 3 wt% Rh/TiO_2 and (c) 5 wt% Rh/TiO_2.

4.2.13. Powder X-ray diffraction (PXRD) analysis of the 1 wt%, 3 wt% and 5 wt% Pt/TiO_2 catalysts.

The crystallographic phases of the Pt/TiO_2 catalysts with 1 wt%, 3 wt% and 5 wt% loadings were studied with PXRD and the patterns are displayed in **Figure 4.25** below. The TiO_2 support displays peaks which represent both the anatase and rutile phases. The anatase phase is still the most dominate phase between the two phases. With the use of EVA it was noted that the peaks at $2\theta = 33^0$, 41^0, 54^0 and 60^0 represent the PtO phase of the Pt/TiO_2 catalysts. This means that after calcination the $H_2PtCl_6.3H_2O$ precursor decomposes into PtO. However all of the PtO phase peaks except the peaks at $2\theta = 33^0$ and 60^0 seem to overlap with the rutile and anatase peaks. Due to this the peaks at $2\theta = 33^0$ and 60^0 were used to calculate the particle sizes of the Pt/TiO_2 catalysts with the use of the Scherrer equation. For the 5 wt% Pt/TiO_2 catalyst the peak at $2\theta = 33^0$ gave a crystallite size of 7.9 nm and the peak at $2\theta = 60^0$ lead to a crystallite size of 7.5 nm. The crystallite sizes of the 1 wt% and 3 wt% catalysts could not be determined as the particles were too small for PXRD analysis.

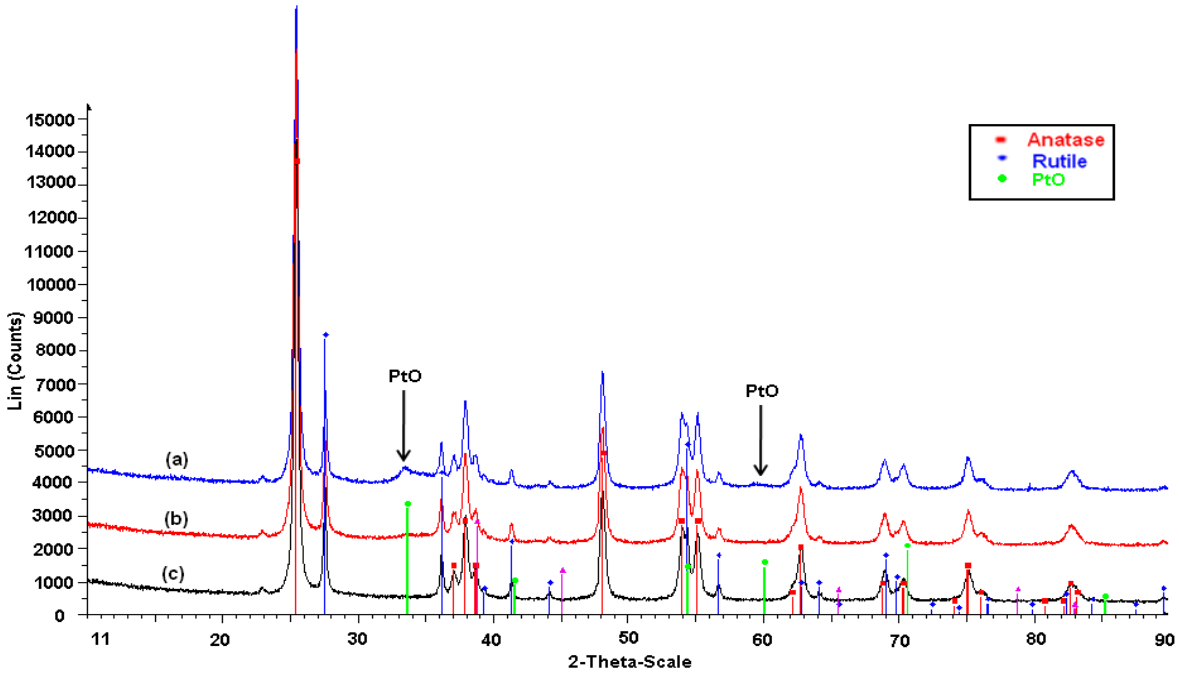


Figure 4.25: PXRD pattern of the Pt/TiO_2 catalysts with different metal loadings **(a)** 5 wt% Pt/TiO_2, **(b)** 3 wt% Pt/TiO_2 and **(c)** 1 wt% Pt/TiO_2.

In order to identify the peak positions of the Pt phase of the Pt/TiO_2 catalyst since this is the active phase of the Pt/TiO_2 catalyst, the prepared 5 wt% Pt/TiO_2 catalyst was reduced in hydrogen and then subjected to PXRD analysis (**Figure 4.26**). The peaks at $2\theta = 40^0$ and 46^0 represent the Pt phase. However the peak at $2\theta = 40^0$ seems to overlap with the anatase peak. The peak at $2\theta = 46^0$ was used to calculate the crystallite size with the use of the Scherrer equation and a crystallite size of 8.8 nm was obtained.

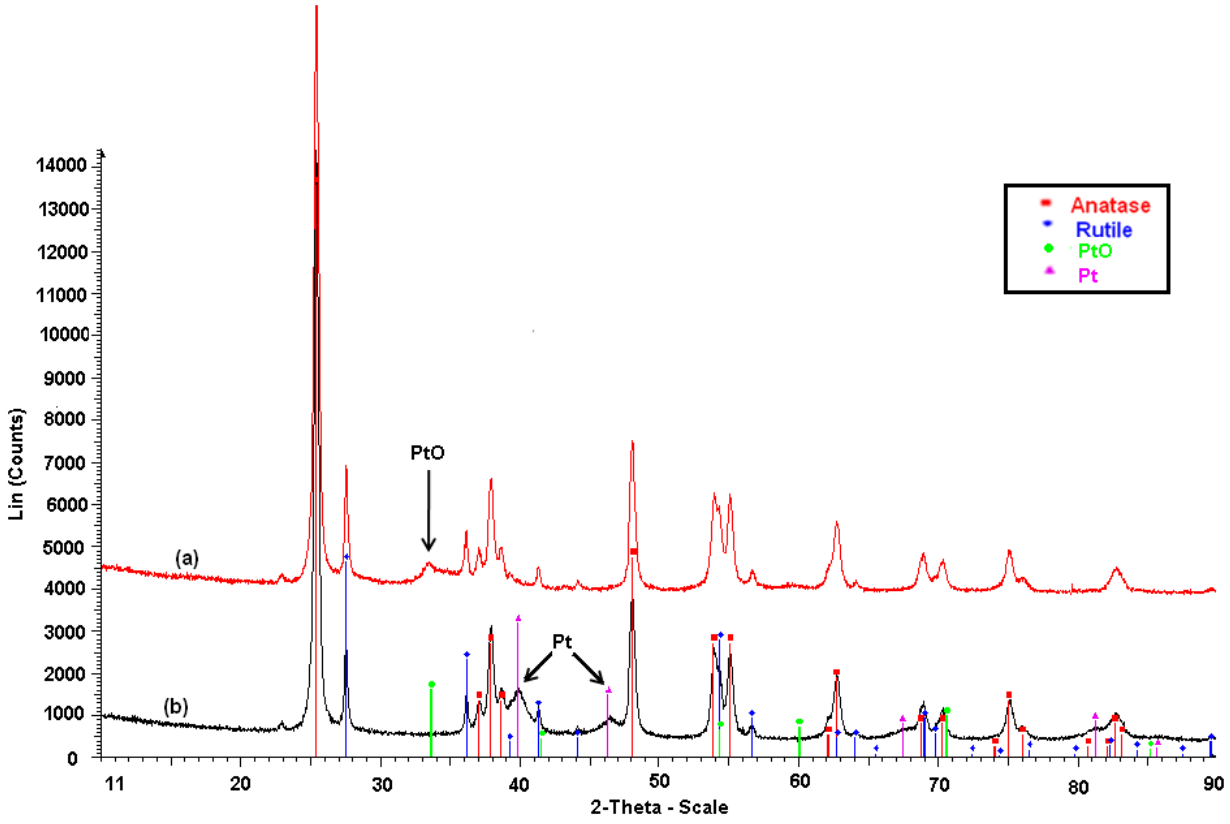


Figure 4.26: PXRD pattern of the 5 wt% Pt/TiO_2 catalysts **(a)** 5 wt% Pt/TiO_2 not reduced and **(b)** 5 wt% Pt/TiO_2 reduced.

4.2.14. BET analysis of the 1 wt%, 3 wt% and 5 wt% Pt/TiO_2 catalysts.

The surface area and pore volume of the Pt/TiO_2 catalysts with different loadings was determined using the BET method and the results are tabulated in **Table 4.4**. Compared to the unloaded TiO_2 support the catalysts decrease in surface area and increase in pore volume. This signals the occupation of the TiO_2 pores by the PtO particles. As the loading decreases so does the extent of the decrease in surface area and increase in pore volume seems to decrease, meaning that the extent of the occupation of the pores decreases with decreasing loadings.

Table 4.4: BET surface area and pore volume of the TiO_2 supported Pt catalysts.

	BET surface area (m^2/g)	Pore volume (cm^3/g)
TiO_2(Degussa,P-25)	49	0.20
1%Pt/TiO_2	41	0.34
3%Pt/TiO_2	37	0.37
5%Pt/TiO_2	36	0.41

4.2.15. TEM analysis of the 5 wt% Pt/TiO_2 catalysts.

Figure 4.27a shows the TEM image of the 5 wt% Pt/TiO_2 catalyst. As it can be noted the particles are well dispersed on the TiO_2 support which seems to form clump like shapes and not the aggregates observed in the other catalysts. The particle width distribution (**Figure 4.27b**) was found to range between 1.0 and 5.5 nm leading to an average particle width of 2.7 nm. This is in good agreement with the mean particle size reported by J.A. Wang et.al.,[17] who investigated

the particle size of a 1 wt% Pt/TiO_2 prepared by the sol-gel method. This closely agrees with the mean particle width reported by T.Ekou et.al.,[15]

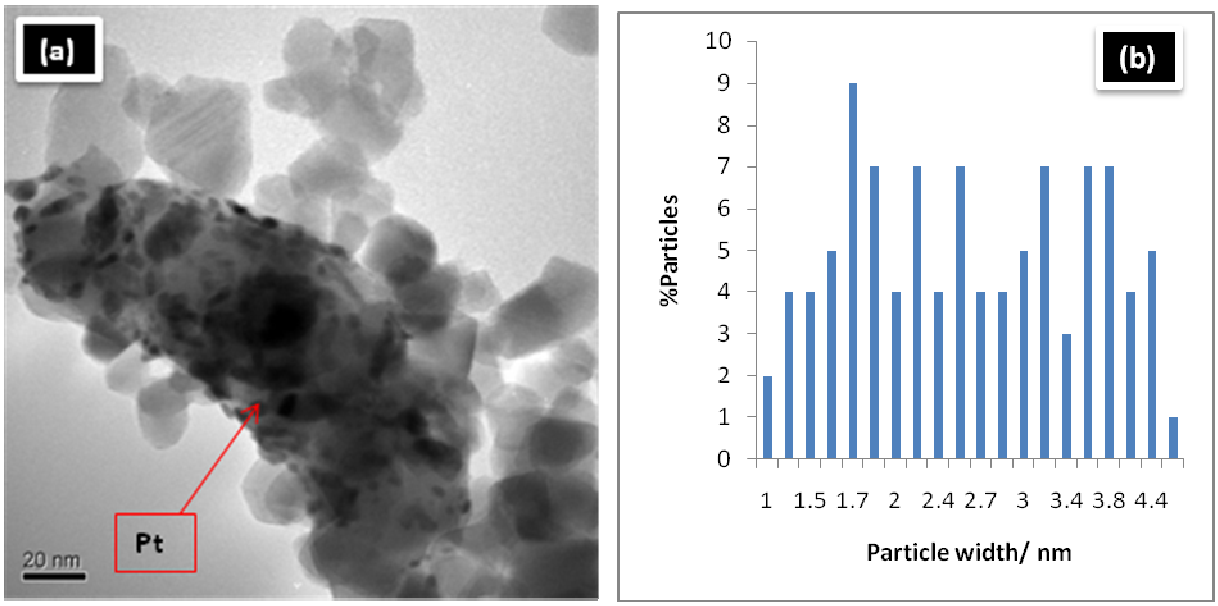


Figure 4.27: TEM image of the 5 wt% Pt/TiO_2 catalyst **(a)** TEM image and **(b)** Particle size distribution

4.2.16. TPR of the calcined 1 wt%, 3 wt% and 5 wt% Pt/TiO_2 catalysts.

Figure 4.28 below displays the TPR profiles of the 1 wt%, 3 wt% and 5 wt% Pt/TiO_2 catalysts. Many attempts were made to try and reduce the Pt/TiO_2 catalysts. Firstly the Pt/TiO_2 catalysts were subjected to TPR analysis after being calcined however this attempt did not lead to any meaningful reduction peaks. Then the catalysts were heated to 200 ^{0}C under the flow of argon to try and get rid of any moisture that might have been present, this did not lead to any success. Then the catalysts were oxidized with the in air at 300 ^{0}C, then 350 ^{0}C, then 400 ^{0}C and lastly at 500 ^{0}C which also did not lead to useful reduction peaks. As a last attempt the catalysts were oxidized in oxygen at the same temperature as for the air attempt which also proved to be

unsuccessful. **Figure 4.28** displays the profiles which were obtained from the last attempt. Many researchers, [16, 17, 18&19] have reported the TPR profiles of the Pt/TiO_2 catalyst and none of these profiles match the one presented in **Figure 4.28**. From the PXRD pattern (**Figure 4.26**) it can be noted that the Pt catalyst should be reduced by H_2 as it contains the PtO phase. T.Huizinga et.al.[20] reported that they oxidised a Pt/TiO_2 catalyst at 673K and observed two reduction peaks, one below 223K and the other just about 273K.These are very low temperature which might perhaps help us explain the absence of reduction peaks with our Pt/TiO_2 catalysts. This could mean that the reduction peaks are not absent but might be appearing at very low temperatures, possible soon as we pass the reduction gas in order to adjust the flow rate the catalyst becomes reduce and by the time analysis begins the catalyst is already reduced. So this could mean that the Pt catalyst is highly reducible (i.e. reduction takes place at sub-ambient temperatures).

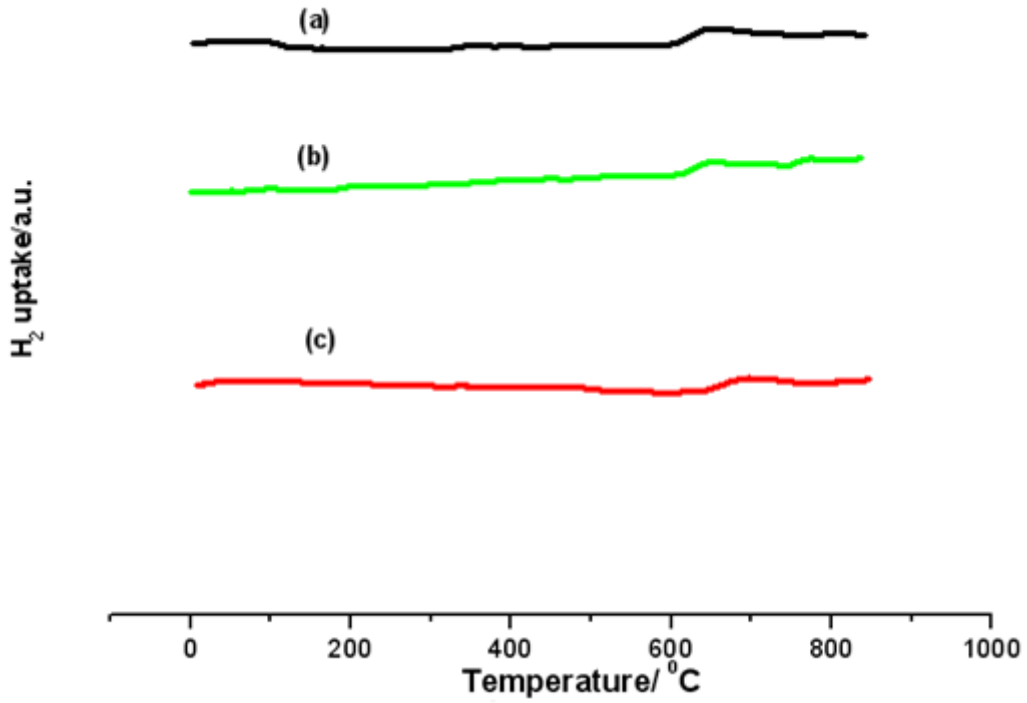


Figure 4.28: TPR profiles of the Pt/TiO_2 catalysts **(a)** 5 wt %, **(b)** 3 wt% and **(c)** 1 wt%

4.3. Catalytic performance tests

This section is divided into three parts, with the first part dealing with the results obtained from the CO methanation results. The second part deals with the CO_2 methanation results while the last part deals with CO/CO_2 methanation results.

4.3.1. CO methanation results

4.3.1.1.CO methanation results of the 5 wt% Ru/TiO_2 catalysts

In this section we began by investigating the activity of the three 5 wt% Ru/TiO_2 catalysts which were prepared by different methods for the CO methanation reaction. The results are summarized in **Figure 4.29** and the catalysts will be symbolized as 5 wt% Ru/TiO_2 **(a)**,5 wt% Ru/TiO_2 **(b)** and 5 wt% Ru/TiO_2 **(c)** corresponding to the preparation method.

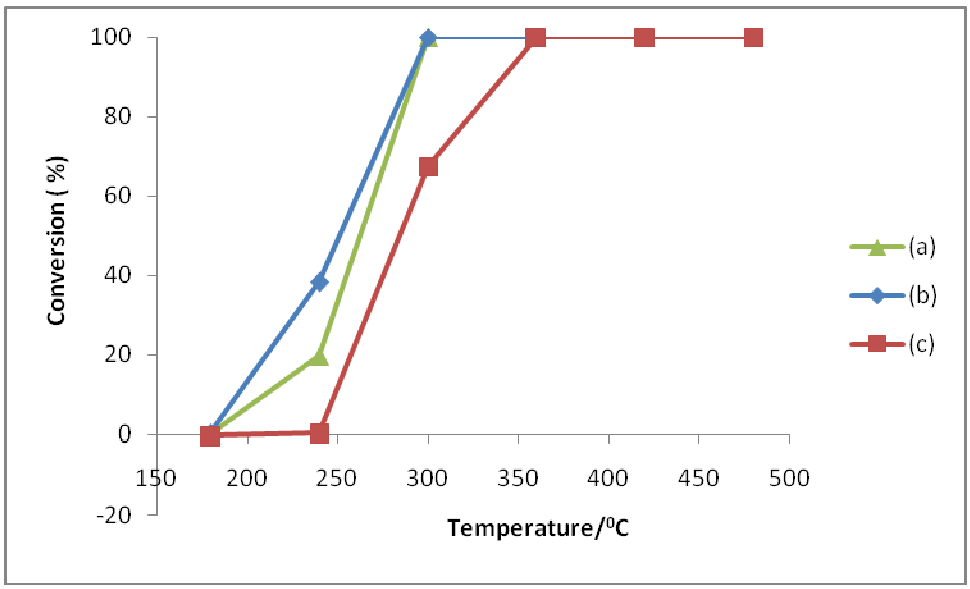


Figure 4.29: Conversions of CO as function of temperature obtained over 5 wt% Ru/TiO_2 catalysts prepared by different methods. **(a)** Dried at 110 ^{0}C for 24 hours and calcined at 400 ^{0}C for 5 hours, **(b)** dried at 110 ^{0}C for 24 hours and **(c)** prepared by deposition-precipitation method, vacuum dried for 20 hours and calcined at 400 ^{0}C for 5 hours.

All of the investigated catalyst led to the production of methane and water meaning that they had 100% methane selectivity. **Figure 4.29** was used to determine the temperature at which CO conversion to CH_4 is at 50 % (T_{50}) and the temperature at which CO conversion reaches 100 %

(T_{100}), above this temperature CO conversion remains at 100% conversion for all catalysts. The T_{50} and T_{100} values for the three catalysts are tabulated in **Table 4.5**. As can be noted from **Table 4.5**, T_{50} is reached at 260 ^{0}C and T_{100} is reached at 300 ^{0}C for the 5 wt% Ru/TiO_2 **(a)** catalyst. The 5 wt% Ru/TiO_2 **(b)** catalysts has a T_{50} value of 250 ^{0}C, this value is 10 ^{0}C lower than the T_{50} value of the 5 wt% Ru/TiO_2 **(a)** catalyst. The complete conversion of CO to CH_4 (T_{100}) is reached at 300 ^{0}C on the 5 wt% Ru/TiO_2 **(a)** catalyst**.** Based on these observations the 5 wt% Ru/TiO_2 **(b)** displays higher activity for the CO methanation reaction than the Ru/TiO_2 **(a)** catalyst. The 5 wt% Ru/TiO_2 **(c)** seems to be the least active catalyst for the CO methanation reaction because it only reaches T_{50} at 280 ^{0}C.This temperature is 20 ^{0}C higher than the T_{50} of the 5 wt% Ru/TiO_2 **(a)** and 30 ^{0}C higher than that of the 5 wt% Ru/TiO_2 **(b)** catalysts. The 5 wt% Ru/TiO_2 **(c)** catalyst displays T_{100} at 360 ^{0}C, this value is 60 ^{0}C lower than that of the 5 wt% Ru/TiO_2 **(a)** and 5 wt% Ru/TiO_2 **(b)** catalysts. The Ru/TiO_2 **(a)** and Ru/TiO_2 **(b)** catalysts were prepared by the same method but were subjected to different catalyst pre-treatment conditions. The Ru/TiO_2 **(c)** catalyst was prepared by a totally different method which is why it could be showing lower activities. The 5 wt% Ru/TiO_2 **(b)** catalyst is the most active out of the three catalysts and activity decreases in this order**:** 5 wt% Ru/TiO_2 **(b) >** 5 wt% Ru/TiO_2 **(a) >** 5 wt% Ru/TiO_2 **(c).**

There have been no studies which report the investigation of the CO methanation reaction with the use of 5 wt% Ru/TiO_2 catalysts prepared by different methods. **Table 4.5** also includes results which were obtained from other authors who investigated the activity of Al_2O_3 supported catalysts for the CO methanation reaction. Eckle et.al.,[21] investigated the activity of a 5 wt% Ru/Al_2O_3 catalyst for the CO methanation reaction and reported that 50% CO conversion occurs at 200 ^{0}C and 100% CO conversion occurs at 210 ^{0}C. Eckle et.al.,[21] used different reaction conditions (210 mg catalyst and 41.6 ml/min gas flow), different catalyst preparation (commercial catalyst) and different gas composition (0.6% CO, 2.8% N_2 and 96.6% H_2) as compared to this study. This could explain why the values reported by Eckle et.al. are different from the values in **Table 4.5**. Panagiotopoulou et.al.,[22] used similar reaction conditions (150 mg catalyst and 200 ml/min gas flow) as in this study. From the results reported by Panagiotopoulou et.al.,[22] it could be noted that T_{50} occurs at about 280 ^{0}C and T_{100} occurs at about 320 ^{0}C. Both of

these values are higher than those of the 5wt% Ru/TiO_2 **(b)** catalyst meaning that the 5wt% Ru/TiO_2 **(b)** catalyst has higher activity for the CO methanation reaction than this catalyst.

Table 4.5: Temperature for 50% and 100% CO conversion in the CO methanation reaction (5 wt% Ru/TiO_2).

Catalyst	T_{50} = 50% conversion (CO) / ^0C	T_{100} = 100% conversion (CO) / ^0C
5% Ru/TiO_2[a]	260	300
5% Ru/TiO_2[b]	250	300
5% Ru/TiO_2[c]	280	360
5% Ru/Al_2O_3 (ref. 21)	200	210
0.5% Ru/Al_2O_3 (ref. 22)	~ 280	~ 320

[a] Prepared by wetness-incipient method dried at 110 ^0C for 24 hours and calcined at 400 ^0C for 5 hours , [b] prepared by wetness-incipient method dried at 110 ^0C for 24 hours, [c] prepared by deposition-precipitation method, vacuum dried for 20 hours and calcined at 400 ^0C for 5 hours.

Based on PXRD (**Figure 4.2**) and TEM (**Figure 4.7**) results the 5 wt% Ru/TiO_2 **(b)** had the smallest Ru particles compared to the 5 wt% Ru/TiO_2 **(a)** and 5 wt% Ru/TiO_2 **(c)** catalysts**.** From the TEM images the particles appeared to be well dispersed on the TiO_2 support. Even during BET analysis the 5wt% Ru/TiO_2 **(b)** catalyst displayed the least change in BET surface area compared to the two catalysts. By looking at the TPR profiles of the three catalysts it can be noted that the 5wt% Ru/TiO_2 **(b)** had a different TPR profile (**Figure 4.10**) which had two reduction peaks, one at about 120 ^0C and the other at 330 ^0C. This could mean preparing the Ru/TiO_2 by the wetness-incipient impregnation method, drying the catalyst and not subjecting it to calcination may have led to the creation of a catalyst with small particles which are well dispersed on the support which has high activity for the CO methanation reaction.

4.3.1.2. CO methanation results of the 1wt% and 3wt% Ru/TiO_2 catalysts

In order to verify if metal loading has an effect on the catalytic activity of the Ru/TiO_2 for the CO methanation reaction, catalysts with Ru loadings of 1 wt% and 3 wt% were analyzed. **Figure 4.30** illustrates the %conversions of the 3 wt% Ru/TiO_2 catalysts as a function of temperature. By looking at **Figure 4.29** and **Figure 4.30** it can be noted that the 1wt% and the 3wt% catalysts display similar S-shaped curves as the 5 wt% catalysts.

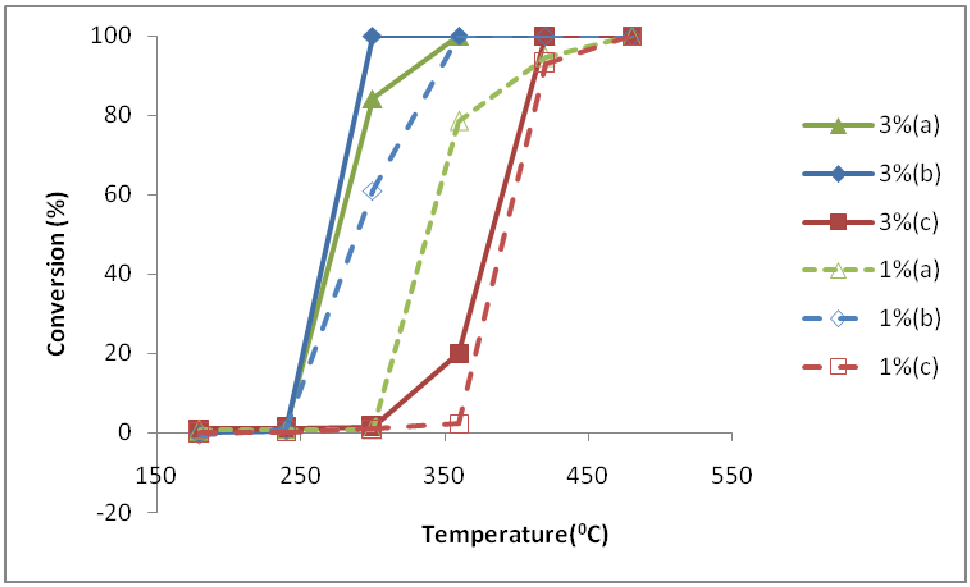


Figure 4.30: Conversions of CO as function of temperature obtained from 1 wt% and 3 wt% Ru/TiO_2 catalysts prepared by different methods. **(a)** Dried at 110 ^{0}C for 24 hours and calcined at 400 ^{0}C for 5 hours, **(b)** dried at 110 ^{0}C for 24 hours and **(c)** prepared by deposition-precipitation method, vacuum dried for 20 hours and calcined at 400 ^{0}C for 5 hours.

Figure 4.30 was used to determine the temperature at which 50 % of CO was converted to CH_4 (T_{50}) and the temperature of complete CO conversion (T_{100}). The values which were obtained are presented in **Table 4.6**. The values in **Table 4.6** illustrate that catalyst activity decreases with decreasing loading. For both the 1 wt% and the 3 wt% the Ru/TiO_2 **(b)** seems to have the highest activity while the Ru/TiO_2 **(c)** catalyst has the least activity. For the 3wt% catalysts the activity of the catalysts can be ranked as follows: 3 wt% Ru/TiO_2 **(b)** > 3 wt% Ru/TiO_2 **(a)** > 3 wt% Ru/TiO_2 **(c)**. The activity of the 1wt% catalysts is also found to decrease in this order: 1 wt% Ru/TiO_2 **(b)** > 1 wt% Ru/TiO_2 **(a)** > 1 wt% Ru/TiO_2.Compared to the 5wt% reported by Eckle et.al.,[21] the 1vwt% and 3vwt% Ru/TiO_2 catalysts have lower activity, however this could be due

to different experimental conditions and the composition of the CO/H_2 gas mixture. The 0.5wt% Ru/Al2O3 catalyst which was reported by Panagiotopoulou et.al.,[22] has lower activity than the 3wt% Ru/TiO_2 **(b)** catalyst. This could mean that the 3wt% Ru/TiO_2 (b) catalyst is the better catalyst.

Table 4.6: Temperature for 50 % and 100 % CO conversion in the CO methanation reaction (1 wt% and 3 wt% Ru/TiO_2).

Catalyst	T_{50} = 50% conversion (CO) / ^0C	T_{100} = 100% conversion (CO) / ^0C
3% Ru/TiO_2[a]	276	360
3% Ru/TiO_2[b]	270	300
3% Ru/TiO_2[c]	384	420
1% Ru/TiO_2[a]	338	480
1% Ru/TiO_2[b]	290	360
1% Ru/TiO_2[c]	392	480
5% Ru/Al_2O_3 (ref. 21)	200	210
0.5% Ru/Al_2O_3 (ref. 22)	~ 280	~ 320

[a] Prepared by wetness-incipient method dried at 110 ^0C for 24 hours and calcined at 400 ^0C for 5 hours , [b] prepared by wetness-incipient method dried at 110 ^0C for 24 hours, [c] prepared by deposition-precipitation method, vacuum dried for 20 hours and calcined at 400 ^0C for 5 hours.

4.3.1.3. CO methanation over the 5 wt% Pd/TiO_2 catalysts

The effect of the preparation method was also investigated for the Pd/TiO_2 catalysts. Data for metal loadings of 5 wt% are illustrated in **Figure 4.31**. For all catalysts the reaction seems to be initiated at about 240 ^{0}C and reaches a maximum of about 100% conversion above 420 ^{0}C. Compared to the conversion curves of the 5wt% Ru/TiO_2 catalysts (**Figure 4.29**) the conversion curves of the 5wt% Pd/TiO_2 catalysts are shifted towards higher temperatures.

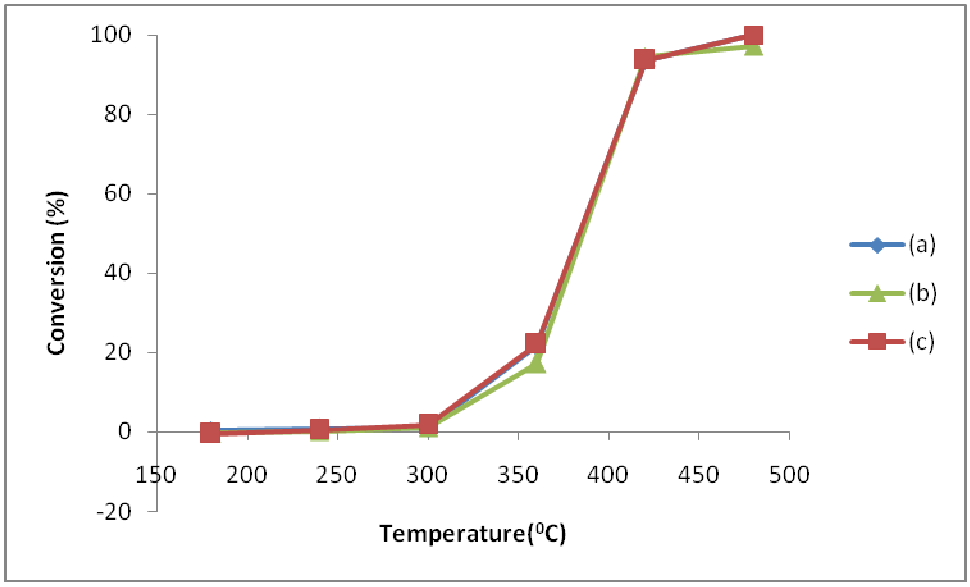


Figure 4.31: Conversions of CO as function of temperature obtained over 5 wt% Pd/TiO_2 catalysts prepared by different methods. **(a)** Dried at 110 ^{0}C for 24 hours and calcined at 400 ^{0}C for 5 hours, **(b)** dried at 110 ^{0}C for 24 hours and **(c)** prepared by deposition-precipitation method, vacuum dried for 20 hours and calcined at 400 ^{0}C for 5 hours.

In **Table 4.7** it can be seen that the 5 wt% Pd/TiO_2 catalysts do not differ in activity as their T_{50} and T_{100} values are the same. This means that preparing the Pd/TiO_2 catalysts by different methods did not have an effect on their catalytic activity for the CO methanation reaction. According to Shen et.al.,[23] preparing the Pd/TiO_2 catalyst by the deposition-precipitation method leads to the creation of cationic palladium species which are not present when the Pd/TiO_2 catalyst is prepared by the wet-incipient method. Shen et al. states that these cationic species enhance the selectivity and activity of the Pd/TiO_2 catalyst in the CO methanation reaction.

However this is not evident in our findings as all of the catalysts have the same activity. Panagiotopoulou et.al.,[22] investigated the activity of a 0.5wt% Pd/Al_2O_3 catalysts for the CO methanation reaction and reported that this catalyst is inactive for the CO methanation reaction because temperatures higher than 440 ^{0}C are required to obtain conversions higher than 10%. The 5wt% Pd/TiO_2 catalysts displays better activity because T_{50} is reached at 384 ^{0}C and T_{100} is reached at 480 ^{0}C.

Table 4.7: Temperature for 50 % and 100 % CO conversion in the CO methanation reaction (5 wt% Pd/TiO_2).

Catalyst	T_{50} = 50% conversion (CO) / ^{0}C	T_{100} = 100% conversion (CO) / ^{0}C
5% Pd/TiO_2[a]	384	480
5% Pd/TiO_2[b]	384	480
5% Pd/TiO_2[c]	384	480
0.5% Pd/Al_2O_3 (ref. 22)	>440	>440

[a] Prepared by wetness-incipient method dried at 110 ^{0}C for 24 hours and calcined at 400 ^{0}C for 5 hours , [b] prepared by wetness-incipient method dried at 110 ^{0}C for 24 hours, [c] prepared by deposition-precipitation method, vacuum dried for 20 hours and calcined at 400 ^{0}C for 5 hours.

4.3.1.4. CO methanation results of the 1wt% and 3wt% Pd/TiO_2 catalysts

The effect of metal loading was also investigated for the Pd/TiO_2 catalyst. **Figure 4.32** displays the CO conversions of the 1 wt% and 3 wt% Pd/TiO_2 catalysts. The activity of the Pd/TiO_2 catalysts decreases with decreasing loadings. Unlike the 1 wt% and 3 wt% Ru/TiO_2 catalysts the 1wt% and 3 wt% Pd/TiO_2 do not reach T_{100} within the investigated temperature range. The 3 wt% Pd/TiO_2 **(a)** catalyst shows 97% CO conversion at 480 ^{0}C and a T_{50} value of 398 ^{0}C. The 3 wt% Ru/TiO_2 **(b)** and 3 wt% Ru/TiO_2 **(c)** catalysts show 89% CO conversion at 480 ^{0}C and T_{50} values of 404 ^{0}C and 390 ^{0}C respectively. Even though the 1 wt% and 3 wt% Pd/TiO_2 catalysts are not as active as the 1 wt% and 3 wt% Ru/TiO_2 catalysts they display better activity than the

Pd/Al_2O_3 catalyst which was reported by Panagiotopoulou et.al. because they have conversions which are higher than 10% at temperatures higher than 440 ^{0}C.

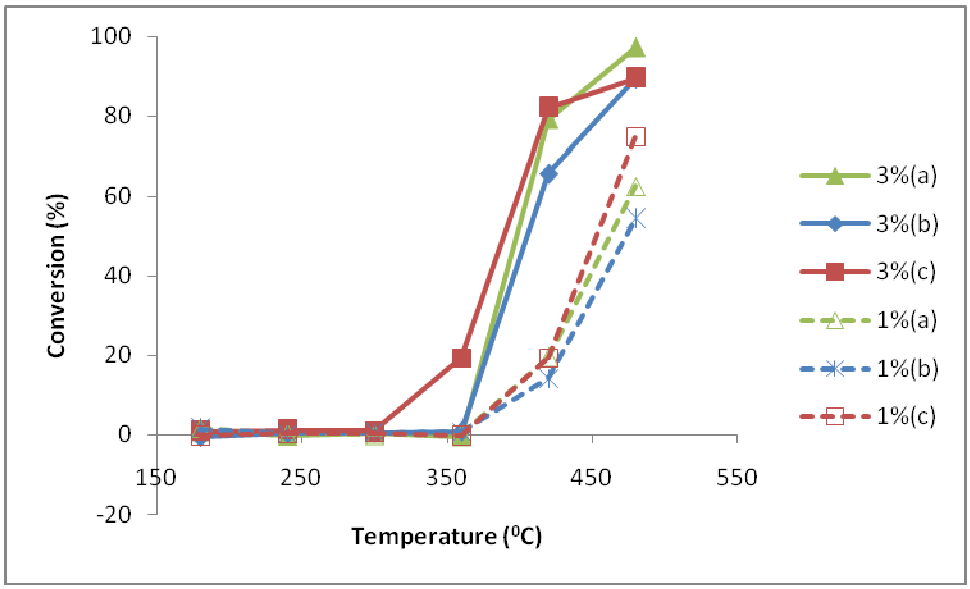


Figure 4.32: Conversions of CO as function of temperature obtained over 1 wt% and 3 wt% Pd/TiO_2 catalysts prepared by different methods. **(a)** Dried at 110 ^{0}C for 24 hours and calcined at 400 ^{0}C for 5 hours, **(b)** dried at 110 ^{0}C for 24 hours and **(c)** prepared by deposition-precipitation method, vacuum dried for 20 hours and calcined at 400 ^{0}C for 5 hours.

It is possible that the difference in activity displayed by the calcined Ru/TiO_2 catalysts could be due to a decreased amount of Ru in the sample due to the evaporation of the RuO_2 species during calcination. To verify this, we subjected the calcined Ru/TiO_2 catalyst to TGA analysis under conditions that are similar to the calcination process (400 ^{o}C for 5 hours). From the data a weight gain (< 5%) was noted which might be due to oxidation of Ru. The data thus suggests that RuO_2 does not evaporate under the calcination conditions. It is also possible that the difference in activity of the differently prepared catalysts was due to varying Ru loadings, i.e. that the Ru loadings did not match the predicted amounts expected. We attempted to verify the loadings with the use of ICP. This attempt was not productive, as the ICP instrument did not produce relliable data for the Ru; the operator suggested that this relates to the analysis of the Ru. This will need to be confirmed.

4.3.1.5. CO methanation results of the 1wt%, 3wt% and 5wt% Rh/TiO_2 catalysts

The activity of Rh/TiO_2 catalysts with different metal loadings was investigated. These were all measured as catalysts subjected to the same preparation method. Results presented in sections **4.3.1.1.** and **4.3.1.2.** demonstrate that the Ru/TiO_2 **(b)** catalysts have the highest activity for the CO methanation reaction. Due to this, only the Rh/TiO_2 catalysts prepared by the wet-incipient method followed by drying at 110 ^{0}C for 24 hours with no calcination were investigated. We also only investigated these catalysts in sections **4.3.2.** and **4.3.3** due to the same reason. The prepared catalysts had varying metal loadings (1 wt%, 3 wt% and 5 wt%) to examine the effect of metal loading on the Rh/TiO_2 catalyst activity. The results which were obtained from the analysis are plotted in **Figure 4.33**.

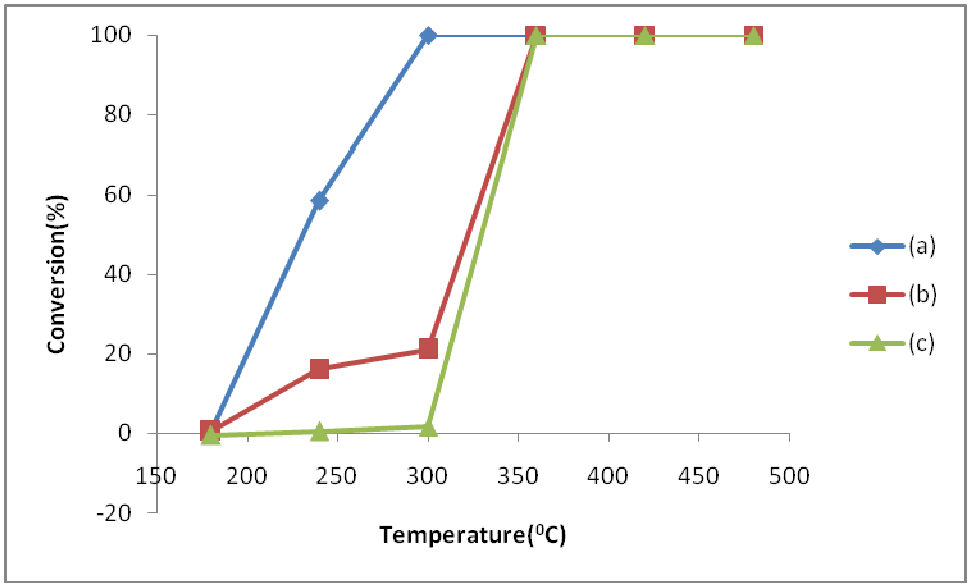


Figure 4.33: Conversions of CO as function of temperature obtained over Rh/TiO_2 catalysts with different metal loadings. **(a)** 5 wt %,**(b)** 3 wt% and **(c)** 1 wt%.

The temperatures at which 50 % CO conversion (T_{50}) and 100% CO conversion (T_{100}) occurs were extrapolated from **Figure 4.33**. The values are tabulated in **Table 4.8**.The catalytic activity of the Rh/TiO_2 catalysts decreases with decreasing metal loadings. The 5wt% Rh/TiO_2 catalyst is the most active catalyst for the CO methanation reaction as it displays a T_{50} value of 230 ^{0}C and a T_{100} value of 300 ^{0}C.The 1wt% and 3wt% have a T_{100} temperature of 360 ^{0}C and T_{50} temperatures of 330 ^{0}C and 320 ^{0}C respectively. Panagiotopoulou et.al.,[22] also investigated the catalytic activity of a 0.5wt% Rh/Al_2O_3 catalyst for the CO methanation reaction. The results

show that T_{50} occurs around 280 ^{0}C and T_{100} is reached at about 320 ^{0}C. Compared with lower loading catalysts the 5wt% Rh/TiO_2 catalyst is a better catalyst than the Rh/Al_2O_3 catalyst.

Table 4.8: Temperature for 50 % and 100 % CO conversion in the CO methanation reaction (1 wt%, 3 wt% and 5 wt% Rh/TiO_2).

Catalyst	T_{50} = 50% conversion (CO) / ^{0}C	T_{100} = 100% conversion (CO) / ^{0}C
5% Rh/TiO_2[b]	230	300
3% Rh/TiO_2[b]	320	360
1% Rh/TiO_2[b]	330	360
0.5% Rh/Al_2O_3 (ref. 22)	~280	~320

[b] Prepared by wetness-incipient method dried at 110 ^{0}C for 24 hours and not subjected to calcination.

4.3.1.6. CO methanation results of the 1 wt%, 3 wt% and 5 wt% Pt/TiO_2 catalysts

Similar studies were performed on 1 wt%, 3 wt% and 5 wt% Pt loaded TiO_2 catalysts. The results are plotted in **Figure 4.34**. Only the catalysts which were prepared by the wet incipient method and uncalcined were investigated as it was noted in sections **4.3.1.1.** and **4.3.1.2** that this preparation method leads to high CO methanation activity. An attempt was made to extrapolate the T_{50} and T_{100} values (**Table 4.9**) from **Figure 4.34** however as it can be observed the Pt/TiO_2 catalysts do reach T_{100} within the investigated temperature range. From **Figure 4.34** it can be noted that out of the three catalysts the 5 wt% catalyst is the most active as it displays a conversion of 13% at 360 ^{0}C. **Table 4.9** illustrates that the 1 wt% catalyst is the least active because the 3 wt% and the 5 wt% catalyst reach T_{50} values at 468 ^{0}C while temperature higher than 480 ^{0}C are needed for the 1 wt% catalyst to reach its T_{50} value. Compared with the 0.5 wt%

Pt/Al_2O_3 catalyst which was investigated by Panagiotopoulou et.al.,[22] the Pt/TiO_2 catalyst are less active for the CO methanation reaction.

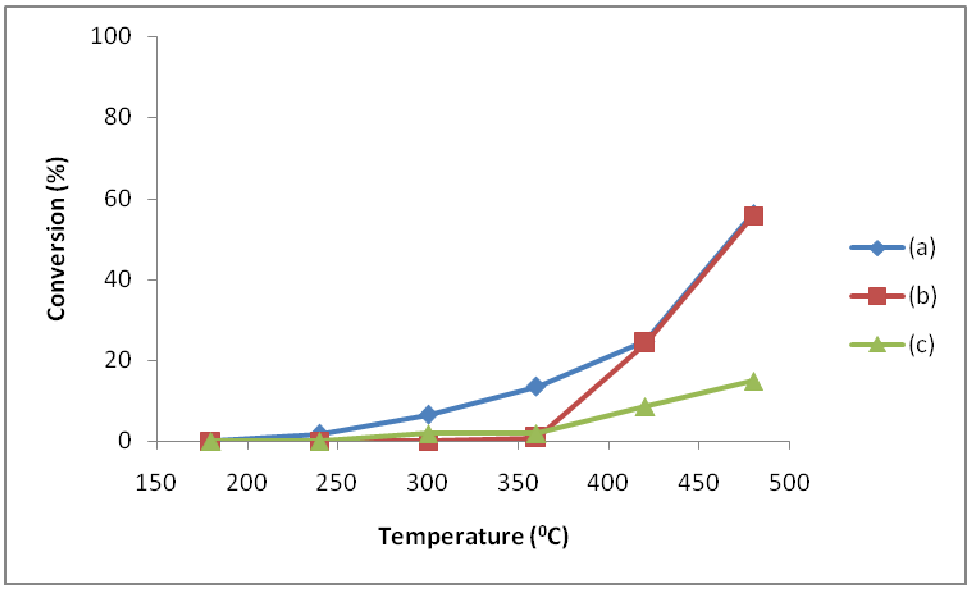


Figure 4.34: Conversions of CO as a function of temperature obtained over Pt/TiO_2 catalysts with different metal loadings. **(a)** 5 wt%, **(b)** 3 wt% and **(c)** 1 wt%.

Table 4.9: Temperature for 50 % and 100 % CO conversion in the CO methanation reaction (1 wt% , 3 wt% and 5 wt% Pt/TiO_2).

Catalyst	T_{50} = 50% conversion (CO) / ^0C	T_{100} = 100% conversion (CO) / ^0C
5% Pt/TiO_2[b]	468	>480
3% Pt/TiO_2[b]	468	>480
1% Pt/TiO_2[b]	>480	>480
0.5% Pt/Al_2O_3 (ref. 22)	~280	~320

[b] Prepared by wetness-incipient method dried at 110 ^0C for 24 hours and not subjected to calcination.

4.3.1.7. Summary of the CO methanation results of the 4 PGMs on TiO_2 support catalysts.

The results of the four different PGM catalysts with a metal loading of 5wt% which were prepared by the wet-incipient method (uncalcined) are summarized in **Figure 4.35**. From **Figure 4.35** it can be seen that the Rh/TiO_2 and the Ru/TiO_2 catalysts are significantly more active than the Pd/TiO_2 and Pt/TiO_2 catalysts. The conversion curves of these catalysts lie at higher temperatures as compared to the Rh and Ru catalysts.

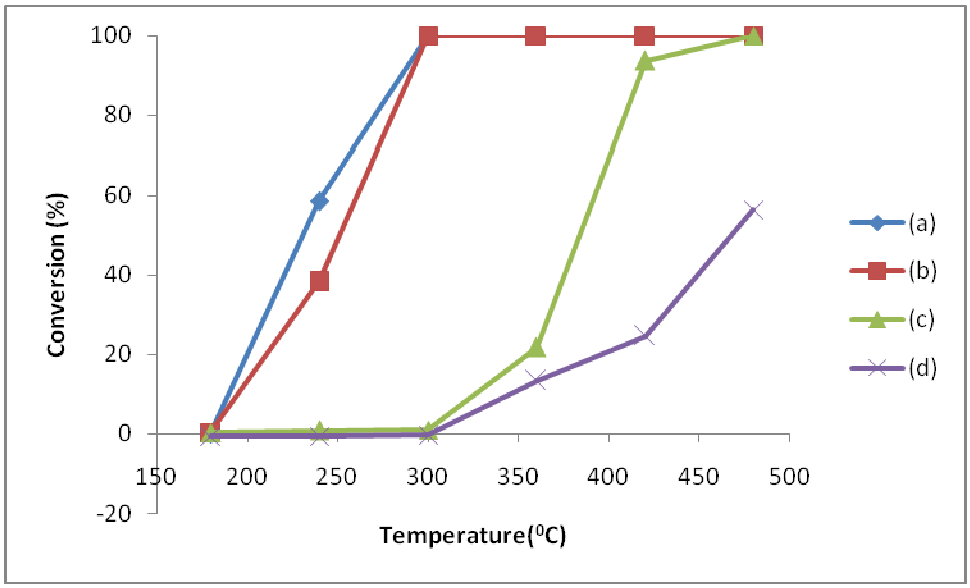


Figure 4.35: Conversions of CO as a function of temperature obtained over different PGMs on TiO_2 support. **(a)** 5 wt% Rh/TiO_2, **(b)** 5 wt% Ru/TiO_2,**(c)**5 wt% Pd/TiO_2 and **(d)** 5 wt% Pt/TiO_2.

For a quantitative comparison, T_{50} and T_{100} values of the individual catalysts are summarized in **Table 4.10**. From **Table 4.10** it can be noted that the Rh/TiO_2 catalyst is slightly more active than the Ru/TiO_2 catalyst as it has a T_{50} value of 230 ^{0}C and the Ru/TiO_2 has a T_{50} value of 250 ^{0}C leading to a difference of 20 ^{0}C. Both catalysts reach 100% CO conversion (T_{100}) at 300 ^{0}C. The two catalysts (Ru &Rh) are more active than the Pd and Pt catalysts as the T_{50} values of these catalysts are 384 ^{0}C and 468 ^{0}C respectively. Even the T_{100} values of Pd and Pt catalysts are high, 480 ^{0}C for the Pd catalysts and higher than 480 ^{0}C for the Pt catalyst. From **Figure 4.35** and **Table 4.10** it can be noted that the activity of the catalysts decreases in this order: $Rh/TiO_2 \sim Ru/TiO_2 > Pd/TiO_2 > Pt/TiO_2$. This ranking is similar to the ranking which was presented by

Panagiotopoulou et.al.,[22] for the Al_2O_3 supported PGMs, which was Ru ~ Rh > Pt > Pd. This ranking also agrees with the ranking reported by Mckee,[24] in which he found the order of activity to be Ru>>Rh ~ Ir > Pt ~ Pd. Mckee,[24] investigated the co-adsorption and interaction of CO and H_2 with the use of unsupported PGMs. Vannice,[25] determined the specific activities of Al_2O_3 supported group five metals in the synthesis of hydrocarbons from CO/H_2 mixtures and found the order of activity to be Ru >> Rh ~ Pd > Pt ~Ir which is also similar to the ranking reported in this study.

Table 4.10: Summary of the 50% and 100% CO conversion in the CO methanation reaction for the 5wt% Rh, Ru, Pd and Pt TiO_2 supported catalysts.

Catalyst	T_{50} = 50% conversion (CO) / ^0C	T_{100} = 100% conversion (CO) / ^0C
Rh/TiO_2[b]	230	300
Ru/TiO_2[b]	250	300
Pd/TiO_2[b]	384	480
Pt/TiO_2[b]	468	>480

[b] Prepared by wetness-incipient method dried at 110 ^0C for 24 hours and not subjected to calcination.

According to Mckee,[24] and Vannice,[25] different experimental conditions and catalyst preparation may affect the ranking of the catalysts, which might explain the slight differences in the rankings. Based on findings from Ojeda et.al.,[26] who investigated the effect of calcining a 3wt% Rh/Al_2O_3 catalysts in the CO/H_2 reaction and the effect of the particle size of a 2wt% Rh/Al_2O_3 catalysts in the CO/H_2 reaction,[27] catalyst preparation is an important parameter in the CO/H_2 reaction. Ojeda et.al., noted that CO conversion and methane selectivity decreases on larger Rh particles which were obtained by calcining the Rh/Al_2O_3 catalyst,[26] or by preparing the Rh/Al_2O_3 catalysts by the microemulsion technology.[27] In addition from X-ray photoelectron spectroscopy (XPS) studies Ojeda et.al., noted that by decreasing the Rh particle size with the use of the microemulsion technique, the electronic metal-support interaction was also increased and this led

to partially oxidized Rh particles.[27] This could mean that preparing the catalysts by the wet-incipient method and not calcining (refer to section 4.2) changed their properties and influenced their activity in the CO methanation reaction. This could also explain why some of the results reported in this section are slightly different from literature results.[21 &22]

According to Mckee,[24] the high activity of the Rh and Ru catalysts is due to their lower affinity for CO which enables an interaction to take place between adsorbed hydrogen and CO. The low activity of the Pd and Pt catalysts is due to their high affinity for CO which then displaces hydrogen from the adsorbed layer and thus preventing an interaction from occuring.[24] This explanation corresponds to the volcano-type curve (**Figure 1.6**, section **1.5**) which was created by Bligaard et.al.,[28] and Norskov et.al.,[29] which relates catalyst activity with the ability of the catalyst to form chemical bonds with the reactants, the intermediates or the products. Vannice,[30] suggested that catalytic activity of the transition metals is related to the molecular CO adsorption energy. Bligaard et.al.,[28] and Norskov et.al.,[29] performed calculations and noted that while there is no correlation between catalytic activity and molecular CO adsorption energy, there is a correlation between catalytic activity and the dissociative adsorption energy of CO. They created the volcano curve which is an important tool in heterogenous catalysts because it can be used as a record for the reaction energies for dissociative CO chemisorptions. The volcano curve is a plot of the activities of different supported transition metals as a function of the reaction energy for dissociative CO chemisorptions.[28] From the volcano curve it can be seen that the maximum activity corresponds to Ru and Rh while lower activities correspond to Pd and Pt. This agrees with the experimental results presented in this study.

4.3.2: CO_2 methanation results

The methanation of CO_2 was studied using the same catalysts (prepared by wet-incipient and uncalcined) as described in section **4.3.1** for the CO methanation reaction. In order to compare CO_2 methanation with CO methanation, data obtained from the separate reactions was plotted in one plot.

4.3.2.1. CO_2 methanation results of the Rh/TiO_2 catalyst.

The CO and CO_2 methanation results were compared for the Rh/TiO_2 catalysts (**Figure 4.36)**. **Figure 4.36** illustrates that the Rh/TiO_2 catalysts have higher activities for CO methanation than CO_2 methanation. For the 5 wt% catalyst CO conversion reaches 100 % conversion above 300 ^{0}C, while CO_2 methanation only undergoes 40 % conversion above 360 ^{0}C. In addition further CO_2 methanation only occurs when CO methanation has reached a maximum. The CO and CO_2 conversion curves of the 1 wt% and 3 wt% Rh/TiO_2 catalysts are shifted towards higher temperatures as compared to the 5 wt% catalyst. Compared to the 1 wt% and 3 wt% catalysts the 5 wt% Rh/TiO_2 catalyst has the largest temperature window at which CO methanation is at a maximum while CO_2 methanation is at a minimum. This temperature window runs from 240 ^{0}C to 480 ^{0}C.

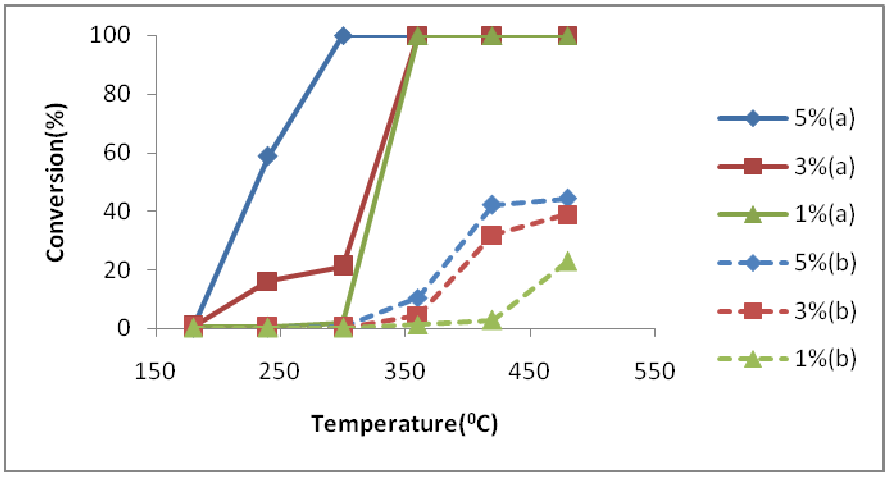


Figure 4.36: Conversions of CO_2 and CO as a function of temperature. The Rh/TiO_2 catalysts were prepared by the wet-incipient method and not calcined. **(a)** CO methanation and **(b)** CO_2 methanation. Feed composition: 25 % CO_2 and 75 % H_2.

In order to determine which Rh/TiO_2 catalyst had the highest selectivity for the CO methanation reaction as compared to the CO_2 methanation reaction, we calculated R values by dividing CO conversions with CO_2 conversions from the individual catalysts corresponding to the investigated temperatures (Equation **(4.5)**). It was assumed that the higher R value is (i.e. the more it approaches infinity), it would mean that the catalyst has a higher selectivity for CO methanation compared to CO_2 methanation.

$$\mathbf{R} = \frac{\%CO\ conversion}{\%CO_2\ conversion} \rightarrow \infty$$

The results which were obtained are presented in **Figure 4.37**. As it can be noted the 5 wt% Rh/TiO_2 has the highest R value (R = 293) maximum at 240 ^{0}C compared to the two lower loading catalysts. The 3wt% Rh/TiO_2 catalyst has the second highest maximum R value (R = 211) at 300 ^{0}C and the 1wt% Rh/TiO_2 catalyst has the lowest R value (R = 80) maximum at 360 ^{0}C. This means that the 5wt% Rh/TiO_2 catalyst is more selective to CO methanation as compared to CO_2 methanation than the 1wt% and 3wt% Rh/TiO_2 catalysts.

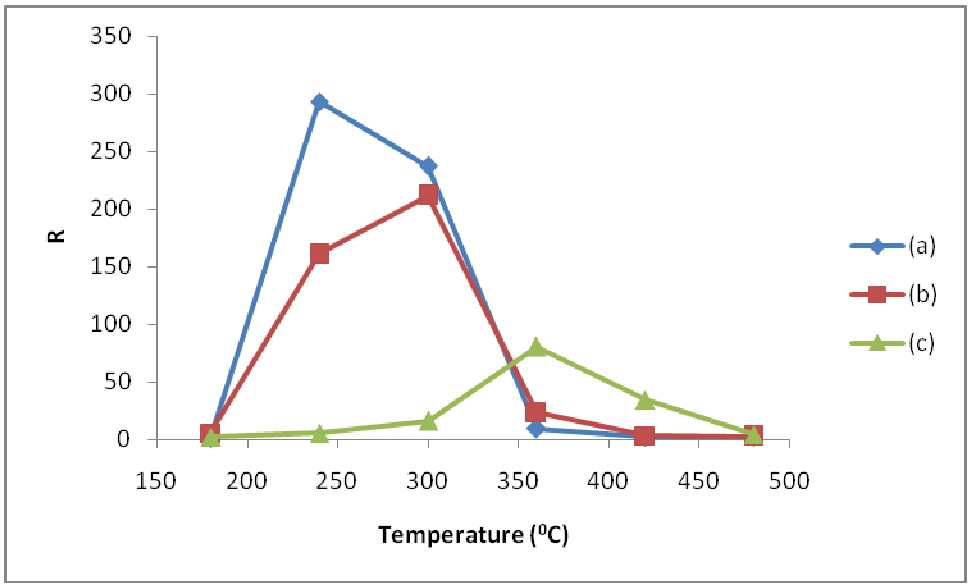


Figure 4.37: Comparison of the R values (R = CO conversion/CO_2 conversion) of the Rh/TiO_2 catalysts as a function of temperature. The Rh/TiO_2 catalysts were prepared by the wet-incipient method and not calcined.(a) 5wt% Rh/TiO_2 ,(b) 3wt% Rh/TiO_2 and (c) 1wt% Rh/TiO_2.

4.3.2.2. CO_2 methanation results of the Ru/TiO_2 catalysts.

Figure 4.38 shows the CO_2 methanation conversion curves together with the CO methanation conversion curves. As with the 5 wt% Rh/TiO_2 catalyst, the 5 wt% Ru/TiO_2 catalyst also has a high activity for CO methanation and a markedly lower activity for CO_2 methanation. Even here the temperature window at which CO methanation is favoured is quite large. CO_2 methanation does not reach 100% conversion as is the case with CO methanation, it only reaches around 40% conversion under the conditions studied. Similar to the 1 wt% and 3 wt% Rh/TiO_2 catalysts, the CO and CO_2 conversion curves of the 1 wt% and 3 wt% catalysts are shifted towards higher temperatures. In order to determine which of the three Ru/TiO_2 catalysts was more selective for the CO methanation reaction we calculated R values similar to the Rh/TiO_2 catalysts and the results which were obtained are presented in **Appendix A1**. The 5 wt% Ru/TiO_2 catalysts has the highest R value maximum (R = 192) at 240 ^{0}C and the 1 wt% and 3 wt% displayed maximum R values of R=12 and R = 16 at 300 ^{0}C respectively. This means that the 5 wt% Ru/TiO_2 is more selective to the CO methanation than the 1 wt% and 3 wt% catalysts.

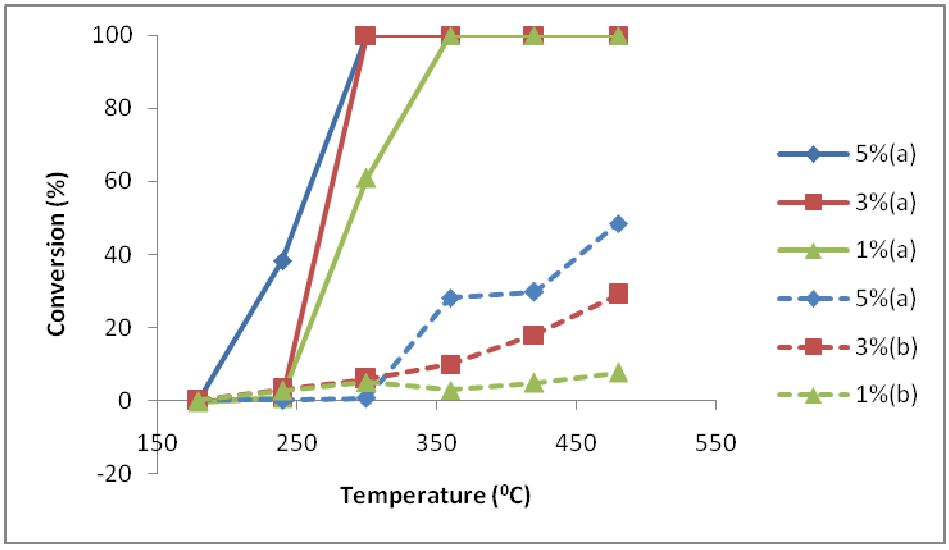


Figure 4.38: Conversions of CO_2 and CO as a function of temperature. The Ru/TiO_2 catalysts were prepared by the wet-incipient method and not calcined. **(a)** CO methanation and **(b)** CO_2 methanation. Feed composition: 25 % CO_2 and 75 % H_2.

4.3.2.3. CO_2 methanation results of the Pd/TiO_2 catalysts.

The CO methanation and CO_2 methanation conversion curves obtained from the Pd/TiO_2 catalyst are plotted in **Figure 4.39**. The 5 wt% Pd/TiO_2 catalyst also displays higher activity for CO methanation and not CO_2 methanation. But the maximum for CO_2 methanation is lower (about 20% conversion) than that of the 5 wt% Rh/TiO_2 catalyst. In addition the temperature window at which CO methanation is at a maximum is not as wide as that of the 5 wt% Rh/TiO_2 catalyst. Nonetheless as with the Rh/TiO_2 catalyst, CO_2 methanation only takes place after significant CO methanation has reached a maximum. As with the other above catalysts, the lower loading catalysts (1 wt% and 3 wt%) have conversions which lie at higher temperatures. Similar to the Rh/TiO_2 and Ru/TiO_2 catalysts R values were calculated for the Pd/TiO_2 catalysts (**Appendix A2**).From the R values it could be noted that the Pd/TiO_2 catalysts are not that selective to the CO methanation reaction as compared to the CO_2 methanation reaction. The 5wt% Pd/TiO_2 catalyst has a low maximum R value (R = 5) at 420 ^{0}C, the 3 wt% Pd/TiO_2 catalyst has a maximum R value of R = 4 at 420 ^{0}C and the 1wt% has a maximum R value of R = 2 at 420 ^{0}C.

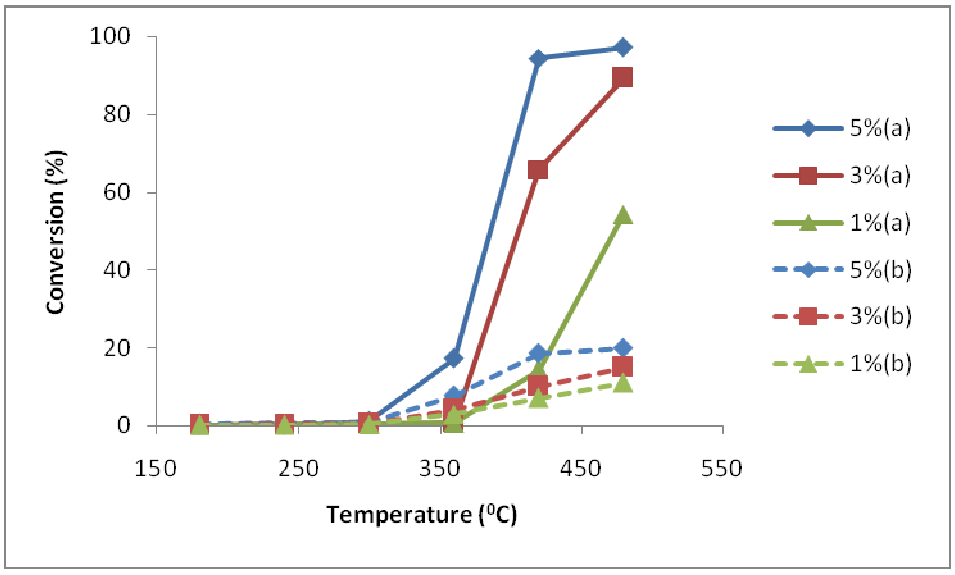


Figure 4.39: Conversions of CO_2 and CO as a function of temperature for the Pd/TiO_2 catalysts. The catalysts were prepared by wet-incipient method and not calcined. **(a)** CO methanation and **(b)** CO_2 methanation. Feed composition: 25 %CO_2 and 75 %H_2.

4.3.2.4. CO_2 methanation results of the 5 wt% Pt/TiO_2 catalyst.

The CO_2 methanation reaction was also studied with the Pt/TiO_2 catalysts (**Figure 4.40)**. Unlike the other catalysts (Rh, Pd and Ru) the Pt/TiO_2 catalysts seem to have a higher tendency for CO_2 methanation below 360 ^{0}C. The CO_2 methanation conversion curve lies above the CO methanation conversion curve from 180 ^{0}C to about 360 ^{0}C. Above 420 ^{0}C the Pt/TiO_2 catalysts show higher activities for CO methanation. Furthermore unlike the other catalysts the very important temperature window at which CO methanation is at a maximum and CO_2 methanation is a minimum does not exist. As it can be noted from **Figure 4.40** the Pd/TiO_2 catalysts have higher selectivity for the CO_2 methanation as compared to the CO methanation reaction. The Pt/TiO_2 catalysts displayed very low R values (**Appendix A3**), meaning that the Pt/TiO_2 catalysts are more selective towards the CO_2 methanation reaction.

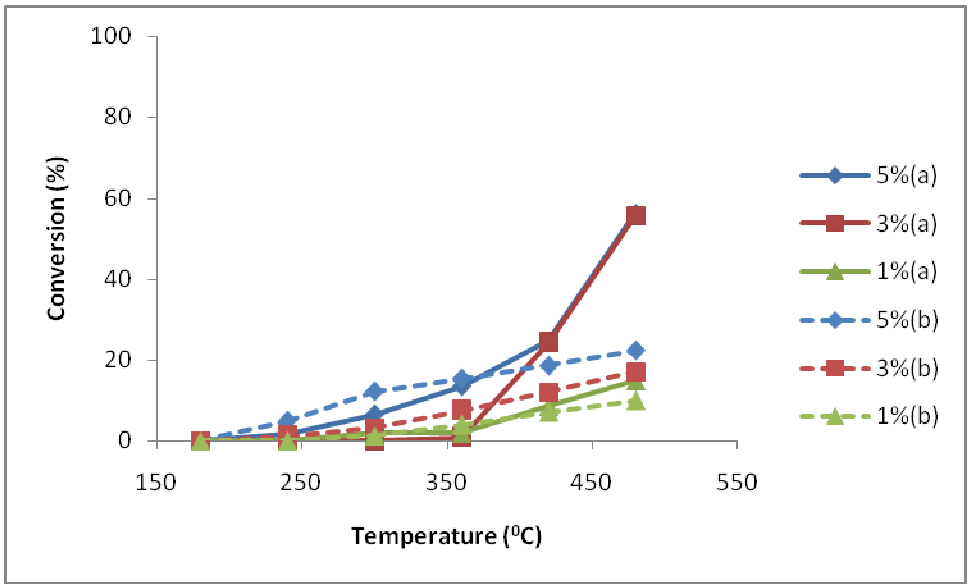


Figure 4.40: Conversions of CO_2 and CO as a function of temperature for 5 wt%Pt/TiO_2 .The catalysts prepared by wet-incipient method and not calcined. **(a)** CO methanation and **(b)** CO_2 methanation. Feed composition: 25 % CO_2 and 75 % H_2.

4.3.2.5. Summary of the CO_2 methanation results of the 4 PGMs on TiO_2 support catalysts.

In this section and throughout the remainder of this study we only investigated the performance of the 5wt% catalysts, since it was noted in the above sections that the activity and selectivity of the catalytsts for CO methanation decreases with decreasing metal loadings. In order to summarize the CO_2 methanation results of the TiO_2 supported 5 wt% PGM catalysts, we determined the CO_2 conversions at 360 ^{0}C and at 480 ^{0}C from **Figure 4.36** to **Figure 4.40** because CO_2 methanation increases with increasing temperature and the catalyst do not show 50% (T_{50}) and 100% (T_{100}) CO_2 conversions within the investigated temperature range. The CO_2 conversions at 360 ^{0}C and 480 ^{0}C are tabulated in **Table 4.11** and are labeled as $Conv_{360}$ and $Conv_{480}$ respectively. **Table 4.11** also includes the CO_2 conversions at 360 ^{0}C and 480 ^{0}C which were determined from the literature.

Table 4.11: CO_2 conversions at 360 ^{0}C and 480 ^{0}C in the CO_2 methanation reaction for the for the 5 wt% Rh, Ru, Pd and Pt, TiO_2 supported catalysts.

Catalyst	$Conv_{360}$ = CO_2 conversion at 360^{0}C / %	$Conv_{480}$ = CO_2 conversion at 480^{0}C / %
Rh/TiO_2[b]	10	44
Ru/TiO_2[b]	28	48
Pt/TiO_2[b]	15	22
Pd/TiO_2[b]	18	20
Rh/Al_2O_3 (ref.22)	~20	~50
Ru/Al_2O_3(ref.22)	~30	~50
Pt/Al_2O_3(ref.22)	~10	~40
Pd/Al_2O_3(ref.22)	-	-

[b] Prepared by wetness-incipient method dried at 110 ^{0}C for 24 hours and not subjected to calcination.

Table 4.11 illustrates that the $Conv_{360}$ and $Conv_{480}$ values of the Ru/TiO_2 catalyst are quite high as compared to the other catalysts; the Rh/TiO_2 catalyst has the second largest values then followed by the Pd/TiO_2 and the Pt/TiO_2 catalysts. The conversions which are reported for the CO_2 methanation reaction in **Table 4.11** are comparable to those which were determined from Panagiotopoulou et. al., [22] they did not report the CO_2 conversion for the Pd/Al_2O_3 catalyst because it displayed low activities which were lower than 5% at 450 ^{0}C. The order of activity of the catalysts for the CO_2 methanation reaction can be ranked as: $Ru/TiO_2 > Rh/TiO_2 > Pd/TiO_2 \sim Pt/TiO_2$. Panagiotopoulou et. al., [22] found the order of activity for the CO_2 methanation reaction of the noble metals on Al_2O_3 support to vary in this order: Ru > Rh > Pt > Pd. Leitenburg et. al.,[31] found the activity of CeO_2 supported noble metals to decrease in this order: Ru >Rh >> Ir ~ Pd > Pt. Similar ordering of the noble metals on Al_2O_3 support was reported by Solymosi et.al.,[32] who found the order to be : Ru> Rh>> Pt ~ Ir ~ Pd. This illustrates that the ordering of the activity of the PGM catalysts on TiO_2 support for the CO_2 methanation reaction in this present study is comparable to literature results.

All of the investigated catalysts led to the production of methane and no other hydrocarbon was detected. However considerable amounts of CO could be detected above 300 ^{0}C during the CO_2 methanation reactions of the individual catalysts. **Figure 4.41** illustrates the results obtained from the Pt/TiO_2 catalyst during the CO_2 methanation reaction at 480 ^{0}C. As it can be noted in addition to CH_4, CO was also produced.

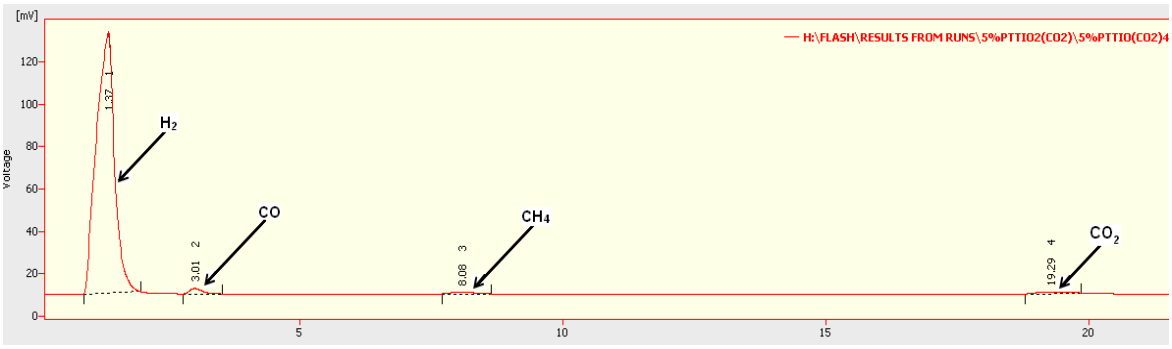


Figure 4.41: CO_2 methanation results obtained from the 5wt% Pt/TiO_2 catalyst at 480 ^{0}C.

The CO is detected during the CO_2 methanation reaction because CO_2 is converted to CO via the RWGS reaction.[22] In order to compare the extent of CO production by the individual catalysts, the degree of CO production from the separate reactions was calculated in terms of CO yield and

the results are presented in **Figure 4.42**. As can be observed the extent of CO production increases with increasing temperature for all of the catalysts. However the production of CO at the expense of CH_4 is more pronounced for the Pt and Pd catalysts. The reason being that the Pt and Pd catalysts have higher selectivity for CO production via the RWGS reaction.[22] The Ru and Rh catalysts also lead to the production of CO as an intermediate which is converted to CH_4,[22] which is why the extent of CO production is not so high for these catalysts. The Ru and Rh catalysts have higher selectivity for methane production.[22] Panagiotopoulou et. al., [22] reported the order of selectivity for methane production to vary in the order of: Ru> Rh >> Pd > Pt. This is also comparable to the selectivity of CH_4 production in this study which can be ranked as: Rh ~ Ru > Pd > Pt. The formation of CO in the CO_2 methanation reaction has been extensively reported in literature.[22]

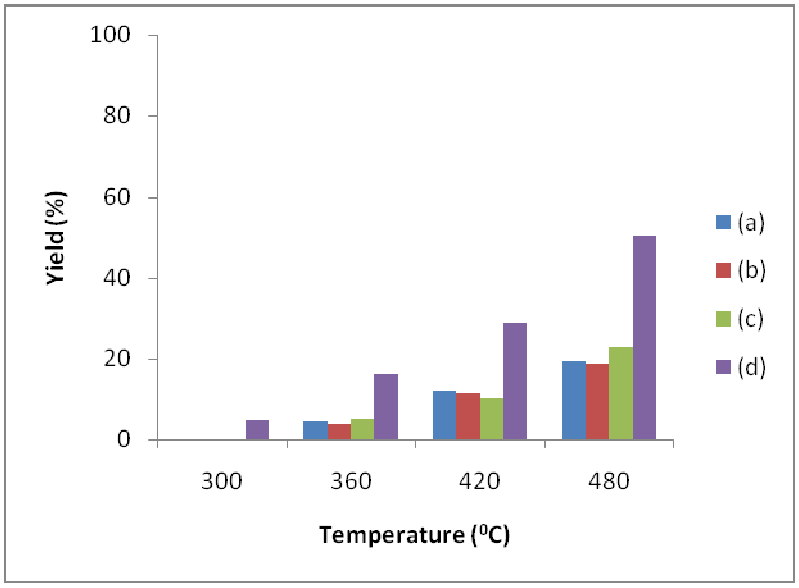


Figure 4.42: Percentage yield of CO produced by the RWGS reaction during CO_2 methanation reaction. **(a)** 5 wt% Rh/TiO_2, **(b)** 5 wt% Ru/TiO_2 , **(c)** 5 wt% Pd/TiO_2 and **(d)** 5 wt% Pt/TiO_2.

In order to compare the R values obtained from the 5 wt% TiO_2 supported PGM catalysts their R values were plotted in **Figure 4.43** as a function of temperature. As it can be noted the 5 wt% Rh and Ru catalysts have the highest maximum R values 293 and 192 at 420 ^{0}C respectively. This means that the 5wt% Rh and Ru catalysts have higher selectivity for the CO methanation

reaction as compared to the CO_2 methanation reaction. Compared to the 5 wt% Rh and Ru catalysts the Pd and Pt catalysts have lower selectivity for the CO methanation reaction because as it can be noted from **Figure 4.43** they have very low R values. The selectivity of the 5wt% TiO_2 supported PGM catalysts for CO methanation compared to CO_2 methanation can be ranked as follows: Rh/TiO_2 >Ru/TiO_2 > Pd/TiO_2 >Pt/TiO_2.

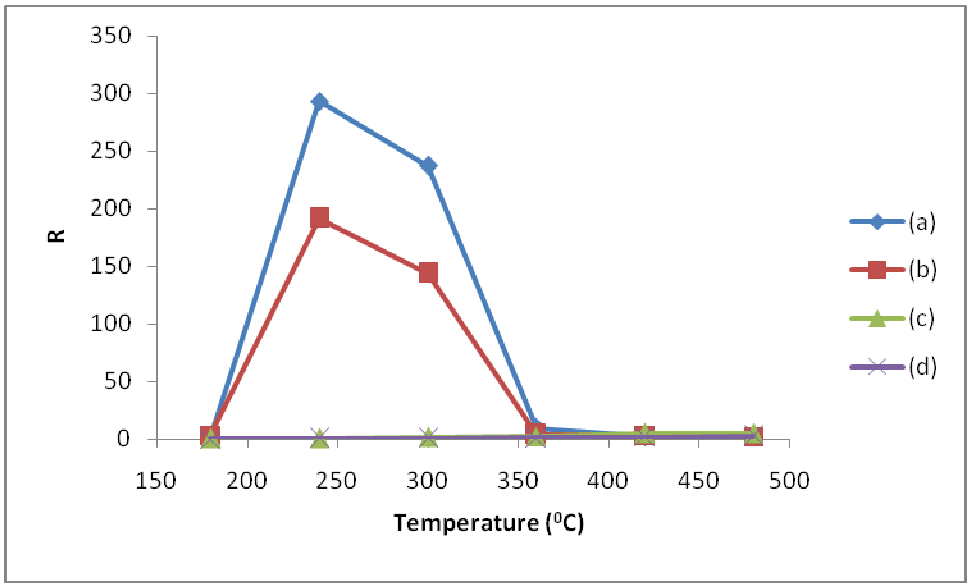


Figure 4.43: Comparison of the R values (R = CO conversion/CO_2 conversion) of the 5 wt% TiO_2 supported PGM catalysts as a function of temperature. The catalysts were prepared by the wet-incipient method and not calcined.(a) 5 wt% Rh/TiO_2 ,(b) 5 wt% Ru/TiO_2 ,(c) 5 wt% Pd/TiO_2 and (d) 5 wt% Pt/TiO_2.

4.3.3. CO/CO_2 methanation results.

4.3.3.1. CO/CO_2 methanation results for the 5 wt% Rh/TiO_2 catalyst.

The selective methanation of CO in a CO/CO_2 gas mixture using the 5 wt% Rh/TiO_2 catalyst was investigated (**Figure 4.44**). It can be observed that CO selective methanation increases with increasing temperature and reaches a maximum of 80% conversion at 300 ^{0}C.This shows that the catalyst is more selective to CO methanation compared to CO_2 methanation. As the temperature increases further CO conversion drops due to the on-set of the reverse water gas shift (RWGS) reaction (Equation **(4.5)**).[22, 33&34]

$$CO_2 + H_2 \leftrightarrow CO + H_2O \qquad (4.5)$$

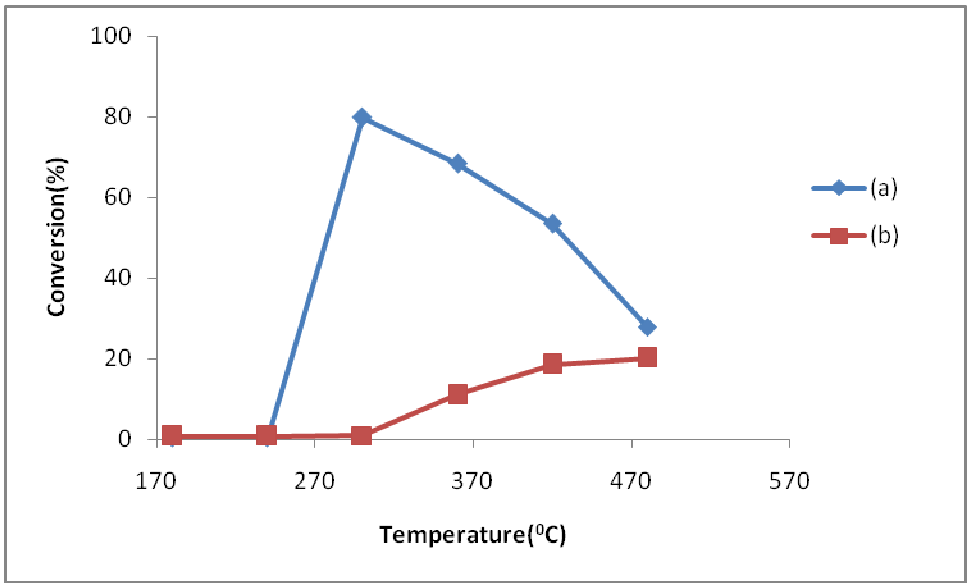


Figure 4.44: Conversions of CO/CO_2 as a function of temperature obtained over 5 wt% Rh/TiO_2 catalysts prepared by wet-incipient method and not calcined. **(a)** CO conversion and **(b)** CO_2 conversion. Feed composition: 8% CO,23% CO_2 and 69% H_2.

In **Figure 4.44**, the RWGS reaction is initiated when CO conversion reaches a maximum and its extent increases with increasing temperature. This is why the conversion of CO_2 increases and the conversion of CO decreases. At 420 ^{0}C, CO conversion is only 53% while CO_2 conversion

increases from 9% at 360 ^{0}C to 19% at 420 ^{0}C. The RWGS reaction is favoured at high temperatures.[35]

4.3.3.2. CO/CO_2 methanation results for the 5 wt% Ru/TiO_2 catalyst.

The 5 wt% Ru/TiO_2 catalyst displayed the same trend as the 5 wt% Rh/TiO_2 catalyst (**Figure 4.45**). The selective CO methanation increases with increasing temperature until it reaches a maximum of 70% conversion at 300 ^{0}C. Beyond this temperature CO conversion decreases due to the RWGS reaction (Equation **(4.5)**).[22,33,36&37]

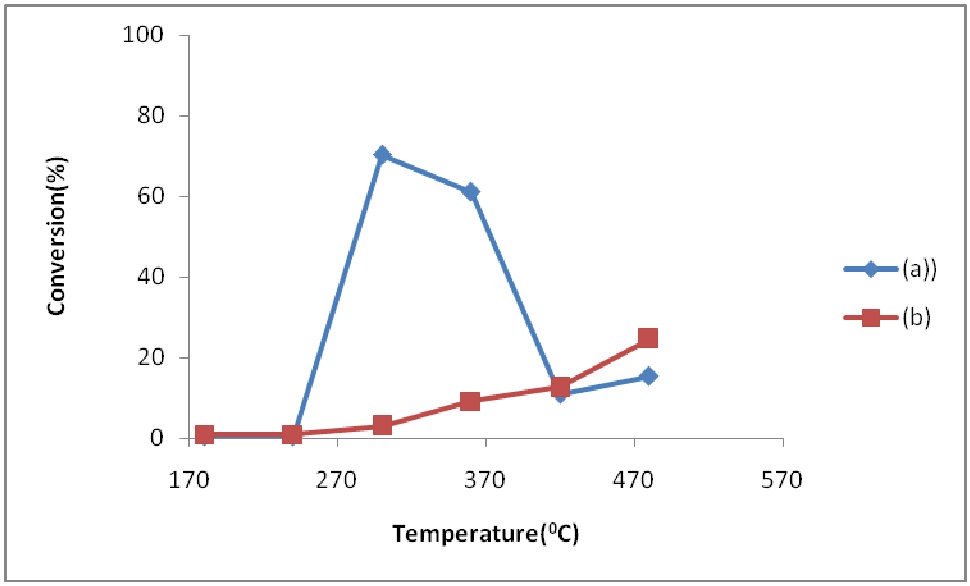


Figure 4.45: Conversions of CO/CO_2 as a function of temperature obtained over 5 wt% Ru/TiO_2 catalysts prepared by wet-incipient method and not calcined. **(a)** CO conversion and **(b)** CO_2 conversion. Feed composition: 8% CO, 23% CO_2 and 69% H_2.

4.3.3.3. CO/CO_2 methanation results for the 5 wt% Pd/TiO_2 catalyst.

The selective methanation of CO in a CO/CO_2 gas mixture was also investigated with the 5wt% Pd/TiO_2 catalyst and the results are presented in **Figure 4.46**.

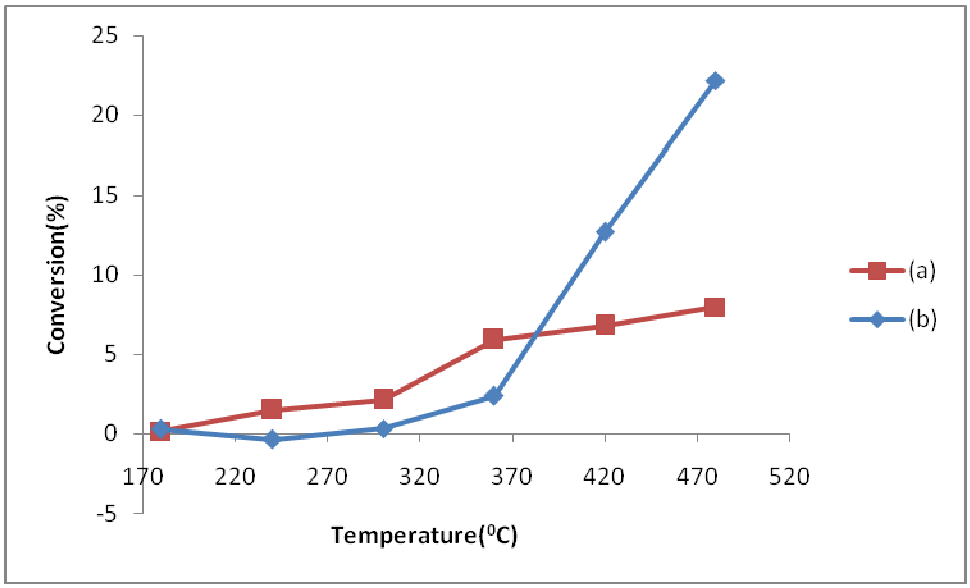


Figure 4.46: Conversions of CO/CO_2 as a function of temperature obtained over 5 wt% Pd/TiO_2 catalysts prepared by wet-incipient method and not calcined.**(a)** CO conversion and **(b)** CO_2 conversion. Feed composition: 8% CO, 23% CO_2 and 69% H_2.

From **Figure 4.46** it can be observed that the Pd/TiO_2 catalyst is more selective towards the CO_2 methanation reaction. Even in **section 4.3.2.3.** the Pd/TiO_2 tends to display higher conversions for CO_2 methanation compared to the other catalysts. CO conversion is only slightly higher than CO_2 conversion at lower temperatures which then switches to high CO_2 conversions at about 380 ^{0}C. At 420 ^{0}C CO_2 conversion is 20% while CO conversion is only 6%. This illustrates that the Pd/TiO_2 catalyst is more selective to CO_2 methanation.

4.3.3.4. CO/CO_2 methanation results for the 5 wt% Pt/TiO_2 catalyst.

Figure 4.47 shows the selective CO methanation results where conversion is plotted as a function of temperature.

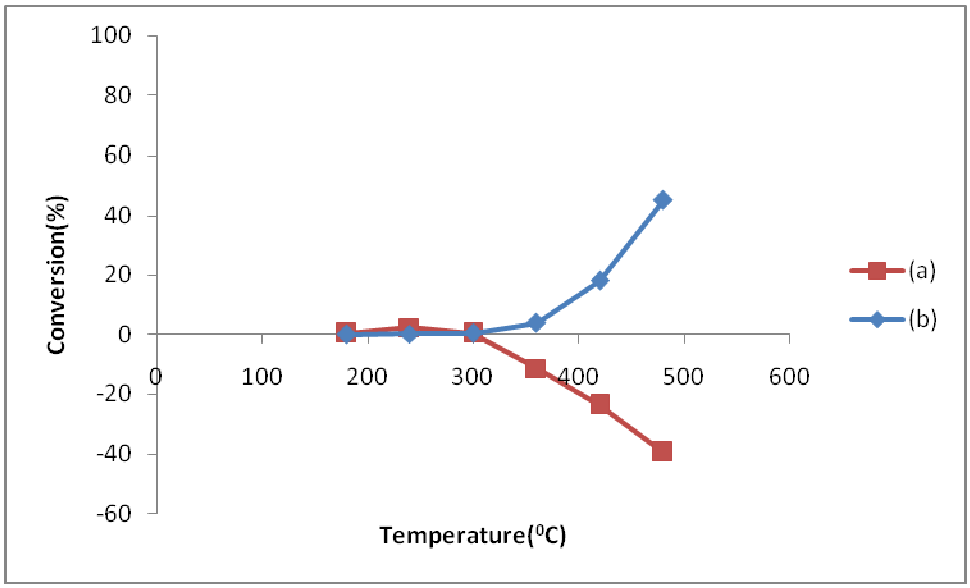


Figure 4.47: Conversions of CO/CO_2 as a function of temperature obtained over 5 wt% Pt/TiO_2 catalysts prepared by wet-incipient method and then not calcined. **(a)** CO conversion and **(b)** CO_2 conversion. Feed composition: 8% CO,23% CO_2 and 69% H_2

Figure 4.47 illustrates that the Pt/TiO_2 catalyst is inactive for the CO selective methanation reaction. This catalyst promotes the RWGS reaction and does not lead to CO methanation.[22] The CO conversion displays negative values because the CO_2 which is present in larger proportions is converted to CO through the RWGS reaction.[22] More CO is made than is being consumed. This effect increases with increasing temperature.

4.3.2.4. Summary of the CO/CO_2 methanation results of the 4 PGMs on TiO_2 support catalysts.

In order to summarize the CO/CO_2 methanation results the highest CO conversion (Max_{CO}) reached by the catalysts and the CO_2 conversion at that temperature (Max_{CO2}) are tabulated in **Table 4.12**. **Table 4.12** also includes the CO ($Conv(CO)_{480}$) and CO_2 ($Conv(CO_2)_{480}$)conversions at 480 ^{0}C. From **Table 4.12** it can be observed that the Rh/TiO_2 catalyst is the most active as it shows Max_{CO} of 80% at 300 ^{0}C while Max_{CO2} is 0% at this temperature. Dissimilar to the CO methanation results, at 480 ^{0}C CO conversion has dropped to 28% while CO_2 conversion is at 20% due to the RWGS reaction which makes the rate of CO consumption lower than the rate of CO production.[22] The Ru/TiO_2 catalyst displays similar behavior and many authors have reported the drop in CO conversion to be due to the onset of the RWGS reaction for this catalyst. [22, 33, 36&37] As it was noted in the CO_2 methanation reaction, the Pt/TiO_2 and Pd/TiO_2 catalysts promote the RWGS reaction and are not highly active for the CO methanation reaction. The activity of the catalysts for the selective methanation of CO in CO/CO_2 gas mixtures can be ranked as follows: $Rh/TiO_2 > Ru/TiO_2 > Pd/TiO_2 > Pt > TiO_2$.

Table 4.12: Summary of the selective methanation of CO in CO/CO_2 mixtures over the TiO_2 supported PGMs.

Catalyst	Max_{CO}= CO conversion at max / %	Max_{CO2}= CO_2 conversion at max / %	$Conv(CO)_{480}$ = CO conversion at 480 ^{0}C / %	$Conv(CO_2)_{480}$ = CO_2 conversion at 480 ^{0}C / %
Rh/TiO_2[b]	80% at 300 ^{0}C	0	28	20
Ru/TiO_2[b]	70% at 300 ^{0}C	3	15	24
Pd/TiO_2[b]	8% at 480 ^{0}C	22	8	22
Pt/TiO_2[b]	2% at 240 ^{0}C	0	-39	45

[b] Prepared by wetness-incipient method dried at 110 ^{0}C for 24 hours and not subjected to calcination.

Panagiotopoulou et. al., [22] also noted that the Rh/Al_2O_3 catalysts shows the highest activity since it had 98% CO conversion at 350 ^{0}C. However activity also dropped with increasing temperature due to the RWGS reaction.[22] The Ru/Al_2O_3 catalyst also displayed similar behavior and the Pt/Al_2O_3 and Pd/Al_2O_3 promoted the RWGS reaction.[22] The order of activity was reported to decrease in this order: $Rh/Al_2O_3 > Ru/Al_2O_3 >> Pt/Al_2O_3 > Pd/Al_2O_3$.[22] Galleti et.al.,[33] looked at the activity of Al_2O_3 supported Ru catalysts in the CO selective methanation reaction and also noted that after complete conversion, CO methanation activity drops due to the onset of the RWGS reaction. Yaccato et.al.,[38] who studied the selective methanation of CO in CO/CO_2 mixture using noble metals, also noted that the Pt catalyst has a high affinity for the RWGS reaction. This was also confirmed by Utaka et.al.,[39] who reported that the Pt/Al_2O_3 catalyst has a high affinity for the RWGS reaction during CO selective methanation in reformate gases. The results which are reported by these authors are comparable to the results obtained in the present study.

From the results in this section it can be noted that the difference between CO methanation and selective CO methanation in CO/CO_2 gas mixtures is that the Rh/TiO_2, Ru/TiO_2 and Pd/TiO_2 catalysts do not reach 100 % CO conversion. In addition after reaching maximum conversion, CO conversion drops due to the start of the RWGS reaction. The Pt/TiO_2 catalyst displays similar behavior for the CO methanation and selective CO methanation as it still shows low activity for CO conversion. The difference between CO_2 methanation and CO/CO_2 methanation is, the Ru/TiO_2 and Rh/TiO_2 catalysts show lower CO_2 conversion in the CO/CO_2 methanation as compared to CO_2 methanation. This could be an indication that CO interacts more strongly with the catalyst surface than CO_2. For the Pt/TiO_2 and Pd/TiO_2 catalysts there is a connection between CO_2 methanation and CO/CO_2 methanation, because in both reactions the catalysts promote the RWGS reaction. Lastly the temperature at which CO methanation is at a maximum and CO_2 methanation is at a minimum is not so large in the actual CO/CO_2 methanation reaction.

Since the 5 wt% Rh/TiO_2 and Ru/TiO_2 catalysts displayed the best performance in terms of activity for the CO methanation reaction as compared to the Pt/TiO_2 and Pd/TiO_2 catalysts, we determined the formation of CH_4 (**Figure 4.48**) from the individual CO/CO_2 methanation reactions of the 5 wt% Rh/TiO_2 and Ru/TiO_2 catalysts. The formation of CH_4 was not determined

for the 5 wt% Pt/TiO_2 and Pd/TiO_2 since they promote the RWGS reaction and do not display high activity for CO methanation.

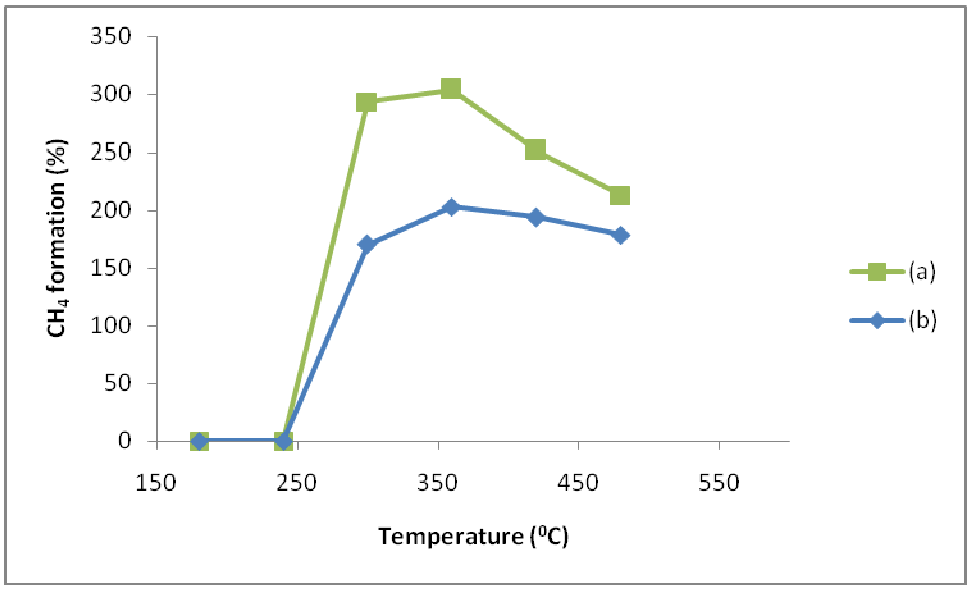


Figure 4.48: CH_4 formation as a function of temperature obtained from the (a) 5 wt% Rh/TiO_2 and (b) 5 wt% Ru/TiO_2 catalysts.

From the CO methanation (Equation **(1.7)**) reaction it can be noted that the molar ratio of CH_4: CO = 1:1. Since CO methanation did not reach 100 % conversion for both catalysts, if CH_4 formation is due to the methanation of CO only and not due to CO_2 then CH_4 formation should be below 100%. However from **Figure 4.45** it can be noted that CH_4 formation is significantly higher than 100% for both catalysts under the investigated temperature range. This means that CO_2 methanation occurs simultaneously with CO methanation under all of the presently investigated temperatures. This decreases the selectivity of both catalysts for the CO methanation reaction. Panagiotopoulou et.al.,[22] also reported similar findings. Galletti et.al.,[40] who performed a study on the selective methanation of CO with the use of Al_2O_3 and CeO_2 supported catalysts also reported that CO_2 methanation occurs together with CO methanation under the reaction conditions that they used. A selective catalyst for the CO selective methanation reaction should display a temperature range at which complete CO methanation occurs without significant CO_2 methanation. A deeper study has to be performed in order to develop a catalyst which retards CO_2 methanation and promotes complete CO conversion. Some of the important factors that

would have to be investigated include catalyst preparation, reaction conditions and gas composition.

4.4. References

1. T. Sreethawong, Y. Yamada, T. Kobayashi, S. Yoshikawa, Journal of Molecular Catalysis A: Chemical, 2006, 248, 226-232.
2. D. Li, N. Ichikuni, S. Shimazu, T. Uematsu, Applied Catalysis A: General, 1999, 180,227-235.
3. N.S. Babu, N. Lingaiah, N. Pasha, J.V. Kumar, P.S.S. Prasad, Catalysis Today, 2009, 141, 120-124.
4. X. Shen, L. Garces, Y. Ding, K. Laubernds, R.P. Zerger, M. Aindow, E. J. Neth and S.L. Suib, Applied Catalysis : A:General, 2008, 335, 187-195.
5. V. Balek, T. Mitsuhashi, A. Watanabe, V. Zelenak, J. Subrt, P.Bezdicka and J. Bohacek, Journal of Colloid and Interface Science, 2003, 260, 70-74.
6. S.A. Corradini, G.G. Lenzi, M.K.Lenzi, C.M.F. Soares, O.A.A. Santos, Journal of Non-Crystalline Solids, 2008, 354, 4865-4870.
7. L.Jinxiang, Y. Lixin, G. Shiuying, H.Lijuan, T. Renyuan, L. Dongbai, Thermochim. Acta, 1988, 123,121.
8. Y.H. Kim, E.D. Park, H. C. Lee, D. Lee, Applied Catalysis A: General, 2009, 366, 363-369.
9. A. Pintar, J. Batista, T. Tisler, Applied Catalysis B: Environmental, 2008, 84, 30-41.
10. G.C. Bond, R.R. Rajaram, R. Burch, Applied Catalysis, 1986, 27, 379.
11. W-J. Shen, M. Okumura, Y. Matsumura, M. Haruta, Applied Catalysis A: General, 2001, 213,225-232.
12. R. Gopinath, K. Narasimha Rao, P.S. Sai Prasad, S.S. Madhavendra, S. Narayanan, G. Vivekanandan, Journal of Molecular Catalysis A, 2002, 181, 215.

13. F.J. Berry, L.E. Smart, P.S. Sai Prasad, N. Lingaiah, P. Kantha Rao, Applied Catalysis A, 1993, 101, 41.

14. Y.V. Larichev, O.V. Netskina, O.V. Komova, V.I. Simagina, International Journal of Hydrogen Energy, 2010, 35, 6501-6507.

15. T. Ekou, A. Vicente, G. Lafaye, C. Especel, P. Marecot, Applied Catalysis A: General, 2006, 314, 64-72.

16. T. Ekou, L. Ekou, A. Vicente, G. Lafaye, S.Pronier, C. Especel, P. Marecot, Journal of Molecular Catalysis A: Chemical, 2011, 337, 82-88.

17. J.A.Wang, A. Cuan, J. Salmones, N. Nava, S. Castillo, M. Moran-Pineda, F. Rojas, Applied Surface Science, 2004, 230,94-105.

18. H. Liang, Y. Zhang, Y. Liu, Journal of Natural Gas Chemistry, 2008, 403-408.

19. P. Panagiotopoulou, A. Christodoulakis, D.I. Kondarides, S.Boghosian, Journal of Catalysis, 2006, 240, 114-125.

20. T.Huizinga, J.Van Grondelle and R. Prins, Applied Catalysis, 1984, 10,199-213.

21. S. Eckle, Y. Denkwitz, R.J Behm, Journal of Catalysis, 2010, 269, 255-268.

22. P. Panagiotopoulou, D. I. Kondarides and X. E. Verykios, Applied Catalysis A: General, 2008, 344, 45-54.

23. W. Shen, M. Okumura, Y. Matsumura and M. Haruta, Applied Catalysis A: General, 2001, 213, 225-232.

24. D.W. McKee, Journal of Catalysis, 1967, 8, 240-249

25. M.A. Vannice, Journal of Catalysis, 1975, 37, 449-461.

26. M. Ojeda, S. Rojas, F. J. Garcia-Garcia, M. L. Granados, P. Terreros and J. L. G. Fierro, Catalysis Communications, 2004, 5, 703-707.

27. M. Ojeda, S. Rojas, M. Boutonnet, F. J. Perez-Alonso, F. J. Garcia-Garcia and J. L. G. Fierro, Applied Catalysis A:General, 2004, 274, 33-41.

28. T. Bligaard, J.K. Norskovs, S. Dahl, J. Matthiesen, C.H. Christensen, J. Sehested, Journal of Catalysis, 2004, 224, 206-217.

29. J.K. Norskov, T. Bligaard, A. Logadottir, S. Bahn, L.B. Hansen, M. Bollinger, H. Bengaard, B. Hammer, Z. Sljivancanin, M. Mavrikakis, Y. Xu, S. Dahl, C.J.H. Jacobsen, Journal of Catalysis, 2002,209,275-278.

30. M.A. Vannice, Journal of Catalysis, 1977, 50,228.

31. C. de Leitenburg, A. Trovarelli, J. Kaspar, Journal of Catalysis, 1997, 166, 98.

32. F. Solymosi, A. Erdöhelyi, T. Bánsági, Journal of Catalysis, 1981, 68, 371.

33. C. Galleti, S. Specchia, G. Saracco, V. Specchia, Chemical Engineering Science, 2010, 65, 590-596.

34. Q. Liu, X. Dong, X. Mo, W. Lin, Journal of Natural Gas Chemistry, 2008, 17, 268-272.

35. E. D. Park, D. Lee, H. C. Lee, Catalysis Today, 2009, 280-290.

36. P. Panagiotopoulou, D.I. Kondarides, X.E. Verykios, Applied Catalysis B: Environmental, 2009, 88,470-478.

37. P. Djinovic, C. Galletti, S. Specchia, V. Specchia, Catalysis Today, 2011,164, 282-287.

38. K. Yaccato, R. Carhart, A. Hagemeyer, A. Lesik, P. Strasser, A.F. Volpe, H. Turner, H. Weinberg, R.K. Grasseli, C. Brooks, Applied Catalysis A, 2005, 296, 30.

39. T. Utaka, T. Takeguchi, R. Kilkunchi, K. Eguchi, Applied Catalysis A, 2003, 246, 117.

40. C. Galletti, S. Specchia, V. Specchia, Chemical Engineering Journal, 2011, 616-621.

Chapter 5

Conclusions and Recommendations

5.1. Conclusions

- The CO, CO_2 and CO/CO_2 methanation reactions with the use of TiO_2 supported Ru, Rh, Pd and Pt catalysts have been investigated. For the CO methanation reaction the Ru/TiO_2 and Pd/TiO_2 catalysts were prepared by different methods, namely deposition-precipitation method and the incipient –wetness impregnation method in which one set was calcined and another set was uncalcined. The uncalcined Ru/TiO_2 and Pd/TiO_2 catalysts exhibited different characteristics compared to the deposition-precipitation method and calcined catalysts. The uncalcined Ru/TiO_2 and Pd/TiO_2 catalysts displayed a second reduction peak which was not present in the other differently prepared catalysts which was due to metal support interactions. In addition the particle size of the uncalcined Ru/TiO_2 was very small while that of the uncalcined Pd/TiO_2 was slightly smaller than the other differently prepared catalysts. The Pd/TiO_2 catalysts did not differ in CO methanation activity however the uncalcined Ru/TiO_2 catalysts displayed high activities for the CO methanation, which is why we prepared the Rh/TiO_2 and Pt/TiO_2 catalysts with this method.

- During the CO methanation reaction the activities of the Rh, Ru and Pd catalysts increased with increasing temperature until a maximum of 100% CO conversion after which the conversion does not change with further increase of temperature. The Pt catalyst does not reach 100% CO conversion during the CO methanation reaction. The activity of all the investigated catalysts for the CO methanation reaction decreases with

decreasing metal loadings. The Ru and Rh catalysts displayed higher activities for the CO methanation than the Pd and Pt catalysts.

- The methanation of CO_2 leads to the production of CO at the expense of CH_4 through the RWGS reaction which is more pronounced for the Pd and Pt catalysts. Activity for CO_2 methanation decreases with decreasing metal loadings for all catalysts investigated. The comparison of CO methanation and CO_2 methanation demonstrates a large temperature window of operation at which CO methanation is at a maximum and CO_2 methanation is at a minimum which is large for the Rh and Ru and smaller for the Pd catalysts. This temperature window does not exist for the Pt catalyst. The Ru and Rh catalyst show higher activities for CO_2 methanation than the Pd and Pt catalysts. In order to determine the selectivity of the catalysts for the CO methanation reaction as compared to CO_2 methanation, R values were calculated by dividing CO conversion with CO_2 conversion. The Rh/TiO_2 and Ru/TiO_2 catalysts displayed the highest R values while the Pd/TiO_2 and Pt/TiO_2 catalysts displayed very low R values. This was an indication that the Rh/TiO_2 and Ru/TiO_2 catalysts are more selective towards CO methanation than CO_2 methanation and the Pd/TiO_2 and Pt/TiO_2 and catalysts are not that selective to CO methanation.

- Dissimilar to CO methanation , during CO/CO_2 methanation the activities of the Rh and Ru catalysts increased until a maximum after which they decreased due to the onset of the RWGS reaction. The Pd and Pt catalysts tend to promote the RWGS reaction during CO/CO_2 methanation to a greater extent than the Rh/TiO_2 and Ru/TiO_2 catalysts. The Ru and Rh catalysts have higher activities for the selective methanation of CO in the CO/CO_2 methanation reaction. The results reported for the CO, CO_2 and CO/CO_2 methanation reactions are consistent with literature results in which different reaction conditions and catalyst supports (mainly Al_2O_3) were used. Since the Rh/TiO_2 and Ru/TiO_2 displayed the best performance in terms of activity for the CO/CO_2 reaction, the formation of CH_4 was determined for both catalysts in order to establish their selectivity towards CO methanation. It was established that CO_2 methanation also occurs during CO methanation for both catalysts because the formation of CH_4 was not solely due to CO

methanation. A temperature range at which complete CO methanation occurs with negligible CO_2 methanation could not be found for both catalysts as the formation of CH_4 was also due to CO_2 methanation. This would mean that a deeper study would have to be conducted in the near future in order to develop a catalyst which would lead to complete CO methanation and minimum if any CO_2 methanation. This study should focus on factors such as catalyst preparation methods, catalyst supports, gas composition and reaction condition (e.g. changing the gas flow rate in such a way that the CO interacts better with the catalyst surface).

5.2. Recommendations for future work

- Future work would include developing a selective catalyst for the CO methanation reaction which shows a temperature range in which complete CO methanation occurs without or with an acceptable low level of CO_2 methanation. In addition this catalyst should not promote the RWGS reaction. A more in depth study should be performed which focuses on factors such as catalyst preparation methods, catalytic supports, gas compositions and reaction conditions.

- In terms of reaction conditions the future study should focus more on issues such as the flow rate of the CO/CO_2 gas mixture. Possibly by increasing or decreasing the gas mixture flow rate the interaction between CO and the catalytic surface might be improved. Thus leading to complete CO methanation and possible minimum CO_2 methanation.

- More advanced characterization techniques such as DRIFTs should be employed to study the catalytic surface of the catalysts. This might shed some light on the species

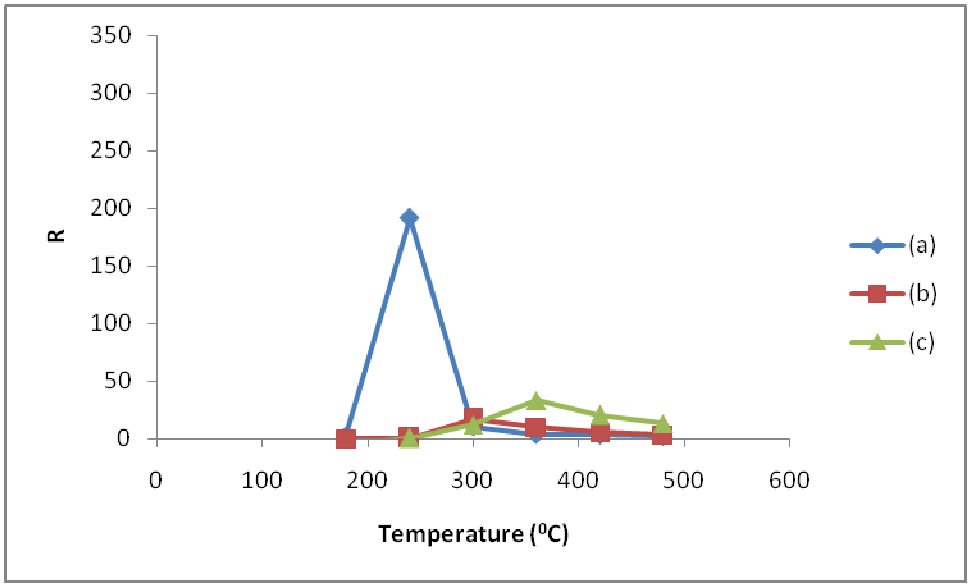
and intermediates which are present on the catalytic surface during the methanation reaction.

- Since it has been established that the Rh/TiO_2 and Ru/TiO_2 catalysts display the best performance for the CO methanation, more focus should be directed to these catalysts and less focus on the Pd/TiO_2 and Pt/TiO_2 catalysts.

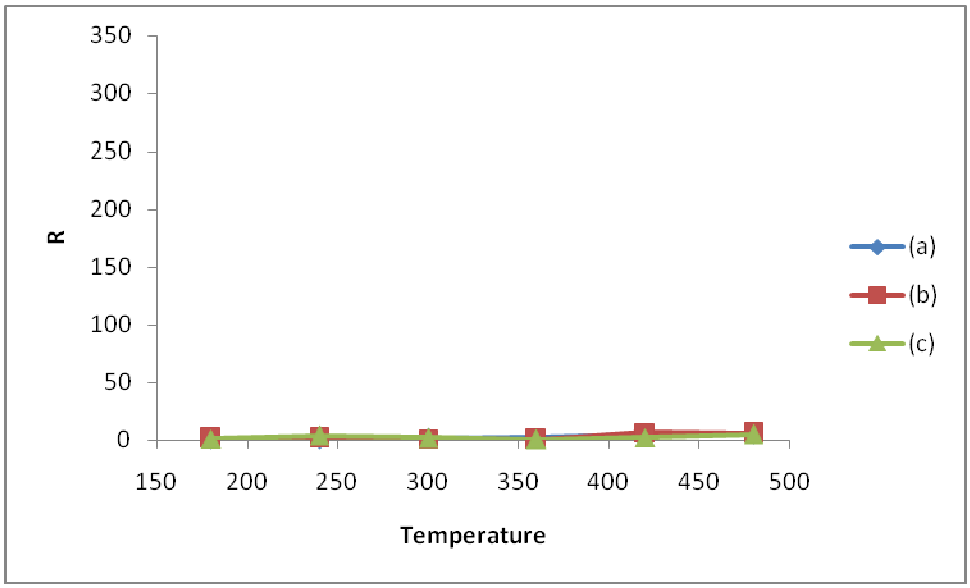
- Since the loadings of the Ru/TiO_2 and Pd/TiO_2 catalysts could not be determined by ICP, future work could involve determining the loadings of the catalysts with a more advanced method. This could involve digesting the catalysts with a method such as fusion and subjecting them to ICP analysis. In addition XRF could be used as an alternative to ICP.

Appendices

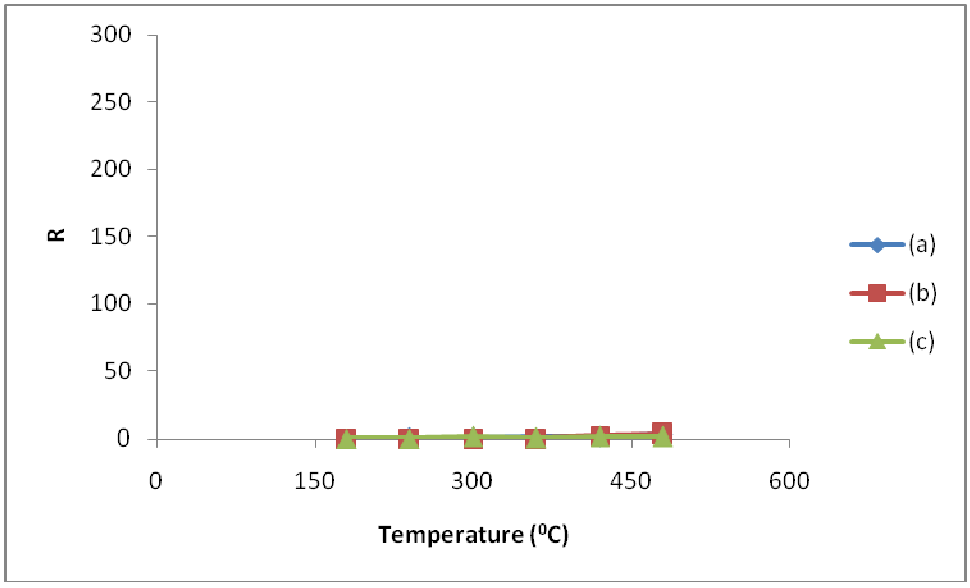
Appendix A



Appendix A1: Comparison of the R values (R = CO conversion/CO_2 conversion) of the Ru/TiO_2 catalysts as a function of temperature. The Ru/TiO_2 catalysts were prepared by the wet-incipient method and not calcined.(a) 5 wt% Ru/TiO_2 ,(b) 3 wt% Ru/TiO_2 and (c) 1 wt% Ru/TiO_2.



Appendix A2: Comparison of the R values (R = CO conversion/CO_2 conversion) of the Pd/TiO_2 catalysts as a function of temperature. The Pd/TiO_2 catalysts were prepared by the wet-incipient method and not calcined.(a) 5 wt% Pd/TiO_2 ,(b) 3 wt% Pd/TiO_2 and (c) 1 wt% Pd/TiO_2.



Appendix A3: Comparison of the R values (R = CO conversion/CO_2 conversion) of the Pt/TiO_2 catalysts as a function of temperature. The Pt/TiO_2 catalysts were prepared by the wet-incipient method and not calcined.(a) 5 wt% Pt/TiO_2 ,(b) 3 wt% Pt/TiO_2 and (c) 1 wt% Pt/TiO_2.